# Dynamics of Stem Cells in Liver

# Homeostasis, Injury and Carcinogenesis

**Wanlu Cao**

The work presented in this thesis was performed in the Department of Gastroenterology and Hepatology at Erasmus MC in Rotterdam, The Netherlands.

The research was funded by:

- Netherlands Organization for Scientific Research (NWO)
- Dutch Digestive Foundation (MLDS)
- Daniel den Hoed Foundation

Financial support for printing of this thesis was provided by:
Erasmus Postgraduate School Molecular Medicine



The cover is modified from ‘A Thousand Li of Rivers and Mountains’ by Wang Ximeng (1096-1119). Layout design: the author of this thesis.

Printed by Ridderprint

ISBN: 978-94-6299-861-2

# Dynamics of Stem Cells in Liver Homeostasis, Injury and Carcinogenesis

De dynamiek van stamcellen in de zieke en gezonde lever

# Thesis

**To obtain the degree of Doctor from the**
**Erasmus University Rotterdam**
**by command of the**
**rector magnificus**

Prof.dr H.A.P.Pols

**and in accordance with the decision of the Doctorate Board**

**The public defense shall be held on**

*Tuesday 6th February 2018 at 13:30 hr*

By

**Wanlu Cao**

Born in Qidong City, Jiangsu Province, China

ERASMUS UNIVERSITEIT ROTTERDAM

Erasmus

# Doctoral Committee

**Promotor:**

Prof. dr. M.P. Peppelenbosch

**Inner Committee:**

Prof. dr. R.A. de Man

Prof. dr. K.K. Krishnadath

Dr. L.J.W. van der Laan

**Copromotor:**

Dr. Q. Pan

# Contents

# CHAPTER 1

## General Introduction and Aim of this Thesis

## Liver Cancer

Liver cancer is the fifth most common cancer and the second most common cause of cancer mortality worldwide. It causes over 800,000 deaths yearly and more than 560.000 patients per year are diagnosed with primary liver cancer worldwide [1]. Primary liver cancer has been traditionally classified into three main types based on the tumor cell type: hepatocellular carcinoma (HCC), cholangiocarcinoma (CC) and hepatocellular-cholangiocarcinoma (CHC). HCC constitutes more than 85% of primary liver cancers. Major risk factors for liver cancer include chronic viral hepatitis (hepatitis B or C), cirrhosis, heavy alcohol use and nonalcoholic fatty liver disease [2]. Surgical resection is the most optimal treatment for liver cancer. However, less than 30% of patients are eligible for surgical resection, because liver cancer is often detected at a late stage. Liver tranplantation has also been established as an effective therapy for liver cancer [3]. However, the major limitations of liver tranplantation are: 1) the shortage of deceased donor living grafts; 2) the strict criteria for selecting patients which are eligible for transplantation; 3) the immunosuppression treatment after liver transplantation weakens the immune system and increases the risk of tumor recurrence or *de novo* formation of different types of cancers. In addition, tumor recurrence is the leading cause of death following surgery and the frequency of recurrence is up to 85% within 5 years. For advanced HCC, the only FDA approved drug for treating liver cancer is Sorafenib, which extends the survival time of patients for approximately 3 months. Thus, understanding the biology and investigation of effective treatment is urgently needed for liver cancer.

## Stem cells in liver homeostasis, injury and carcinogenesis

Liver stem cells are defined by their ability to self-renew and differentiate into both hepatocytes and cholangiocytes. The various functions of liver stem cells are distinct in two aspects: 1) those involved in homeostatic maintenance of the liver compartment under normal physiological conditions; 2) those involved in tissue repair/regeneration under pathological conditions.

During homeostasis, liver stem cells remain quiescent and possess a longer life span compared to the rest of the cells. Classically, the quiescent/slow cycling cells are identified by nucleotide analogs (thymidine or BrDU)-dependent label retaining assays. Different locations in liver have been reported to contain stem cells by virtue of their capacity to incorporate and retain label in such assays. These regions include the canals of Hering,

the bile duct and the peribiliary area [4]. Upon liver injury, liver stem cells start to proliferate and then further differentiate. For example, the leucine-rich-repeat-containing G-protein-coupled receptor 5 (LGR5) marks a stem cell pool which actively proliferates upon carbon tetrachloride (CCL4)-induced liver injury [5]. Isolated LGR5 stem cells can give birth to both cholangiocyte and hepatocyte population *in vitro*. The tranplantation of single $LGR5^+$ cell derived organoid can generate functional hepatocytes in liver function-impaired mice.

However, chronic liver injury can eventually result in the development of liver cancer, possibly because the injury is also accompanied by long-term activation and expansion of stem cells. This has led to the notion that adult stem cells can accumulate genetic/epigenetic changes and subsequently contribute to tumor initiation and progression and this concept has attracted great interest. Because various mutations are necessary for a cell finally turning into cancerous entity, the long-lived and injury-activated stem cells have the highest opportunity to accumulate those cancer-inducing mutations over years. For example, the sex determining region Y-box 9 (SOX9) gene has been demonstrated to be a marker for facultative stem cells in liver [6]. SOX9 liver cells can compensate for the loss of bulk of hepatocytes in several liver injury settings, including CCL4 or 3,5-diethoxycarbonyl-1,4-dihydrocollidine (DDC) induced liver injury, as well as choline-deficient ethionine supplemented (CDE) diet. However, liver SOX9 expressing cells are present in HCC [7], which is the most common type of primary liver cancer. The prognosis of HCC patients correlates to the expression profile of SOX9. Thus, it would be particularly interesting to investigate the dynamics of liver stem cells under normal physiological and different pathological conditions.

**Cancer stem cells**

The definition of cancer stem cell is “a cell within a tumor that possesses the capability to self-renew and to cause the heterogeneous lineages of cancer cells that comprise the tumor” [8]. Cancer stem cells are considered to be responsible for tumor initiation and growth, failure of treatment and tumor recurrence. Functionally, the colony formation and therapy resistance assay are classical and convenient approaches to identify the tumor stem cell *in vitro*. Genetic lineage tracing and limited diluted tumor formation assay are used to demonstrate tumor stemness *in vivo*. For instance, LGR5 marks a cancer stem cell population in intestinal and colorectal carcinoma [9-11]. LGR5 tumor stem cells are highly tumorigenic, and can form tumor when only 100 cells were transplanted into

immunocompromised mice [12]. In addition, LGR5$^{+}$ cancer stem cells play a critical role in the development and maintenance of colorectal cancer derived metastasis [12]. Thus, the investigation of cancer stem cells would provide new insights with respect to the understanding the biology of the tumor, as well as allow for the discovery of more effective therapy.

**Organoids: an innovative model for studying (cancer) stem cells.**

Organoids are stem cell derived, organ-like 3D structures, which have attracted great attention during the recent years. Stem cells are isolated from a particular organ/tissue proliferate and then arrange themselves automatically into a 3-dimensional structure in appropriate culture conditions. The resulting structures contain different cell types which also existed in the original corresponding organ/tissue, where those stem cells derived from. This technique has subsequently been adapted to culture organoids from the intestine [13], liver [5], stomach [14, 15] and prostate [16].

Organoid systems offer one of the most promising platforms for harnessing stem cell research. With respect to regenerative medicine for treating liver disease, material suitable for therapeutic transplantation is always rare, leading to an urgent requirement for developing alternative sources. Human liver organoid have been successfully transplanted into the immunodeficient mouse to compensate for the insufficient liver function [14]. Although extensive investigation is required before clinical application can become commonplace, especially considering the technical, safety, efficacy and ethical issues, organoid-based stem cell therapy does provide a new avenue for transplantation medicine.

Organoid system can also be used for modelling different diseases, including infectious disease, genetic disease, especially different types of cancers. Organoids have already been successfully established from primary tumor of colons [13], stomach [14], prostate [17] and pancreas [18]. There are many advantages of tumor organoid models, but just to highlight a few as following: 1) understanding for the impact of a specific genetic mutation, by combining with the CRISPR/Cas9 genome editing and xenograft/allograft tranplantation assays; 2) allowing the culturing of both primary tumor and tumor surrounding healthy tissue, thus providing personalized information regarding response to therapy *ex vivo* [19, 20]; 3) an innovative model system for studying cancer stem cells [12]. In sum, organoid system representing an unique tool for the research field to advance in-depth research of adult stem cells, cancers and cancer stem cells.

## Cancer stem cell-targeted therapy

Cancer stem cells have been hypothesized to fuel the growth of the tumor by giving birth to offspring that retains the cancer stemness , as well as proliferative progenitor cells that mediate compartment expansion. They are also thought to be resistant to treatment, and thus responsible to the recurrence of the tumor following therapy. These features make cancer stem cells as attractive cancer targets [21].

Over the past decades, several cancer stem cell markers have been identified as potential therapeutic targets [21]. For example, targeting LGR5 colon cancer stem cells has been investigated, by using colorectal mouse cancer model, as well as xenograft cancer model [12, 22]. Those investigations employed the diphtheria toxin-diphtheria toxin receptor (DT-DTR) system, which can specifically ablate LGR5-expressing cells. The depletion of LGR5 colon cancer stem cell were observed to impede the growth of the primary tumor, as well as the metastasis.

However, many cancer stem cell markers are also expressed in the normal stem cells or embryonic stem cells. Thus, it is very important to selectively target tumor stem cells, without compromising normal stem cell homeostasis. Thus, researchers have adopted antibody-drug conjugates (ADCs) and assessed the resulting tumor-targeting efficiency, as well as their safety *in vivo*. The anti-LGR5-antibody-drug conjugates are reported to inhibit the tumor growth effectively, and even improve the survival for the intestinal cancer carrying mouse. Impressively, the anti-LGR5-antibody-drug conjugate has no major effect on the normal stem cell pool [10]. Thus, It will be of particular interesting to further explore novel strategies to target cancer stem cells.

## Aim of this Thesis

Based on the former, the general aims of this thesis are: 1) to investigate the dynamics of LGR5 proliferative stem cells in homeostatis and injury of the liver, and to characterize the role of LGR5 stem cell in maintenance of the stem cell pool *ex vivo*. 2) to demonstrate the existence and function of quiescent stem cells using the long-term label retaining assay 3) to investigate the interrelationship of the proliferative LGR5 stem cells and the quiescent stem cell during liver homeostasis and injury. 4) to establish malignant organoid models from mouse primary liver tumors and demonstrate their applications in liver cancer research. 5) to investigate the existence and function of liver cancer stem cells by adopting

transgenic mouse model and 3D organoid model. 6) to investigate whether normal LGR5 proliferative stem cells participate in the tumor progression and formation by using LGR5 lineage tracing mouse. The results provide a wealth of data on the action and function of the LGR5 stem cell compartment and other stem cell compartment in hepatic physiology and pathology.

## References:


1. Bosch FX, Ribes J, Diaz M, et al. Primary liver cancer: worldwide incidence and trends. Gastroenterology 2004;127:S5-S16.

2. El-Serag HB, Rudolph KL. Hepatocellular carcinoma: epidemiology and molecular carcinogenesis. Gastroenterology 2007;132:2557-76.

3. Duffy JP, Vardanian A, Benjamin E, et al. Liver transplantation criteria for hepatocellular carcinoma should be expanded: a 22-year experience with 467 patients at UCLA. Ann Surg 2007;246:502-9; discussion 509-11.

4. Kuwahara R, Kofman AV, Landis CS, et al. The hepatic stem cell niche: identification by label-retaining cell assay. Hepatology 2008;47:1994-2002.

5. Huch M, Dorrell C, Boj SF, et al. In vitro expansion of single Lgr5+ liver stem cells induced by Wnt-driven regeneration. Nature 2013;494:247-50.

6. Tarlow BD, Finegold MJ, Grompe M. Clonal tracing of Sox9+ liver progenitors in mouse oval cell injury. Hepatology 2014;60:278-89.

7. Liu C, Liu L, Chen X, et al. Sox9 regulates self-renewal and tumorigenicity by promoting symmetrical cell division of cancer stem cells in hepatocellular carcinoma. Hepatology 2016;64:117-29.

8. Clarke MF, Dick JE, Dirks PB, et al. Cancer stem cells--perspectives on current status and future directions: AACR Workshop on cancer stem cells. Cancer Res 2006;66:9339-44.

9. Gregorieff A, Liu Y, Inanlou MR, et al. Yap-dependent reprogramming of Lgr5(+) stem cells drives intestinal regeneration and cancer. Nature 2015;526:715-8.

10. Junttila MR, Mao W, Wang X, et al. Targeting LGR5+ cells with an antibody-drug conjugate for the treatment of colon cancer. Sci Transl Med 2015;7:314ra186.

11. Medema JP. Targeting the Colorectal Cancer Stem Cell. N Engl J Med 2017;377:888-890.

12. de Sousa e Melo F, Kurtova AV, Harnoss JM, et al. A distinct role for Lgr5+ stem cells in primary and metastatic colon cancer. Nature 2017;543:676-680.

13. Sato T, Stange DE, Ferrante M, et al. Long-term expansion of epithelial organoids from human colon, adenoma, adenocarcinoma, and Barrett's epithelium. Gastroenterology 2011;141:1762-72.

14. Bartfeld S, Bayram T, van de Wetering M, et al. In vitro expansion of human gastric epithelial stem cells and their responses to bacterial infection. Gastroenterology 2015;148:126-136 e6.

15. Barker N, Huch M, Kujala P, et al. Lgr5(+ve) stem cells drive self-renewal in the stomach and build long-lived gastric units in vitro. Cell Stem Cell 2010;6:25-36.

16. Chua CW, Shibata M, Lei M, et al. Single luminal epithelial progenitors can generate prostate organoids in culture. Nat Cell Biol 2014;16:951-61, 1-4.

17. Gao D, Vela I, Sboner A, et al. Organoid cultures derived from patients with advanced prostate cancer. Cell 2014;159:176-187.

18. Boj SF, Hwang CI, Baker LA, et al. Organoid models of human and mouse ductal pancreatic cancer. Cell 2015;160:324-38.

19. Wang S, Gao D, Chen Y. The potential of organoids in urological cancer research. Nat Rev Urol 2017;14:401-414.

20. Bartfeld S, Clevers H. Stem cell-derived organoids and their application for medical research and patient treatment. J Mol Med (Berl) 2017;95:729-738.

21. Nassar D, Blanpain C. Cancer Stem Cells: Basic Concepts and Therapeutic Implications. Annu Rev Pathol 2016;11:47-76.

22. Shimokawa M, Ohta Y, Nishikori S, et al. Visualization and targeting of LGR5+ human colon cancer stem cells. Nature 2017;545:187-192.

# CHAPTER 2

# Dynamics of Proliferative and Quiescent Stem Cells in Liver Homeostasis and Injury

Wanlu Cao[1], Kan Chen[1,2], Michiel Bolkestein[3,4], Yuebang Yin[1], Monique M. A. Verstegen[4], Marcel. J. C. Bijvelds[1], Wenshi Wang[1], Nesrin Tuysuz[3], Derk ten Berge[3], Dave Sprengers[1], Herold J. Metselaar[1], Luc J. W. van der Laan[4], Jaap Kwekkeboom[1], Ron Smits[1], Maikel P. Peppelenbosch[1] and Qiuwei Pan[1*]

[1]Department of Gastroenterology and Hepatology, Erasmus MC-University Medical Center, Rotterdam, The Netherlands.
[2]College of Life Sciences, Zhejiang Sci-Tech University, Hangzhou, China.
[3]Department of Cell Biology, Erasmus MC-University Medical Center, Rotterdam, The Netherlands.
[4]Department of Surgery, Erasmus MC-University Medical Center, Rotterdam, The Netherlands.

***Gastroenterology. 2017 Oct;153(4).***

## Abstract:

**Background & Aims**: Adult liver stem cells are usually maintained in a quiescent/slow cycling state. However, a proliferative population, marked by leucine-rich repeat-containing G-protein coupled receptor 5 (LGR5), was recently identified as an important liver stem cell population. We aimed to investigate the dynamics and functions of proliferative and quiescent stem cells in healthy and injured livers.

**Methods**: We studied LGR5-positive stem cells using diphtheria toxin receptor (DTR) and green fluorescent protein (GFP) knock-in mice. In these mice, LGR5-positive cells specifically co-express DTR and the GFP reporter. Lineage tracing experiments were performed in mice in which LGR5-positive stem cells and their daughter cells expressed a YFP/mTmG reporter. Slow-cycling stem cells were investigated using GFP-based, Tet-on controlled transgenic mice. We studied the dynamics of both stem cell populations during liver homeostasis and injury induced by carbon tetrachloride. Stem cells were isolated from mouse liver and organoid formation assays were performed. We analyzed hepatocyte and cholangiocyte lineage differentiation in cultured organoids.

**Results**: We did not detect LGR5-expressing stem cells in livers of mice at any stage of a lifespan, but only following liver injury induced by carbon tetrachloride. In the liver stem cell niche, where the proliferating $LGR5^{+}$ cells are located, we identified a quiescent/slow-cycling cell population, called label-retaining cells (LRCs). These cells were present in the homeostatic liver, capable of retaining the GFP label over 1 year, and expressed a panel of progenitor/stem cell markers. Isolated single LRCs were capable of forming organoids that could be carried in culture, expanded for months, and differentiated into hepatocyte and cholangiocyte lineages in vitro, demonstrating their bona fide stem cell properties. More interestingly, LRCs responded to liver injury and give rise to LGR5-expressing stem cells, as well as other potential progenitor/stem cell populations, including SOX9- and CD44-positive cells.

**Conclusions:** Proliferative LGR5 cells are an intermediate stem cell population in the liver that emerge only during tissue injury. In contrast, LRCs are quiescent stem cells that are

present in homeostatic liver, respond to tissue injury, and can give rise to LGR5 stem cells, as well as SOX9- and CD44-positive cells.

**Keywords**: Liver Stem Cells; LGR5; Quiescent Stem Cells; Proliferative Stem Cells

## Introduction

In general, adult stem cells are maintained in quiescence at homeostatic conditions but are able to exit the quiescent state and rapidly expand and differentiate in response to tissue injury.[1] Counterintuitively, recent studies indicated that LGR5, as a component of the Wnt signaling pathway, robustly marks actively dividing stem cells in the gut,[2] stomach,[3] hair follicle,[4] mammary gland[5] and liver.[6]

In the intestine, proliferative LGR5$^+$ stem cells are present throughout the intestine and populate the crypt and villi within 3 days.[2, 7] Another type of stem cells, marked by BMI1, represent a rarer cell population that are quiescent but can be activated under pathological conditions and give birth to proliferative LGR5$^+$ cells in the intestine.[8]

In the liver, the early streaming liver theory has proposed that normal liver turnover is originated from the portal zone and migrates towards the central vein, mainly driven by mature hepatocyte proliferation.[9, 10] Liver stem cells, as a small population of cells, are thought to reside around the portal zone and maintained in quiescence.[11] As an emerging field, a recent study reported that an Axin2 marked population of proliferating and self-renewing cells adjacent to the central vein can also contribute to generation of new hepatocytes.[12] Upon tissue injury, in particular in the setting of chronic liver diseases, long-term (10-30 years) chronicity triggers continuous inflammation, liver regeneration and possible development of liver cancer which coordinately initiate the activation and expansion of hepatic stem cells, though recent studies in experimental models have indicated that hepatocytes are probably the main cell-of-origin in liver canecr.[13-16] In fact, this proposed quiescent liver stem cell population has not been functionally demonstrated yet; whereas the proliferative LGR5$^+$ liver stem cells have been recently identified. These LGR5$^+$ stem cells were activated upon carbon tetrachloride ($CCl_4$) induced injury in a *Lgr5-lacZ* knock-in mouse model. Single isolated LGR5$^+$ cells can initiate organoids *ex vivo*. Upon transplantation, those organoids can repopulate the injured liver of the fumarylacetoacetate hydrolase mutant mice.[6]

Previously, the liver quiescent/slow-cycling cell population, also termed as label retaining cells (LRCs), was identified by labeling with nucleotide analogs that incorporate into genomic DNA in mice.[11] However, this classical approach was not able to functionally characterize these cells due to technical limitations. In this study, we applied a green florescent protein (GFP) based, Tet-on controlled transgenic mouse model that enables us to identify, isolate and functionally study these liver LRCs. Secondly, we have investigated

the interrelationship of the proliferative LGR5 stem cells and the LRCs during liver homeostasis and injury.

## Materials and Methods:

### *Tamoxifen (TAM) Labelling Experiments*

*Lgr5-creERT2* mice (kindly provided by Genentech)[8] were crossed with *B6.129X1-Gt(ROSA)26Sortm1(EYFP)Cos/J* (Rosa26-YFP, The Jackson Laboratory) and *Gt(ROSA)26Sortm4 (ACTB-tdTomato,-EGFP)Luo/J (Rosa26-mTmG*, The Jackson Laboratory*)*[17] Cre reporter mice respectively. Offspring (8-12 weeks) were administrated with single or weekly repeated intraperitoneal (i.p.) $CCl_4$ injection (10 µL/20 g body weight of 10% $CCl_4$ solution in corn oil or corn oil as control). A single dose of TAM (5 mg per mouse) was i.p. injected 5 days after the last $CCl_4$/oil injection for initiating lineage tracing. Mice were sacrificed at post day 5 and 25 of TAM injection, and tissues were collected for analyzing the presence of daughter cells derived from $LGR5^+$ cells. For *Rosa26-YFP* reporter mice, the daughter cells derived from $LGR5^+$ cells expressed yellow florescent protein (YFP); For *Rosa26-mTmG* reporter mice, regular cells expressed membrane-targeted tandem dimer Tomato florescent protein (mT), but the offspring derived from $LGR5^+$ cells expressed membrane-targeted green fluorescent protein (mG).

### *Diphtheria Toxin (DT) Cell Ablation*

*Lgr5-DTR-GFP* transgenic mice (kindly provided by Genentech)[8] specifically co-express the diphtheria toxin (DT) receptor (DTR) and GFP under the control of the *Lgr5* promotor. Thus, $LGR5^+$ cells will be marked by GFP, and LGR5-$GFP^+$ cells can be selectively ablated by treatment with DT. To deplete LGR5-$GFP^+$ cells in cultured organoids, DT (concentrations ranged from 1 ng/ml to 100 ng/ml) was added it to organoid expansion medium for three days, followed by further analysis or passage.[18] For organoid initiation assay, DT was supplied constantly with organoid initiation medium since organoids were seeded.

### *In vivo Label Retaining System*

The transgenic mouse model expressing the reverse tetracycline transactivator (rtTA) under a particular promoter (*Cag* promoter; *Rosa26* promoter; *HnRNP* promoter) was mated with *tetO-HIST1H2BJ/GFP (H2BGFP)* mice (JAX laboratory), which carried a

Histone2B fused GFP protein (H2B-GFP) under control of a TetO-responsive promoter.[19-21] Young adult transgenic mice (4-6 weeks of age) carrying heterozygous *rtTA/H2BGFP* and control littermates were administered with doxycycline (dox, Sigma-Aldrich) at 1 mg/ml in 5% sucrose (Sigma-Aldrich) containing drinking water for 7 days. GFP will be expressed upon dox administration, in all cells of the mice which have the corresponding promoter (*Cag*/*Rosa26*/*HnRNP* promoter). After withdrawing the dox water, GFP will not be produced anymore and proliferating cells will progressively dilute the GFP, but quiescent/slow cycling cells can retain the GFP label. GFP expression in mice was analyzed from 0 till 65 weeks after dox induction. All animal experiments were approved by the Committee on the Ethics of Animal Experiments of the Erasmus Medical Center.

## Results

### *LGR5$^+$ Stem Cells Are Absent in the Homeostatic Liver Over the Life Span of a Mouse, But Emerge Upon Injury*

A previous study has reported the activation of liver LGR5 proliferative stem cells by $CCl_4$ induced injury.[6] By adopting *Lgr5-DTR-GFP* knock-in mice,[8] we observed that LGR5-expressing cells (marked by GFP) are absent in the homeostatic liver over the life span of a mouse (Supplementary Figure 1*A*). Indeed, single/repeated administration of $CCl_4$ for inducing acute/chronic hepatic injury triggered the emergence of LGR5-GFP$^+$ cells (mean ± SEM, 1 × $CCl_4$: 0.02 ± 0.01%, n = 3; 4 × $CCl_4$: 0.04 ± 0.01%, n = 3; 17 × $CCl_4$: 0.11 ± 0.01%, n = 4) in the liver (Supplementary Figure 1*B-D,* and Supplementary Figure 2: immunohistochemistry). Isolated single LGR5-GFP$^+$ cells derived from 4 months of chronically injured livers formed organoids with the ability of serial passage (Supplementary Figure 1*E*). Meanwhile, we found that LGR5-GFP$^-$ cells also formed organoids with the ability of serial passage, although with a lower organoid initiation efficiency compared to LGR5-GFP$^+$ cells (Supplementary Figure 1*F-G*).

We further investigated the daughter cells (marked by YFP) derived from LGR5-expressing cells by *Lgr5-CreERT2/Rosa26-YFP* lineage tracing mice (Supplementary Figure 3*A-B*).[8] Upon acute liver injury, less than 0.05% or 0.1% of liver cells during a 5-day or 25-day lineage tracing period were labelled with YFP, respectively. Even when $CCl_4$ was administrated for 4 months (17 × $CCl_4$) to induce chronic injury, there was still a very low percentage of YFP-expressing cells (less than 0.2%) identified in the liver (Supplementary Figure 3*C-E*). To further confirm and better visualize LGR5 daughter cells,

we next employed a *mTmG* reporter mouse for LGR5 lineage tracing (Supplementary Figure 3*F*).[17] Due to the specific membrane localization of fluorescent protein in the *mTmG* reporter mice, the daughter cells of LGR5 stem cells were clearly visible both in liver as well as the intestine. After using the same acute injury and lineage tracing strategy as mentioned above, we confirmed the low percentages of LGR5 offspring contributing to injury recovery in the liver, both in 5-day and 25-day lineage tracing period (Supplementary Figure 3*G*, and Supplementary Figure 4: immunohistochemistry). Our results indicated that, unlike other progenitor/stem cells (*e.g.* Sox9$^+$ cells),[22] hepatic LGR5 stem cells contribute a relatively low number of daughter cells to injury recovery of the liver.

## *Bile Duct Gives Birth to LGR5$^+$ Stem Cells, and LGR5 Cells Are Dispensable for Organoid Formation*

Since we and others[6] have observed that LGR5-expressing cells are present around or within the bile duct of the portal triad area (Figure 1*A*, and Supplementary Figure 2*B-C*), we asked whether bile duct indeed gives rise to LGR5$^+$ liver stem cells. Therefore, we first isolated bile ducts (no LGR5$^+$ cells) from the liver of the healthy *Lgr5-DTR-GFP* mice and seeded the bile ducts in matrigel for organoid initiation (Figure 1*B* and *D*). We found that LGR5-GFP$^+$ cells emerged during organoid initiation and were stably maintained during organoid expansion (Figure 1*C* and *E*), indicating that bile duct can give rise to LGR5$^+$ cells. Furthermore, both LGR5-GFP$^+$ and LGR5-GFP$^-$ cells dissociated from bile duct derived organoids and isolated by FACS sorting can re-initiate organoids. LGR5-GFP$^+$ cells were maintained in the organoids derived from LGR5-GFP$^+$ cells, but also appeared in the organoids formed by the LGR5-GFP$^-$ cells (Figure 1*F and G*).

We further investigated whether the depletion of LGR5-expressing cells will affect organoid expansion. Since the *Lgr5-DTR-GFP* mice co-express DTR, LGR5-GFP$^+$ cells can be selectively ablated by treatment with DT (Figure 1*H* and *I*). We first found that 1 ng/ml of DT was sufficient to specifically kill LGR5$^+$ cells (Figure 1*J* and Supplementary Figure 5*A*). Interestingly, specific ablation of LGR5$^+$ cells by DT did not strongly affect the growth of formed organoids (Figure 1*K*). LGR5-depleted organoids can still be passaged, with similar efficiency of re-initiating organoids, compared to organoids containing LGR5$^+$ cells (control vs. DT treatment: 3.30 ± 1.33% vs. 3.07 ± 0.70%, mean ± SEM, n = 3; *P* = NS) (Figure 1*L*).

To further investigate whether the depletion of LGR5-expressing cells will affect organoid initiation, we supplied the organoid culture medium with DT since the initial

culture of isolated bile ducts (Figure 1*M*). No clear difference of organoid morphology was observed between DT treated and untreated groups. FACS analysis confirmed the efficient ablation of LGR5-expressing cells (Figure 1*O*, and Supplementary Figure 5*B*). Organoids derived from wild type mouse were taken as control and also showed similar results (Figure 1*P*, and Supplementary Figure 5*C-D*). Furthermore, organoids of the DT treated group could be weekly passaged for more than 2 months with the persistent supplement of DT. The DT treated group showed similar organoid re-initiation efficiency, compared to the untreated group (Figure 1*N*). Interestingly, the LGR5-depleted organoids showed significant upregulation of a panel of progenitor/stem cell markers, including *Oct4*, *Sox2*, *Cd44*, *Cd133*, *Sox9*, *Lrig1* and *Mex3a,* suggesting a possible compensatory mechanism (Figure 1*Q*). Thus, these data suggest that bile ducts harbor an early stem cell population that can give rise to $LGR5^+$ stem cells, but liver $LGR5^+$ cells are dispensable for organoid initiation and further expansion.

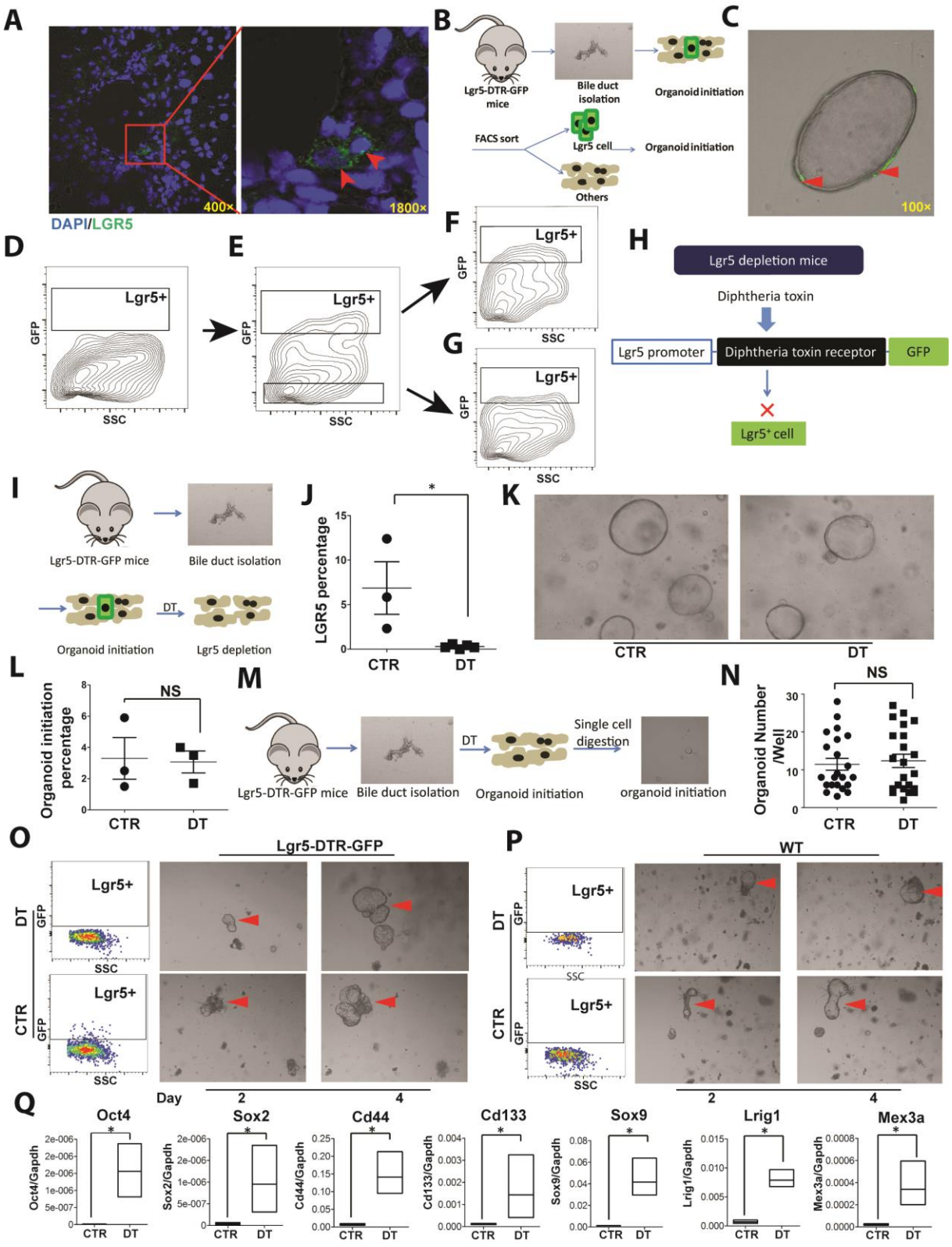


**Figure 1.** Bile ducts could give birth to LGR5 stem cells which were dispensable for organoid initiation and expansion. (*A*) LGR5 stem cells (green) localized around the portal triad, which indicated by anti-GFP immunofluorescence staining; Red arrow: LGR5$^{+}$ cell. DAPI: blue; LRCs: Green. (*B*) An outline of the experimental strategy used. (*C*) Representative pictures showing bile ducts derived organoids containing LGR5-expressing cells; Red arrow: LGR5$^{+}$ cell. (*D-G*) Bile duct isolated from healthy *Lgr5-DTR-GFP* mice and initiated organoids *ex vivo*. Then, LGR5-GFP$^{+}$ and LGR5-GFP$^{-}$ cells were isolated from organoids by FACS sorter for further organoid initiation. Representative flow cytometry plots show that bile duct (*D*) can give rise to LGR5$^{+}$ stem cells (*E*), LGR5-GFP$^{+}$ stem cells could give rise to both LGR5-GFP$^{+}$ and LGR5-GFP$^{-}$ cells (*E, F*), and LGR5-

GFP$^-$ cells could give birth to LGR5-GFP$^+$ cells (*E, G*). (*H*) A schematic of the *Lgr5-DTR-GFP* transgenic mouse model used. (*I*) Bile ducts isolated from *Lgr5-DTR-GFP* mice initiated organoids and were further treated with DT for LGR5 depletion as indicated in the scheme. (*J*) DT efficiently depleted LGR5-GFP$^+$ cells (n = 3, **P* < .05). (*K*) Representative microscopic pictures of control (CTR) and LGR5 depleted (DT) organoids. Original magnifications were ×40. (*L*) LGR5-depleted organoids showed similar re-initiating efficiency compared to control group (n = 3, *P* = NS. NS: not significant). (*M*) Bile ducts isolated from *Lgr5-DTR-GFP* transgenic mice were directly treated with DT to initiate organoids as indicated in the scheme. (*N*) The organoid re-initiation efficiency for control and LGR5 depleted groups (n = 21, *P* = NS. NS: not significant). (*O*) Depletion of LGR5 stem cells did not influence organoid initiation. Representative flow cytometry (Left panel) and microscopic pictures for control and LGR5 depleted organoids, at post Day 2 (Middle panel) and Day 4 (Right panel) of DT treatment. CTR: control, without adding DT. Original magnifications were ×40 (n = 3). (*P*) DT treatment did not affect the initiation of organoids derived from wild type mouse livers (n = 3). (*Q*) Progenitor markers were upregulated upon LGR5 depletion (n = 3, **P* < .05).

## *Identification of Label Retaining Cells (LRCs) within the LGR5$^+$ Stem Cell Niche in the Liver*

An intriguing question is the origin of these proliferative LGR5$^+$ stem cells in the liver. We hypothesize that within the same niche there may be an earlier-stage but quiescent stem cell population, which permanently resides there, but becomes activated during injury and gives rise to LGR5$^+$ cells. Although the classical Bromodeoxyuridine (BrdU) labeling technique has been used to identify slow-cycling cells in the portal triad area,[23] these cells have not been functionally confirmed due to the intrinsic limitations of this approach, i.e. Brdu cannot incorporate into fully quiescent populations and the labeled cells cannot be isolated for functional characterization.

To overcome these limitations, we employed a cell cycle independent approach, i.e.*in vivo* pulse-chase labeling with H2B-GFP to identify quiescent/slow-cycling cells.[19] This *rtTA/Tet-on-H2BGFP* system conditionally expresses H2B-GFP only in the presence of dox. Adopting 7 days of dox induction followed by a long term chasing period, we expect to be able to identify quiescent/slow-cycling cells that retain GFP fluorescence over time in the liver (Supplementary Figure 6*A*-*B*).

To obtain an optimal label retaining mouse line, we first crossed *Tet-on-H2BGFP* transgenic mice with three different promoter controlled *rtTA* mouse lines: *Cag-rtTA*, *HnRNP-rtTA* and *Rosa26-rtTA*. Upon 7-day dox induction, the *Cag-rtTA/GFP*, *HnRNP-rtTA/GFP* and *Rosa26-rtTA/GFP* mouse lines achieved 80%, 65% and 55% of GFP positivity in the liver respectively, which was confirmed by both FACS and immunofluorescence (Supplementary Figure 6*C*-*D*). Both *HnRNP-rtTA/GFP* and *Rosa26-rtTA/GFP* mouse lines showed limited GFP induction in cholangiocyte areas (Supplementary Figure 6*C*: middle and right panels). In contrast, the *Cag-rtTA/GFP* transgenic mouse showed no leaky expression without dox (Figure 2*A*:

immunohistochemistry, Figure 2*E*: immunofluorescence) and high labeling efficiency both in the hepatocyte and cholangiocyte compartment upon dox induction (Figure 2*B*: immunohistochemistry, Figure 2*F* and left panel of Supplementary Figure 6*C*: immunofluorescence). Thus, the *Cag-rtTA/GFP* transgenic mouse line was used for further experimentations because of its highest induction efficiency.

To investigate label fading during the chasing period, we first checked GFP expression post-dox induction from months 0 to 7. We observed that most of the liver cells gradually lost the GFP label, confirmed by FACS, immunofluorescent and immunohistochemistry staining (Supplementary Figure 7, Figure 2*B-D* and 2*F-H*). As expected, the immunofluorescence based on GFP expression was much more sensitive, compared to the anti-GFP immunohistochemistry staining; whereas immunohistochemistry provided much better histology. At post-dox induction of five months, GFP-retaining cells (named as label retaining cells, LRCs) were localizing around the portal triad (Figure 2*C* and *G*). Of those, around 66% (128 out of 194) were close to the portal vein (PV), but not to the central vein (CV). This localization became much clearer at months 6-7 (83%, 200 out of 240). qRT-PCR revealed that LRCs compared with non-LRCs expressed higher levels of *Ck19* (Figure 2*I*), but not *Hnf4α* (Figure 2*J*). After further staining with cholangiocyte marker CK19, we found that around 32% LRCs expressed CK19 (133 out of 344) (Figure 2*K*). In contrast, no LRCs (0 of 338) expressed hepatocyte marker HNF4α (Supplementary Figure 8). Thus, these results revealed that LRCs are localized around or within the bile duct structure.

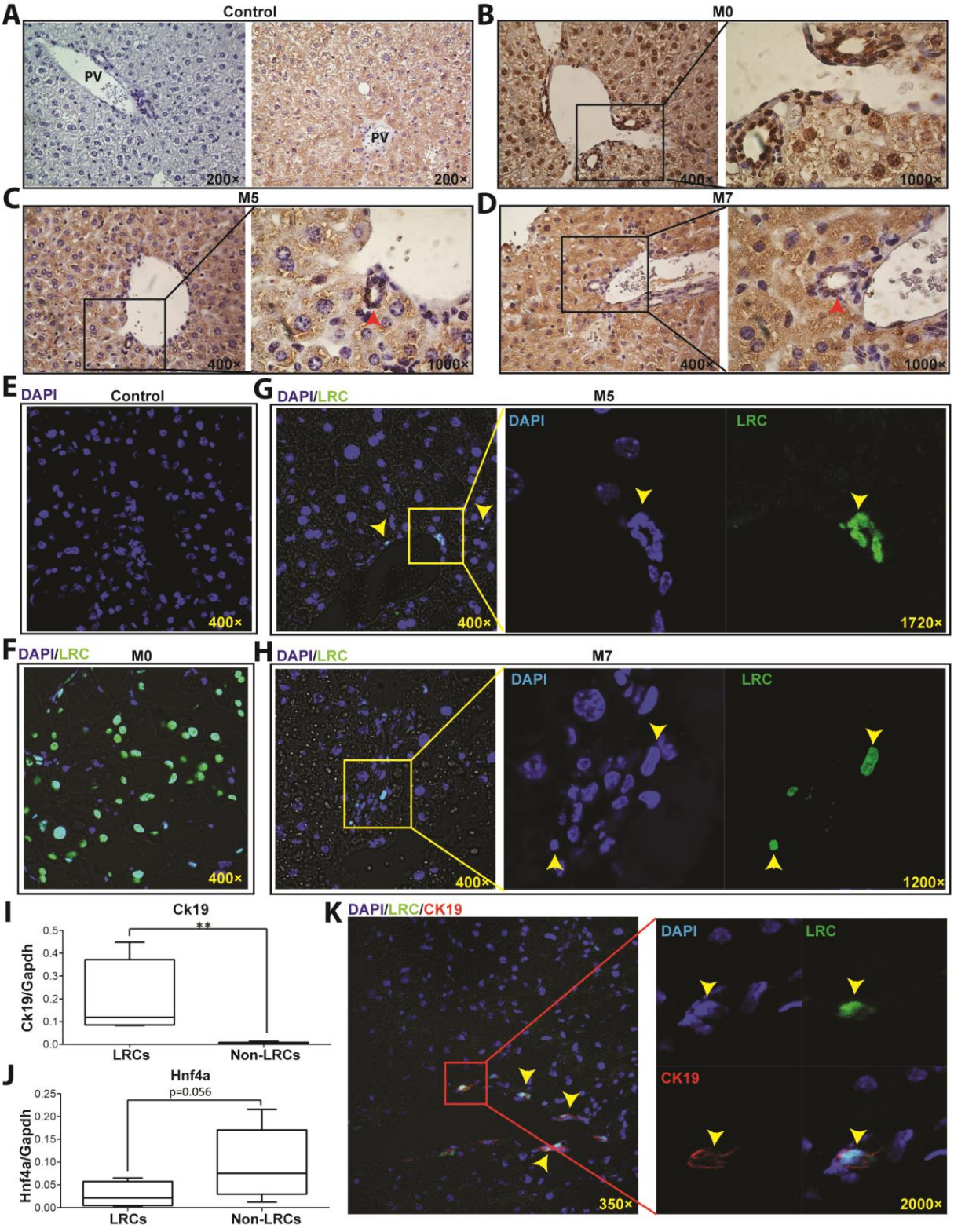


**Figure 2.** Localization and characterization of liver LRCs. (*A*) Representative anti-GFP immunohistochemistry pictures showing that the *rtTA/GFP* mice liver did not have leaky expression of GFP. Left panel: negative control for GFP staining; Right panel: the anti-GFP staining of *rtTA/GFP* mice liver without dox induction. PV: portal vein. (*B-D*) Representative immunohistochemistry pictures showing GFP label immediately after dox induction (*B*), post induction month 5 (*C*) and month 7 (*D*). Red arrows: LRCs. (*E-H*). Representative immunofluorescence pictures showing that the *rtTA/GFP* mice liver did not have leaky expression of GFP (*E*) and expressed GFP label immediately after dox induction (*F*), post induction month 5 (*G*) and month 7 (*H*). Yellow arrows: LRCs. (*I-J*) LRCs and non-LRCs were isolated from normal

mouse liver by FACS sorter and RNA was isolated directly. Gene expression quantified by qRT-PCR showed that non-LRCs expressed higher levels of *Hnf4α* and lower level of *Ck19*, compared to LRCs. Values were normalized against *Gapdh* expression (n = 3, ***P* < .01). (*K*) Representative confocal images for the expression of cholangiocyte marker CK19 in LRCs. CK19: red; DAPI: blue; LRCs: Green.

## *LRCs Are Bona Fide Stem Cells with Capability of Initiating Organoids*

To functionally prove whether LRCs are stem cells, organoid initiation assays were performed. After 3-7 months of chasing, both LRCs ($GFP^+$) and non-LRCs ($GFP^-$) were isolated from the digested liver by FACS sorting. A sorting strategy by combining Propidium Iodide (PI) and CD45 staining was used to exclude dead cells and immune cells (Figure 3*A*). Excitingly, freshly isolated single LRCs initiated organoids with a efficiency of 0.09 ± 0.03% (mean ± SEM, n = 5) after seeding in matrigel; whereas the non-LRCs did not form any organoid (Figures 3*B* and Supplementary Figure 9*A*). Since we found that LRCs are present around or within the bile duct structure, to further characterize LRCs, we also performed the organoid initiation assay for bile duct derived LRCs and non-LRCs (Figure 3*C*). The duct derived LRCs also showed higher organoid initiation ability compared to duct non-LRCs, and higher efficiency compared to LRCs isolated from the entire liver (Duct-LRCs: 0.50 ± 0.14%; Duct-Non-LRCs: 0.02 ± 0.015%: mean ± SEM, n = 3.) (Figure 3*D* and *E*, and Supplementary Figure 9*B*). Those LRCs-derived organoids can be maintained over eight months with in expansion culture medium, by weekly passaging at 1:2-1:4 ratio.

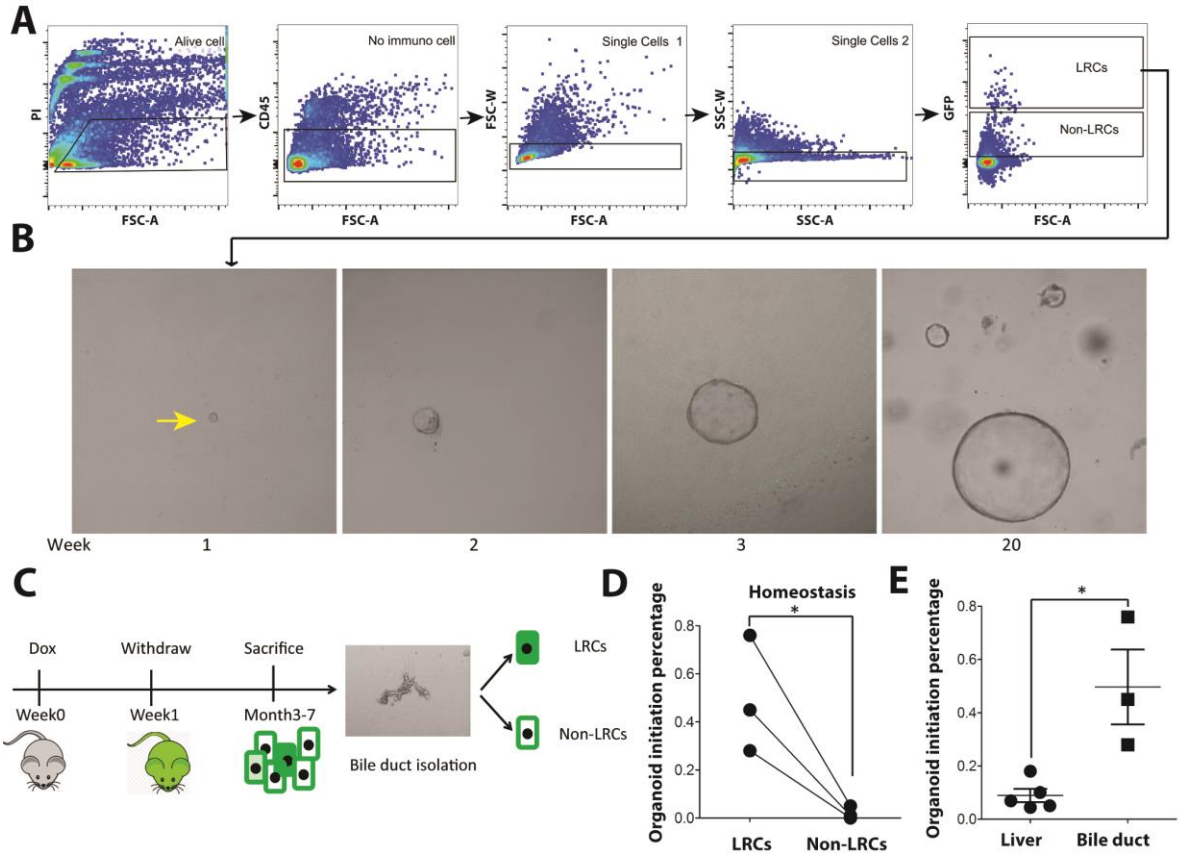


**Figure 3.** Liver LRCs were able to initiate organoids. (*A*) The sorting strategy of LRCs. (*B*) Serial images showing the outgrowth of a single LRC. Original magnifications were ×100. (*C*) Transgenic *Cag-rtTA/GFP* mice were fed with dox water to induce H2BGFP expression for one week, before cessation of 3-7 month for chasing as indicated in the scheme. Then, bile ducts were isolated and digested into single cell suspension, for further duct-LRCs/non-LRCs isolation. (*D*) The organoid initiation efficiency of LRCs and non-LRCs from homeostatic liver, isolated from bile duct (n = 3, **P* < .05). (*E*) The organoid initiation efficiency comparison between entire liver isolated LRCs and bile duct isolated LRCs (**P* < .05).

## *Extremely Quiescent Cells Retaining the Label Over One Year Have Strong Stem Cell Characteristics*

To further investigate the existence of extremely quiescent cells, we carried the H2B-GFP dependent pulse-chase experiment up to 15 months. Surprisingly, a very small proportion of cells persistently retained the label (0.68 ± 0.20%, mean ± SEM, n = 3). To better visualize GFP, we stained these LRCs with an anti-GFP antibody. We found that these long-term LRCs are also localized within the bile duct structure (Figure 4*A*). We next isolated the bile ducts and determined the percentage of LRCs. FACS analysis confirmed the significant enrichment of LRCs in bile duct structure (7.31 ± 1.37%, mean ± SEM, n = 3) (Figure 4*B*).

Functionally, LRCs exerted significantly higher organoid initiation ability compared to non-LRCs (Figure 4*C and D*, and Supplementary Figure 9*C* and *D*). These LRC-derived

organoids have been maintained over three months as tested so far. Compared to LRCs detected after 5 months of chasing, these extremely quiescent cells expressed higher levels of progenitor/stem cell markers, including *Sox2*, *Oct4*, *Lrig1*, *Cd44*, *Mex3a* and *Bmi1* (Figure 4*E*). Thus, these results revealed that the liver harbors extremely quiescent cells with strong stem cell characteristics.

Furthermore, isolated LRCs (identified from month 3-15 post dox induction) expressed higher levels of a panel of stem/progenitor cell markers, including, *Sox9*, *Nanog, Lrig1*, *Tert* and *Mex3a*, when compared to non-LRCs (Figure 4*F*, Supplementary Figure 10). Interestingly, a set of stem cell markers, including *Lgr5*, S*ox9*, *Cd133 and Cd44* (Figure 4*G*), were absent or lowly expressed in the initial isolated LRCs, but emerged during organoid formation. We further confirmed the protein expression of CD44 and SOX9 in the organoid initiated by LRCs derived from healthy liver by immunofluorescent staining (Figure 4*H-I*). These results indicate that quiescent LRCs can give birth to other types of potential progenitor/stem cells during *ex vivo* expansion.

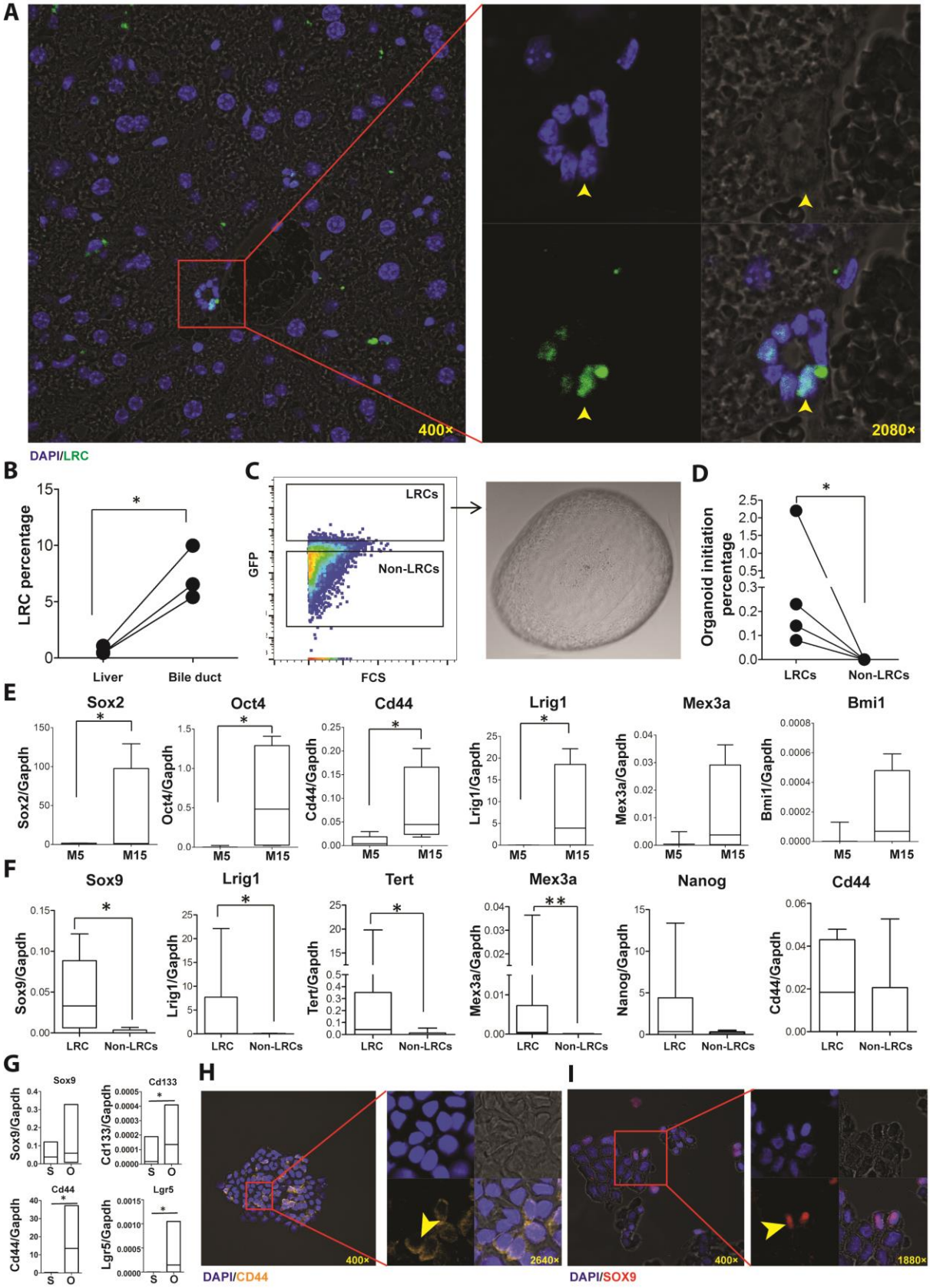


**Figure 4.** Characterizing the extremely quiescent cells that retain the GFP label over one year. (*A*) Representative confocal images showing long-term LRCs (stained with anti-GFP antibody) localized around portal triad, at month 15 post GFP fading. DAPI: blue; LRCs: Green. (*B*) Comparison of the percentages of entire liver and bile duct isolated LRCs (n = 3, *$P$ < .05). (*C*) Representative images showing the outgrowth of a single LRC. Original magnification was ×100. (*D*) The organoid initiation efficiency of LRCs and non-LRCs from homeostatic liver, isolated from

entire liver (n = 4, *$P$ < .05). (*E*) Freshly isolated LRCs derived from post dox induction month 15 compared to month 5 expressed higher levels of progenitor/stem cell markers, as quantified by qRT-PCR. Values were normalized against *Gapdh* expression (*$P$ < .05, n = 3). (*F*) LRCs (freshly isolated, from month 3-15) were enriched of a particular panel of progenitor markers, compared to non-LRCs (*$P$ < .05; **$P$ < .01; n = 6). (*G*) Compared to freshly sorted LRCs (S) from normal mice livers, gene expression quantified by qRT-PCR showed that LRCs derived organoids (O) expressed higher levels of a particular set of progenitor/stem cell markers (*$P$ < .05; n = 6). (*H-I*) LRCs derived organoids expressed CD44 (*H*) and SOX9 (*I*). DAPI: Blue; CD44: yellow; SOX9: red. Yellow arrow: LRCs expressed CD44/SOX9 protein.

## *LRCs Can Differentiate Towards Hepatocyte and Cholangiocyte Lineages*

To further investigate the lineage differentiation ability of LRCs, as one of the stem cell properties, we performed hepatocyte and cholangiocyte differentiation assays. By switching to a hepatocyte-fate differentiation medium, these organoids were differentiated towards hepatocyte-like cells. Upon hepatic differentiation, the progenitor/stem cell markers were downregulated (Figure 5*A*, *and* Supplementary Figure 11*A-B*); whereas the hepatocyte marker *Hnf4a*, the essential liver maturation genes (*Pparg*) and mature hepatocyte markers (*Cyp3a11*, *Fah*, *Albumin* and *G6pc*) showed trends of upregulation after differentiation (Figure 5*B*). Immunofluorescent staining confirmed that Albumin and HNF4α proteins were expressed in over 35% (81 out of 208) and over 7% (34 out of 458) of the differentiated organoid cells, respectively (Figure 5*E-F*). In contrast, undifferentiated organoids did not express HNF4α and Albumin protein during the expansion phage (Figure 5*E-F*: upper panel). The differentiated cells also displayed larger nuclei, as a hepatocyte characteristic, compared to undifferentiated organoid cells (Figure 5*H*).

During this differentiation process, we also observed significant upregulation of cholangiocyte markers, including *Ck7* and *Ck19* (Figure 5*C*). Thus, we next adopted a cholangiocyte-directed differentiation protocol to enhance cholangiocyte-fate differentiation. After switching the medium, cholangiocyte markers including *Ck19*, *Ck7*, *Muc5ac* and *Muc1* were significantly upregulated (Figure 5*D*). The expression of CK19 was also validated at the protein level by immunofluorescent staining (Figure 5*G*). In contrast, the progenitor/stem cell markers, including *Lgr5*, *Sox9*, *Sox2*, *Nanog*, *Sox17* and *Cd44* were downregulated (Supplementary Figure 12). These results demonstrated that LRC stem cells have the potential of differentiating towards both hepatocyte and cholangiocyte lineages.

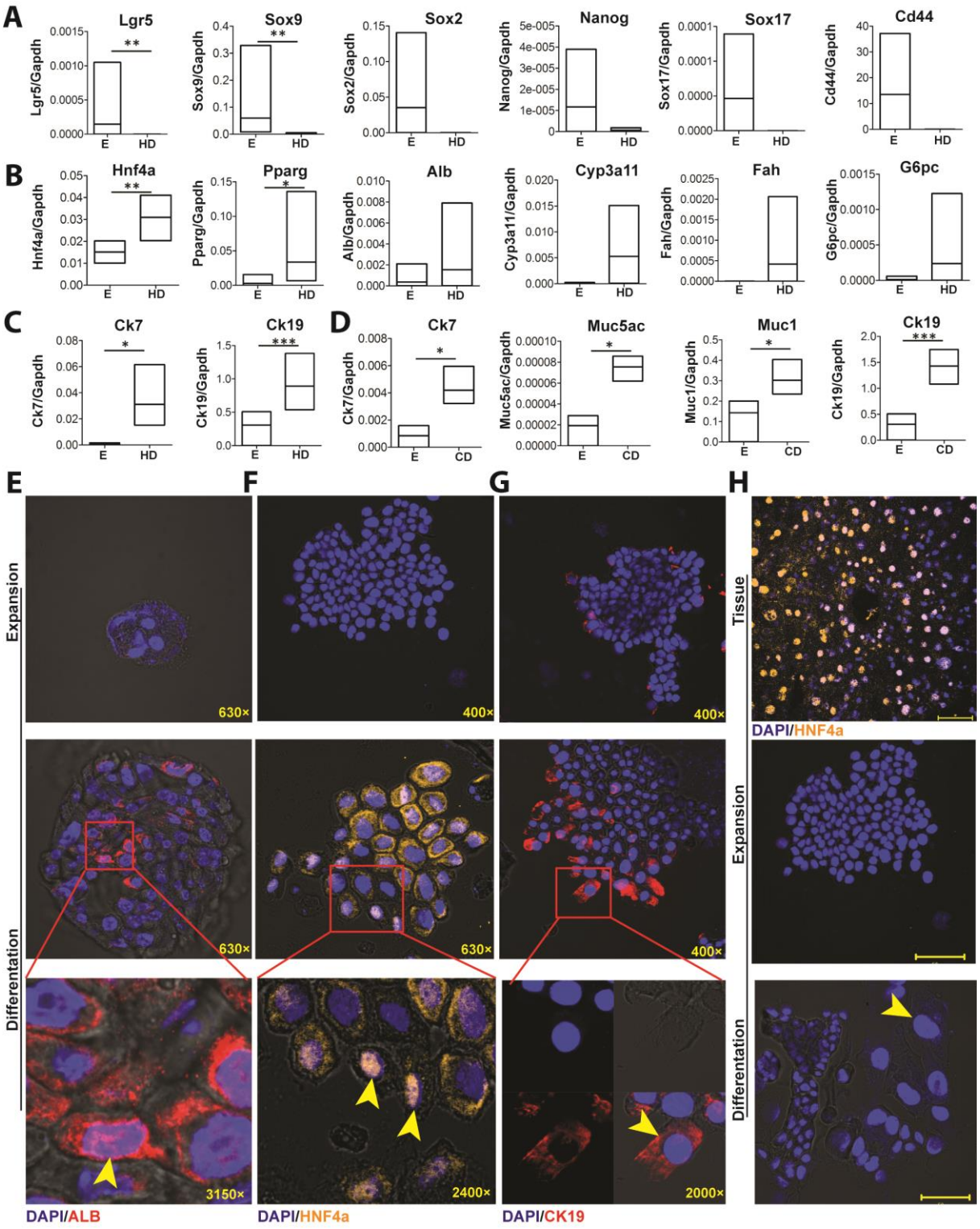


**Figure 5.** LRCs could differentiate towards hepatocyte and cholangiocyte lineages. (*A-D*) Gene expression of progenitor/stem cell, hepatocyte and maturation markers in LRCs derived organoids, compared between expansion and differentiation phase. E: expansion. HD: hepatocyte directed differentiation. CD: cholangiocyte directed differentiation. Values were normalized against *Gapdh* expression (**P* < .05; ***P* < .01; ****P* < .001; n = 4). (*E-F*) Representative confocal images for hepatocyte-specific markers: ALB (*E*, red) and HNF4α (*F*, yellow). Upper panel: LRCs derived organoids in expansion medium. Middle and lower panel: LRCs derived organoids in hepatocyte differentiation medium. Yellow arrow: cells which expressed ALB/HNF4α protein. (*G*) Representative confocal images for a cholangiocyte-specific marker, CK19 (red). Upper panel: LRCs derived organoid in expansion medium. Middle and lower panels: LRCs derived organoid in cholangiocyte differentiation medium. Yellow arrow: cells which expressed CK19 protein. (*H*)

Similar to hepatocytes in liver tissue (upper panel; HNF4α: yellow), the differentiated cells after culture in hepatocyte differentiation medium showed larger nuclei (lower panel), compared to undifferentiated cells (middle panel). Yellow scale: 50 μm. Yellow arrow: cell which showed large nucleus.

## *LRCs Respond to Liver Injury and Induce Lgr5 Expression In Vivo*

To investigate whether LRCs can respond to liver injury, we induced an acute injury by a single treatment of $CCl_4$ in mice after 3-7 months of chasing. Compared to LRCs in the homeostatic liver, we observed that LRCs from the injured liver shifted towards lower expression of GFP (n = 5; Figure 6*A* and Supplementary Figure 13*A*). This result indicated that $CCl_4$-treatment triggered the proliferation of LRCs, therefore diluting the GFP levels per cell. To better clarify this effect, we further defined the LRCs population into high-GFP-LRCs (*e.g.* GFP expression level > $1\times 10^4$, GFP-bright) and low-GFP-LRCs (GFP expression level < $1\times 10^4$) populations. We found that there were 41.8 ± 3.4% of high-GFP-LRCs and 58.2 ± 3.4% low-GFP-LRCs in homeostasis (mean ± SEM, n = 5). At day 3 of post-$CCl_4$ injection, the bright GFP population was dramatically decreased from 41.8 ± 3.4% to 23.8 ± 3.0% of the total label retaining population (n = 5) (Figure 6*B-D*, and Supplementary Figure 13*B*). Similar results were observed, when defining the high-GFP-LRC population based on different levels of GFP expression (Supplementary Figure 13*C-D*). This indicated that a large proportion of the quiescent LRCs entered the cell cycle in response to injury, although the percentage of LRCs within the entire cell population did not significantly change (Supplementary Figure 9*H*).

We further confirmed the activation of LRCs in the injured liver by visualization of the expression of the proliferation marker KI67 by immunofluorescence (Figure 6*E*). In contrast, LRCs in homeostatic liver did not express KI67 (Supplementary Figure 14*A*). qRT-PCR also confirmed the upregulation of *Ki67* expression in LRCs isolated from the injured liver; whereas it is not expressed in LRCs isolated from the homeostatic liver (Figure 6*F*).

Furthermore, LRCs from injured liver can form organoids, with similar efficiency as normal liver derived LRCs (Figure 6*G*, and Supplementary Figure 9*E* and *G*). However, LRCs from injured liver formed significantly larger organoids, which also grew faster, as shown by the organoid diameters measured at day 7 (Normal vs Injury = 101 ± 21 μm vs. 187 ± 35 μm). The same pattern was also observed on day 11 and 15 (Figure 6*G-H*). These observations were also found in the bile duct derived LRCs from homeostatic and injured livers (Figure 6*I-L,* and Supplementary Figure 9*F* and *G*).

Most interestingly, we detected *Lgr5* expression by qRT-PCR in LRCs directly isolated from the injured liver; whereas it was not expressed in LRCs isolated from the homeostatic liver or non-LRCs from both types of livers (Figure 7*A*). This is consistent with our observation that *Lgr5* expression emerges during organoid culture, but is absent in the initial isolated LRCs derived from the healthy liver (Figure 4*G*). In addition, we found that injury triggered the upregulation of CD44 and SOX9 in LRCs, as demonstrated by qRT-PCR of isolated single cells (Figure 7*A*) and immunofluorescent staining of *in situ* protein expression (Figure 7*B-C*). CD44 and SOX9 expression were retained in LRCs cultured organoids (Figure 7*D-E*). Isolated LRCs from injured compared to homeostatic liver also showed a trend of upregulation of other progenitor/stem cell markers, including *Sox17*, *Cd133*, *Oct4*, *Nanog* and *Sox2* (Figure 7*A*). In contrast, LRCs expressed relatively lower levels of maturation markers including *Tbx3*, *Cyp3a11*, *Pparg* and *Alb*, compared to non-LRCs (Figure 7*A*). Taken together, these results indicated that quiescent LRCs rapidly respond to liver injury and give rise to *Lgr5*-expressing cells, as well as other potential progenitor/stem cells.

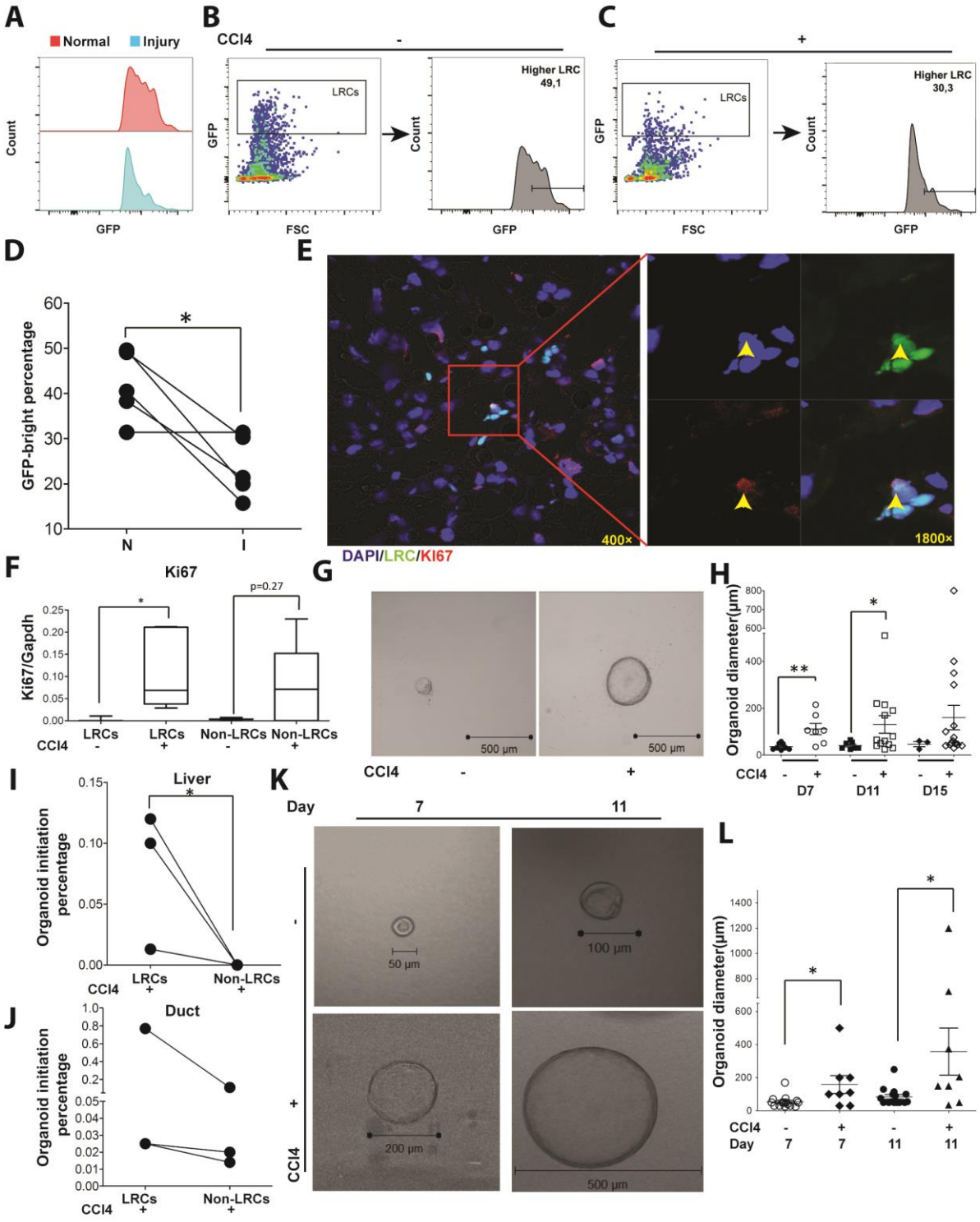


**Figure 6.** LRCs responded to liver injury. (*A*) Representative FACS results showing that the LRCs shifted towards a relatively lower expression of GFP, upon 3 days of $CCl_4$ injury. (*B-C*) Representative flow cytometry pictures showing that liver LRCs responded to injury indicated by the decreased percentage of $GFP^{bright}$-LRC population. FSC: forward scatter. (*D*) Absolute numbers of all five paired samples showing that liver LRCs responded to injury indicated by the decreased percentage of $GFP^{bright}$-LRC population (*$P$ < .05; n = 5). (*E*) Representative confocal images showing the expression of proliferation marker KI67 in injured liver. Yellow arrow: LRCs with KI67 expression in injured liver. KI67: red; DAPI: blue; LRCs: Green. (*F*) Gene expression quantified by qRT-PCR showed that injured liver LRCs expressed higher levels of proliferation marker *Ki67*, compared to homeostatic liver derived LRCs (*$P$ < .05; n = 3). (*G*) Organoids cultured

from LRCs derived from healthy or $CCl_4$ treated mice liver. (*H*) Injury stimulated the growth of LRCs derived organoids. The differences of organoid diameters were measured at day 7 (**$P$ < .01), day 11 (*$P$ < .05) and day 15 of culture. Cells analyzed here were derived from three groups of mice. (*I*) The organoid initiation efficiency of LRCs and non-LRCs from injured liver, isolated from entire liver (n = 3, *$P$ < .05). (*J*) The organoid initiation efficiency of LRCs and non-LRCs from injured liver, isolated from bile duct. (*K*) Representative pictures of organoids cultured from Duct-LRCs derived from healthy or $CCl_4$ treated mice. (*L*) Injury stimulated the growth of Duct-LRCs derived organoids. The differences of organoid diameters were measured at post day 7 and day 11 of culture (*$P$ < .05). Cells analyzed here were derived from three groups of mice.

**Figure 7.** LRCs expressed low levels of hepatocyte markers, but high level of progenitor markers. (*A*) For freshly isolated LRCs and non-LRCs derived from normal and injured mice livers (paired mice), gene expression quantified by qRT-PCR showed that LRCs expressed relatively higher levels of progenitor markers and lower levels of hepatic/mature markers, compared to non-LRCs.(*$P$ < .05; **$P$ < .01; n = 5). Values were normalized against *Gapdh* expression. (*B-C*) Representative confocal images showing the expression of CD44 (*B*) and SOX9 (*C*) in LRCs, upon liver injury. CD44: yellow; DAPI: blue; SOX9: red; LRCs: green. Yellow arrow: LRCs expressed CD44/SOX9 protein. (*D-E*) Injured liver derived LRCs initiated organoids which expressed CD44 (*D*) and SOX9 (*E*). DAPI: Blue; CD44: yellow; SOX9: red. Yellow arrow: cells expressed CD44/SOX9 protein

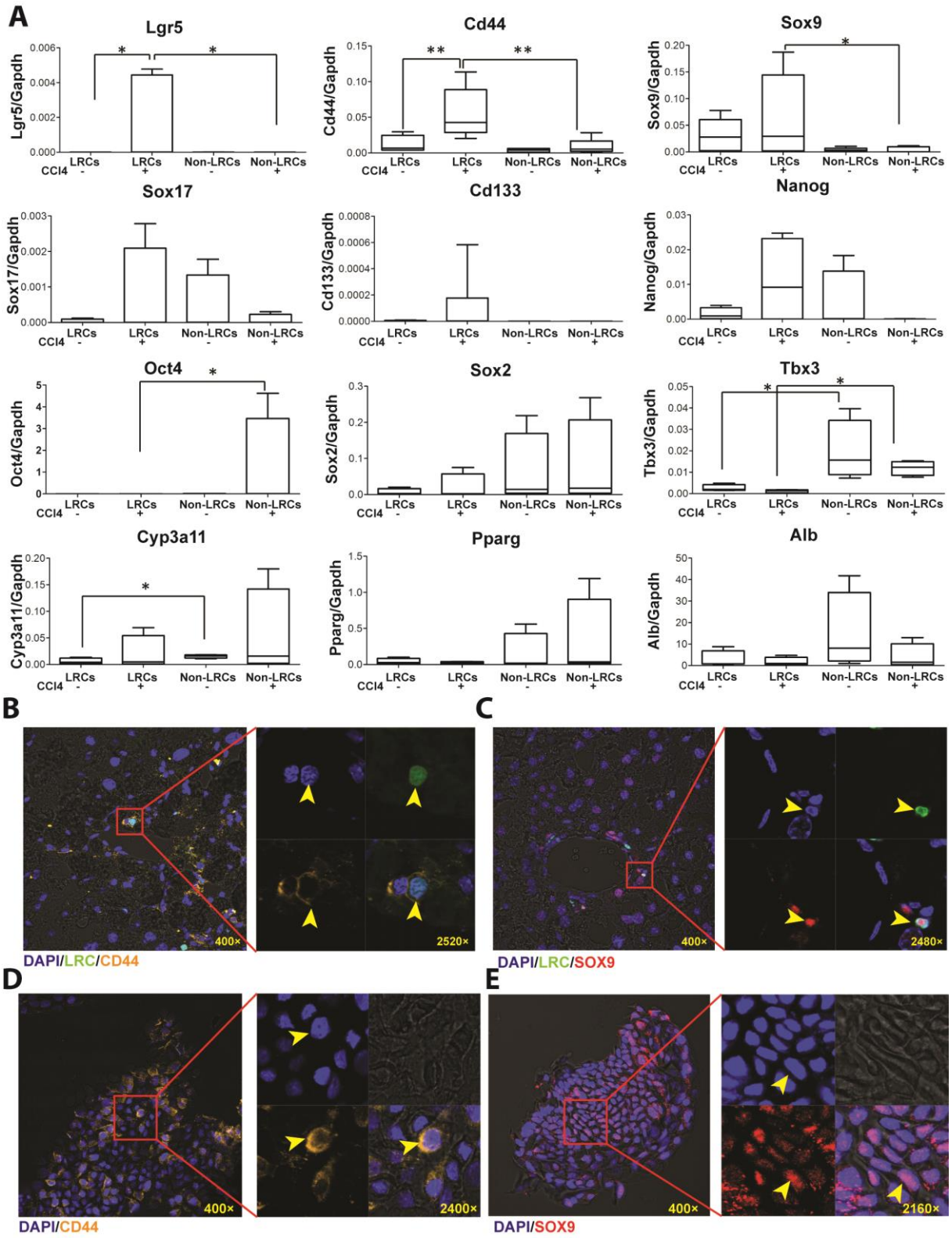
A
Lgr5
Lgr5/Gapdh
Cd44
Cd44/Gapdh
Sox9
Sox9/Gapdh
Sox17
Sox17/Gapdh
Cd133
Cd133/Gapdh
Nanog
Nanog/Gapdh
Oct4
Oct4/Gapdh
Sox2
Sox2/Gapdh
Tbx3
Tbx3/Gapdh
Cyp3a11
Cyp3a11/Gapdh
Pparg
Pparg/Gapdh
Alb
Alb/Gapdh
CCl4 - LRCs + LRCs - Non-LRCs + Non-LRCs
B
400×
2520×
DAPI/LRC/CD44
C
400×
2480×
DAPI/LRC/SOX9
D
400×
2400×
DAPI/CD44
E
400×
2160×
DAPI/SOX9

## Discussion:

This study has demonstrated that slow-cycling/quiescent cells (LRCs) identified by label retaining technique are *bona fide* stem cells in the mouse liver. In fact, LGR5 proliferative stem cells are absent in the homeostatic liver but only activated by liver injury, which is dispensable for injury recovery. More interestingly, we revealed that quiescent LRCs can be activated by liver injury and give rise to LGR5 proliferative stem cells.

Unlike in the liver, LGR5 stem cells in intestine, colon and skin are present at homeostatic status and participate in tissue renewal by compensating the loss of differentiated cells.[2, 24, 25] Despite their essential role in homeostatic maintenance in these tissues, loss of LGR5 stem cells in the intestine can be compensated by transdifferentiation from the quiescent stem cell pool,[8, 26] or through plasticity of their enterocyte-lineage daughters.[27] This is in line with our findings that liver LGR5 stem cells are dispensable for organoid initiation and expansion *ex vivo*, and are limited in tissue repair *in vivo*.

Although slow-cycling cells have been identified in the mouse liver,[23, 28] their function however has never been studied mainly because of technical limitations. Classically, nucleotide analogs that incorporate into genomic DNA have been widely used to identify slow-cycling cells including in liver, intestine, esophagus and stomach.[23, 29, 30] However, these compounds, such as BrdU, have major drawbacks: 1) It preferentially labels proliferating cells; 2) *in vivo* labeled cells are unable to be isolated for further functional investigation; 3) in turn trigger cell proliferation from quiescent stage.[19, 26] The unique advantage of this study is to use transgenic mice that can conditionally and efficiently label cells by a nuclear localized GFP reporter. This model allows identification of *bona fide* quiescent cells with a labeling efficiency higher than 80% and over 450 days of label fading (Figure 4, and Supplementary Figure 6). Most importantly, living LRCs can be isolated based on GFP expression and subjected to functional experimentation.

Here we reveal that similar to LGR5 cells, LRCs are localized around/within the bile duct, a well-accepted liver stem cell niche,[31] and consistent with streaming liver theory.[21, 26] Isolated LRCs express relatively low levels of hepatic markers, including *Hnf4a*, *Tbx3*, *Pparg*, *Cyp3a11*, *Fah* and *Albumin*. Functionally, isolated LRCs are able to initiate organoids, which can be expanded and passaged for months, confirming their stem cell property. By switching expansion medium into lineage differentiation media, these organoids switch into hepatocyte or cholangiocyte fate. This is consistent with a previous study of lineage differentiation of human liver organoids.[32]

Impressively, the liver harbors a small proportion of extremely quiescent cells that are capable of retaining the GFP label over one year. These LRCs have strong stem cell characteristics, showing the capability of organoid initiation and enriched expression of quiescent stem cell markers, including *Mex3a*, *Bmi1* and *Lrig1*.[33]

LRCs do not express *Lgr5* at homeostatic status, but are activated by injury and give birth to *Lgr5* proliferative stem cells *in vivo*. This is similar to the intestine that Bmi1-marked quiescent stem cells can compensate for the loss of LGR5 proliferative stem cells.[8] it is however very different from another scenario in the intestine that LGR5 stem cells can be generated through dedifferentiation of their enterocyte-lineage daughters.[27] In the liver, LRCs are present in homeostasis and LGR5 cells only emerge upon injury, which preclude the possibility of LRCs as daughter cells of LGR5 stem cells. In response to injury, LRCs also give birth to other progenitor/stem cell populations, including SOX9 and CD44 cells. SOX9-expressing cells are enriched both in the LRCs from homeostatic (Figure 4*F*) and injured liver (Figure 7*A*) and have been demonstrated to be able to replace the bulk of the hepatocyte mass in several settings.[22] CD44-expressing cells are not enriched in LRCs or non-LRCs from homeostatic liver (Figure 4*F*), but specifically emerged upon injury within the LRC population (Figure 7*A*). CD44-expressing cells are considered as an important mesenchymal/neural stem cells marker or cancer stem cell marker for several types of cancers[34-38]. Our results indicate a potential role of CD44 in the liver stem cell compartment, deserving further investigation. Here, we provide evidence that multiple progenitor/stem cell populations dynamically respond and participate in injury recovery of the liver and LRCs likely serve as an early-stage stem cell population.

In summary, our study functionally proved that quiescent/slow-cycling cells in the mouse liver are stem cells. They respond to tissue injury and can give rise to the *Lgr5* proliferative stem cells. It will be of particular interest to also study these stem cell populations in human liver. However, innovative techniques need to be developed for identification of quiescent/slow-cycling cells in human, which will enable functional studies of the identified cells.

**Acknowledgements:**

We gratefully thank Genentech for providing the *Lgr5-DTR-GFP* and *Lgr5-creERT2* mouse strains. We thank W. Koole, M. Schewe , R. Lieshout, K. de Groot –Kreefft, S.A. van der Heide – Mulder, M.J. Teeuwssen, P.Y. Hernanda, A. Mooppilmadham Das, M.C.G.N. Van den Hout-van Vroonhoven and W.F.J. van IJcken for technical assistance. We also thank Prof. R. Fodde for discussing the project.

This research is supported by the Daniel den Hoed Foundation for a Centennial Award fellowship (to Q. Pan), a KWF Young Investigator Grant 10140 (to Q. Pan) from the Dutch Cancer Society, a Key Laboratory Grant of Zhejiang Province (to C. Kan), and the China Scholarship Council for funding PhD fellowships to W. Cao (201307060013), Y. Yin (201307720045) and W. Wang (201303250056).

**Author contributions**

W.C., M.P.P., and Q.P. designed research; R.S., M.M.A.V., M.J.C.B., W.W., K.C., Y.Y., N.T., M.B., L.J.W.L., D.T.B., D.S, H.J.M., and J.K contributed new reagents/analytic tools; W.C. and Q.P. performed research; W.C, R.S and Q.P. analyzed data; and W.C. and Q.P. wrote the paper. R.S., L.J.W.L., D.T.B., D.S., J.K, and Q.P. revised the manuscript critical for important intellectual content. K.C and M.B contributed equally and share co-second authorship.

## References


1. **Arai F**, **Hirao A,** Ohmura M, et al. Tie2/angiopoietin-1 signaling regulates hematopoietic stem cell quiescence in the bone marrow niche. Cell 2004;118:149-61.

2. Barker N, van Es JH, Kuipers J, et al. Identification of stem cells in small intestine and colon by marker gene Lgr5. Nature 2007;449:1003-7.

3. **Barker N**, **Huch M**, Kujala P, et al. Lgr5(+ve) stem cells drive self-renewal in the stomach and build long-lived gastric units in vitro. Cell Stem Cell 2010;6:25-36.

4. **aks V**, **Barker N**, **Kasper M**, et al. Lgr5 marks cycling, yet long-lived, hair follicle stem cells. Nat Genet 2008;40:1291-9.

5. **Plaks V**, **Brenot A**, Lawson DA, et al. Lgr5-expressing cells are sufficient and necessary for postnatal mammary gland organogenesis. Cell Rep 2013;3:70-8.

6. **Huch M**, **Dorrell C**, Boj SF, et al. In vitro expansion of single Lgr5+ liver stem cells induced by Wnt-driven regeneration. Nature 2013;494:247-50.

7. Koo BK, Clevers H. Stem cells marked by the R-spondin receptor LGR5. Gastroenterology 2014;147:289-302.

8. Tian H, Biehs B, Warming S, et al. A reserve stem cell population in small intestine renders Lgr5-positive cells dispensable. Nature 2011;478:255-9.

9. Zajicek G, Oren R, Weinreb M, Jr. The streaming liver. Liver 1985;5:293-300.

10. Arber N, Zajicek G. Streaming liver. VI: Streaming intra-hepatic bile ducts. Liver 1990;10:205-8.

11. Duncan AW, Dorrell C, Grompe M. Stem cells and liver regeneration. Gastroenterology 2009;137:466-81.

12. Wang B, Zhao L, Fish M, et al. Self-renewing diploid Axin2(+) cells fuel homeostatic renewal of the liver. Nature 2015;524:180-5.

13. Yamashita T, Wang XW. Cancer stem cells in the development of liver cancer. J Clin Invest 2013;123:1911-8.

14. **Shin S**, **Wangensteen KJ**, **Teta-Bissett M**, et al. Genetic lineage tracing analysis of the cell of origin of hepatotoxin-induced liver tumors in mice. Hepatology 2016;64:1163-77.

15. **Tummala KS, Brandt M**, Teijeiro A, et al. Hepatocellular Carcinomas Originate Predominantly from Hepatocytes and Benign Lesions from Hepatic Progenitor Cells. Cell Rep 2017;19:584-600.

16. **Michalopoulos GK**, **Khan Z**. Liver Stem Cells: Experimental Findings and Implications for Human Liver Disease. Gastroenterology 2015;149:876-82.

17. Muzumdar MD, Tasic B, Miyamichi K, et al. A global double-fluorescent Cre reporter mouse. Genesis 2007;45:593-605.

18. Sasaki N, Sachs N, Wiebrands K, et al. Reg4+ deep crypt secretory cells function as epithelial niche for Lgr5+ stem cells in colon. Proc Natl Acad Sci U S A 2016;113:E5399-407.

19. Wang Y, Sacchetti A, van Dijk MR, et al. Identification of quiescent, stem-like cells in the distal female reproductive tract. PLoS One 2012;7:e40691.

20. Woltjen K, Michael IP, Mohseni P, et al. piggyBac transposition reprograms fibroblasts to induced pluripotent stem cells. Nature 2009;458:766-70.

21. Katsantoni EZ, Anghelescu NE, Rottier R, et al. Ubiquitous expression of the rtTA2S-M2 inducible system in transgenic mice driven by the human hnRNPA2B1/CBX3 CpG island. BMC Dev Biol 2007;7:108.

22. Tarlow BD, Finegold MJ, Grompe M. Clonal tracing of Sox9+ liver progenitors in mouse oval cell injury. Hepatology 2014;60:278-89.

23. **Kuwahara R**, **Kofman AV**, Landis CS, et al. The hepatic stem cell niche: identification by label-retaining cell assay. Hepatology 2008;47:1994-2002.

24. Boddupally K, Wang G, Chen Y, et al. Lgr5 marks neural crest derived multipotent oral stromal stem cells. Stem Cells 2016.

25. Haegebarth A, Clevers H. Wnt signaling, lgr5, and stem cells in the intestine and skin. Am J Pathol 2009;174:715-21.

26. Buczacki SJ, Zecchini HI, Nicholson AM, et al. Intestinal label-retaining cells are secretory precursors expressing Lgr5. Nature 2013;495:65-9.

27. Tetteh PW, Basak O, Farin HF, et al. Replacement of Lost Lgr5-Positive Stem Cells through Plasticity of Their Enterocyte-Lineage Daughters. Cell Stem Cell 2016;18:203-13.

28. **Li F**, **Lu L**, Lu J. Identification and location of label retaining cells in mouse liver. J Gastroenterol 2010;45:113-21.

29. **Jaks V**, **Kasper M**, Toftgard R. The hair follicle-a stem cell zoo. Exp Cell Res 2010;316:1422-8.

30. **Pan Q**, **Nicholson AM**, **Barr H**, **Harrison LA**, et al. Identification of lineage-uncommitted, long-lived, label-retaining cells in healthy human esophagus and stomach, and in metaplastic esophagus. Gastroenterology 2013;144:761-70.

31. Petersen B, Shupe T. Location is everything: the liver stem cell niche. Hepatology 2008;47:1810-2.

32. **Huch M**, **Gehart H**, **van Boxtel R**, et al. Long-term culture of genome-stable bipotent stem cells from adult human liver. Cell 2015;160:299-312.

33. Barriga FM, Montagni E, Mana M, et al. Mex3a Marks a Slowly Dividing Subpopulation of Lgr5+ Intestinal Stem Cells. Cell Stem Cell 2017.

34. **De Coppi P**, **Bartsch G, Jr.**, Siddiqui MM, et al. Isolation of amniotic stem cell lines with potential for therapy. Nat Biotechnol 2007;25:100-6.

35. Takaishi S, Okumura T, Tu S, et al. Identification of gastric cancer stem cells using the cell surface marker CD44. Stem Cells 2009;27:1006-20.

36. Patrawala L, Calhoun T, Schneider-Broussard R, et al. Highly purified CD44+ prostate cancer cells from xenograft human tumors are enriched in tumorigenic and metastatic progenitor cells. Oncogene 2006;25:1696-708.

37. Brown MD, Gilmore PE, Hart CA, et al. Characterization of benign and malignant prostate epithelial Hoechst 33342 side populations. Prostate 2007;67:1384-96.

38. Klonisch T, Wiechec E, Hombach-Klonisch S, et al. Cancer stem cell markers in common cancers - therapeutic implications. Trends Mol Med 2008;14:450-60.

**Author names in bold designate shared co-first authorship.**

**Supplementary data for:**

# Dynamics of Proliferative and Quiescent Stem Cells in Liver Homeostasis and Injury

## Table of contents



## Supplementary Materials and Methods:

### *Bile Duct Derived Organoid Culture*

Biliary ducts were isolated from mouse liver using digestion solution I: 125 µg/ml of Collagenase type XI (Sigma-Aldrich), 125 µg/ml of Dispase (Gibco), 100 µg/1ml of Dnase-1 (Sigma-Aldrich), 1% FBS in DMEM medium (Lonza) (37°C, 30min). Isolated bile ducts were mixed with matrigel (BD Bioscience) and seeded on 24/48 well plate, as described previously.[1] Medium was added after the matrigel formed a solid gel. Organoid culture

medium was based on advanced DMEM/F12 (Invitrogen), which is supplemented with 2% (vol/vol) of B27 and 1% (vol/vol) of N2 (Invitrogen), 1.25 μM N-acetylcysteine (Sigma-Aldrich, antioxidant agent), 10 nM gastrin (Sigma-Aldrich), 50 ng/ml EGF (Peprotech, epidermal growth factor), 10% (vol/vol) of R-spondin-1 (conditioned medium produced by 293T-H-RspoI-Fc cell line, WNT/β catenin signaling pathway activator), 100 ng/ml FGF10 (Peprotech, fibroblast growth factor 10), 10 mM nicotinamide (Sigma-Aldrich) and 50 ng/ml HGF (Peprotech, hepatocyte growth factor). For the first 4 days, the organoids were also supplemented with 10% (vol/vol) of Noggin (conditioned medium produced by 293T-HA-Noggin cell line, bone morphogenic protein ligands antagonist) and 30% (vol/vol) of Wnt3a (conditioned medium produced by L-Wnt3a cell line, WNT/β-catenin signaling pathway activator). Medium was refreshed every 2-3 days and passage was performed in 1:2-1:4 split ratio once per week.

### *Single Cell Derived Organoid Culture*

Digestion solution II (500μg/ml of collagenase type XI, 200μg/ml of Dnase-1, 1% FBS in DMEM medium) was used to digest liver tissues into single cell suspension (37°C, 30min). A FACSAria$^{TM}$ II cell sorter (BD Biosciences) was used to isolate the target cell population. Propidium iodide (PI) staining was performed to exclude dead cells and CD45 staining was adopted for excluding leucocytes. Single-sorted LGR5-GFP$^{+}$ cells, LGR5-GFP$^{-}$ cells, LRCs and non-LRCs were mixed with matrigel separately and seeded for organoid initiation. Cells were cultured in organoid culture medium mentioned above. For the first 8-12 days, the organoids were supplemented with 10 μM Y-27632 (Sigma-Aldrich, RHO/ROCK pathway inhibitor), Noggin and Wnt3a conditioned medium. Medium was refreshed every 2-4 days and passage was performed in split ratios of 1:2-1:4 weekly for at least 8 months.

### *Hepatocyte Differentiation*

To enhance hepatocyte fate, LRC-derived organoids were first seeded and maintained in organoid culture medium as described above for 2-4 days. Then, the medium was changed to organoid differentiation medium. Organoid differentiation medium was based on organoid culture medium, which no longer contained R-spondin 1, HGF and nicotinamide but contained 50 nM A8301 (Tocris Bioscience, TGF-βRI inhibitor) and 10 nM DAPT (Sigma-Aldrich, Notch inhibitor). For the last 3 days of the differentiation, cultures were also supplemented with dexamethasone (30 μM, Sigma-Aldrich, Glucocorticoid pathway activator). Medium was changed every other day for a period of 9 to 18 days.[2]

## *Cholangiocyte Differentiation*

To enhance cholangiocyte fate, LRC-derived organoids were first seeded and maintained in organoid culture medium as described above for 2-4 days. Then, the medium was changed to cholangiocyte directed differentiation medium (phase 1) for 4 days. Phase 1 medium was based on advanced DMEM/F12, which was supplemented with B27, 50 ng/ml FGF10, 50ng/ml activin-A (Sigma-Aldrich, TGF-β family member) and 3 μM RA (Sigma-Aldrich, *all−trans*−Retinoic acid). Next, medium was changed to cholangiocyte directed differentiation medium (phase 2), Phase 2 medium was also based on advanced DMEM/F12, which was supplemented with 10 mM nicotinamide, 17 mM sodium bicarbonate (Sigma Aldrich), 0.2 mM 2-Phospho-L-ascorbic acid trisodium salt (Sigma-Aldrich), 6.3 mM sodium pyruvate (Invitrogen, carbon source), 14 mM glucose (Sigma-Aldrich), ITS+ premix (BD Biosciences, contains insulin, human transferrin, and selenous acid mainly), 0.1 uM dexamethasone, 2 mM Glutamax (Invitrogen) and 20 ng/ml EGF. Medium was changed every other day for two weeks.[3]

## *FACS Analysis*

For FACS analysis, single cells derived from liver, intestine and organoids were suspended in DMEM plus 2% FBS. Cell suspensions were analyzed using a BD FACSCalibur or BD FACSAria™ II.

## *Histology, Immunohistochemistry and Immunofluorescence*

Liver or intestine was fixed in 4% paraformaldehyde (PFA) overnight at 4°C. For immunofluorescence, samples were further dehydrated with 30% sucrose (Sigma-Aldrich) at 4°C overnight, embedded in OCT gel, stored at -80°C and then sectioned at 8 μm for further analysis. Images were acquired with a Zeiss LSM510META confocal microscope. For histology and immunohistochemistry, materials were dehydrated with 70% ethanol, embedded with paraffin, sectioned at 4 μm for staining. Images were acquired with a Zeiss Axioskop 20 microscope. All antibodies are listed in Supplementary Table 1.

## *qRT–PCR*

For organoids, Machery-NucleoSpin RNA II kit (Bioké) was used to extract RNA; for freshly sorted cells, RNeasy Micro Kit (QIAGEN) was used to isolate RNA. After

quantification with Nanodrop ND-1000 (Wilmington), RNA was converted to cDNA using a cDNA Synthesis kit (TAKARA BIO INC.). Real-time PCR reactions were performed with SYBRGreen-based real-time PCR (Applied Biosystems®) and amplified in a thermal cycler (GeneAmp PCR System 9700) according to the manufacturer's instructions. Glyceraldehyde 3-phosphate dehydrogenase (*Gapdh*) gene was used as reference. All primers are listed in Supplementary Table 2.

### *Statistical Analysis.*

Prism software (GraphPad Software) was used for all statistical analysis. For statistical significance of the differences between the means of two groups, we used Mann-Whitney U-test. Differences were considered significant at a *P* value less than 0.05.

## Supplementary References


1. **Huch M**, **Dorrell C**, Boj SF, et al. In vitro expansion of single Lgr5+ liver stem cells induced by Wnt-driven regeneration. Nature 2013;494:247-50.

2. **Jaks V**, **Kasper M**, Toftgard R. The hair follicle-a stem cell zoo. Exp Cell Res 2010;316:1422-8.

3. Sampaziotis F, Cardoso de Brito M, Madrigal P, et al. Cholangiocytes derived from human induced pluripotent stem cells for disease modeling and drug validation. Nat Biotechnol 2015;33:845-52.


Author names in bold designate shared co-first authorship.

## Supplementary Figures and Legends

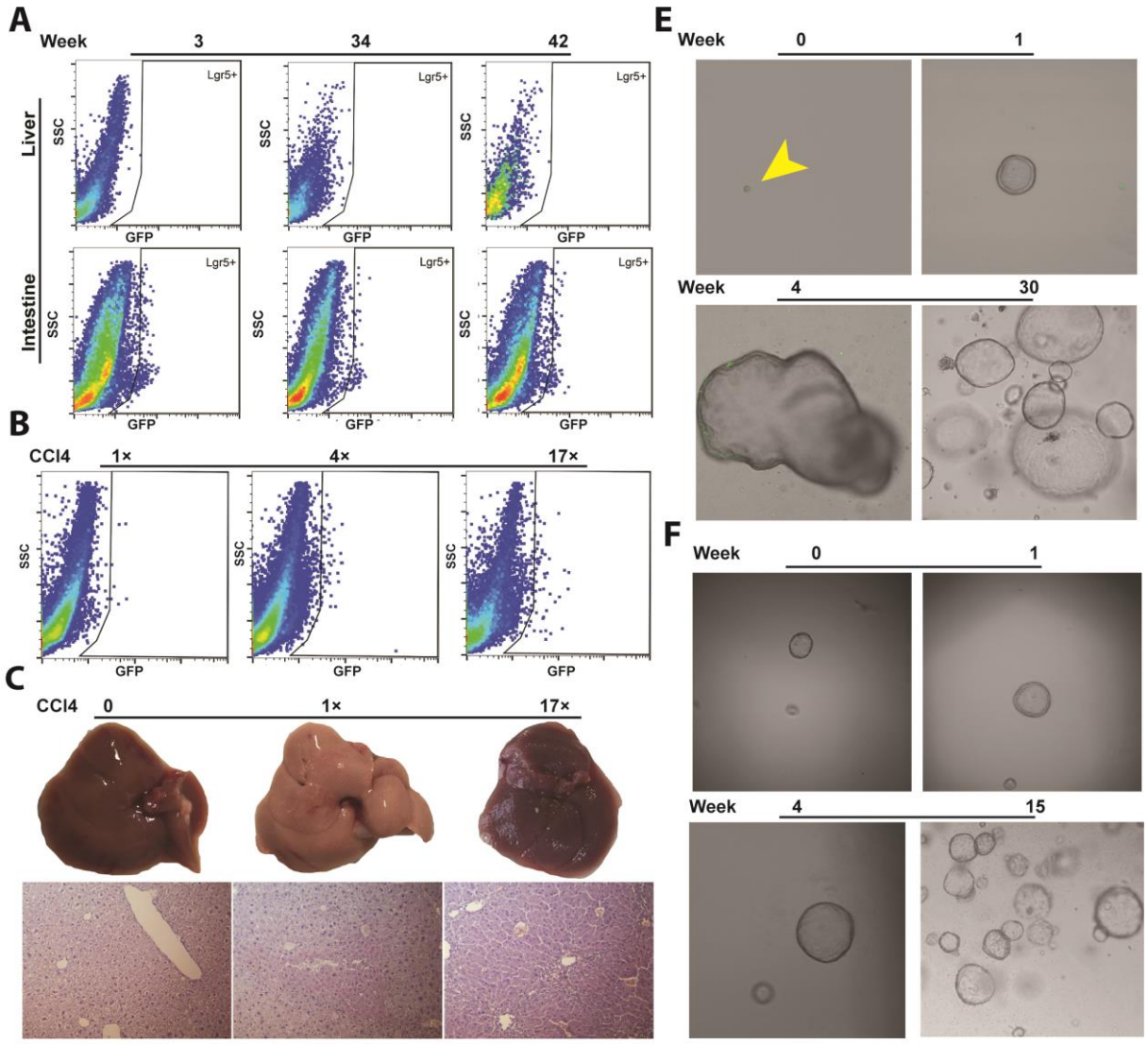


G

| Injury | Experiment 1 | | Experiment 2 | |
|---|---|---|---|---|
| | Lgr5-GFP+ | Lgr5-GFP- | Lgr5-GFP+ | Lgr5-GFP- |
| Cells input | 1577 | 17267 | 122 | 67153 |
| Organoid number | 11 | 10 | 1 | 22 |
| Colony formation percentage | 0.7% | 0.06% | 0.8% | 0.03% |

**Supplementary Figure 1.** LGR5 stem cells were absent in the homeostatic liver over the life span of a mouse, but emerged upon injury. (*A*) Representative flow cytometry plots for LGR5-GFP$^+$ cells at different age of mice (in week, n = 3). (*B*) Representative flow cytometry plots for LGR5-GFP$^+$ cells in injured livers by single or repeated $CCl_4$ injections. (*C*) Representative liver and H&E staining showing normal (left panel), injury by single $CCl_4$ (middle panel) and injury by multiple $CCl_4$ injections (right panel). Original magnifications were ×40. (*D*) Absolute percentages for LGR5-GFP$^+$ cells in $CCl_4$ injured livers. (*E-F*) Serial images showing the outgrowth of a single sorted LGR5-GFP$^+$ cell (*E*) and two sorted LGR5-GFP$^-$ cells (*F*). Original magnifications were ×100. (*G*) The organoid initiation efficiency of LGR5-GFP$^+$ and LGR5-GFP$^-$ from chronic injured livers with 4 months of repeated $CCl_4$ induction (n = 2).

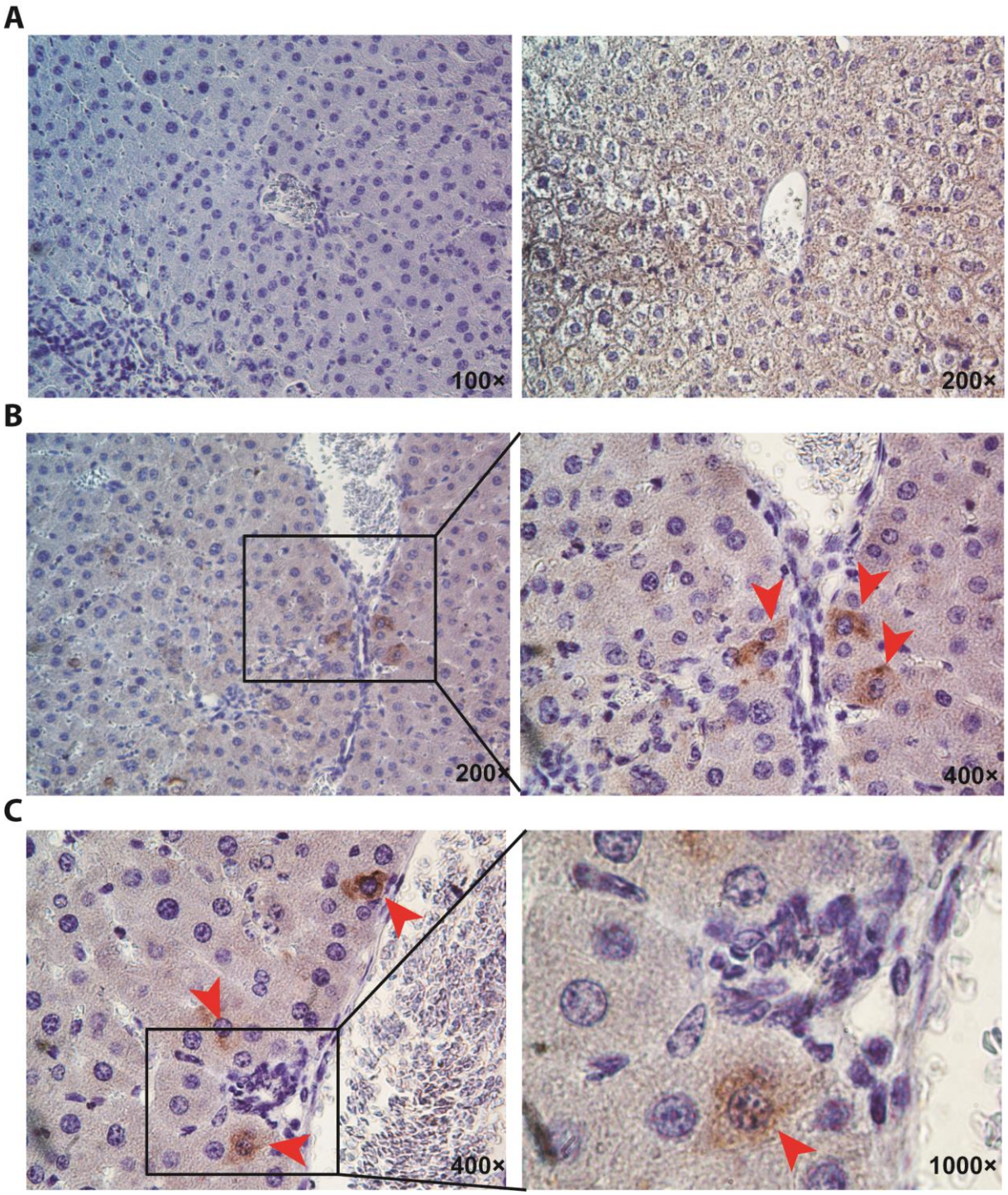
A
100×
200×
B
200×
400×
C
400×
1000×

**Supplementary Figure 2.** The immunohistochemistry staining of $LGR5^+$ cells which expressed GFP. (*A*) Representative immunohistochemistry pictures of negative control for anti-GFP staining. Without adding primary antibody: left panel; the negative sample which did not express GFP: right panel. (*B-C*) Representative immunohistochemistry pictures of LGR5-$GFP^+$ cells (presenting sample: long term $CCl_4$ induced injured liver), which was stained with anti-GFP antibody. Red arrow: $LGR5^+$ cells. Nuclear: blue; GFP: brown.

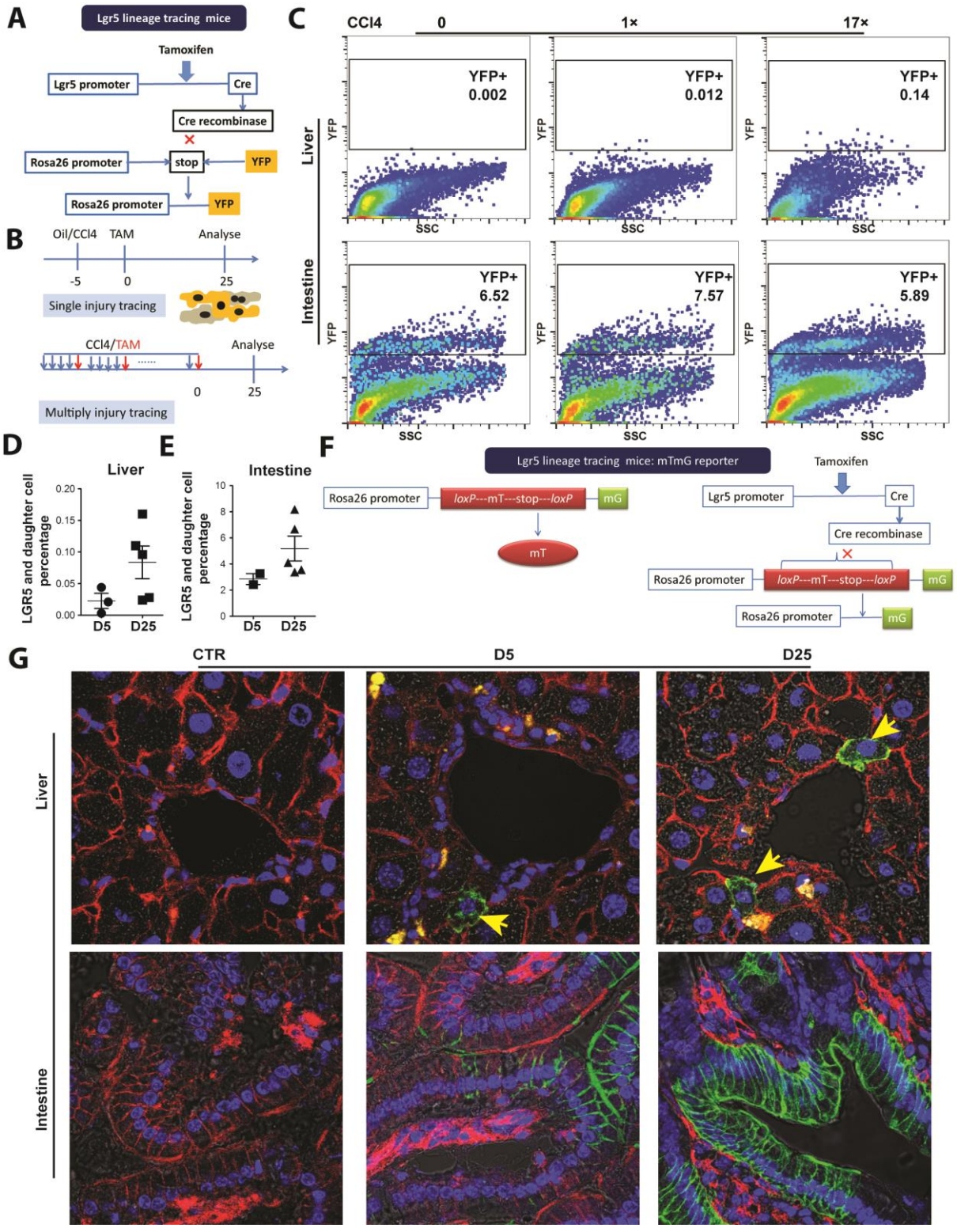
A
Lgr5 lineage tracing mice
Tamoxifen
Lgr5 promoter
Cre
Cre recombinase
Rosa26 promoter
stop
YFP
Rosa26 promoter
YFP
B
Oil/CCl4
TAM
Analyse
-5
0
25
Single injury tracing
CCl4/TAM
Analyse
0
25
Multiply injury tracing
C
CCl4
0
1×
17×
Liver
Intestine
YFP
SSC
YFP+ 0.002
YFP+ 0.012
YFP+ 0.14
YFP+ 6.52
YFP+ 7.57
YFP+ 5.89
D
Liver
LGR5 and daughter cell percentage
0.20
0.15
0.10
0.05
0.00
D5
D25
E
Intestine
LGR5 and daughter cell percentage
10
8
6
4
2
0
D5
D25
F
Lgr5 lineage tracing mice: mTmG reporter
Rosa26 promoter
loxP---mT---stop---loxP
mG
mT
Tamoxifen
Lgr5 promoter
Cre
Cre recombinase
Rosa26 promoter
loxP---mT---stop---loxP
mG
Rosa26 promoter
mG
G
CTR
D5
D25
Liver
Intestine

**Supplementary Figure 3**. LGR5 stem cells in recovery of liver injury. (*A*) A schematic illustration of *Lgr5-CreERT2/Rosa26-YFP* transgenic mice used. (*B*) Schemes showing the lineage tracing strategies. (*C*) Representative flow cytometry plots for daughter cells (YFP) derived from $LGR5^+$ cells in the liver and intestine with *Lgr5-CreERT2/Rosa26-YFP* transgenic mice without or with $CCl_4$ induced injury (number showed in percentage). SSC: side scatter. (*D-E*) Percentages of the daughter cells (YFP) derived from LGR5 cell with single $CCl_4$ injury in liver (*D*) and intestine (*E*), post day 5 and day 25. (*F*) A schematic illustration of the *Lgr5-CreERT2/Rosa26-mTmG* transgenic mice used. (*G*) Representative confocal images showing LGR5 derived offspring cells in *Lgr5-CreERT2/Rosa26-mTmG* mice after acute liver injury, at day 5 and 25 of post TAM induction. CTR: no TAM induced control; DAPI: blue; LGR5 derived offspring: green; Normal cells: red; Yellow arrow: daughter cells derived from liver $LGR5^+$ cells.

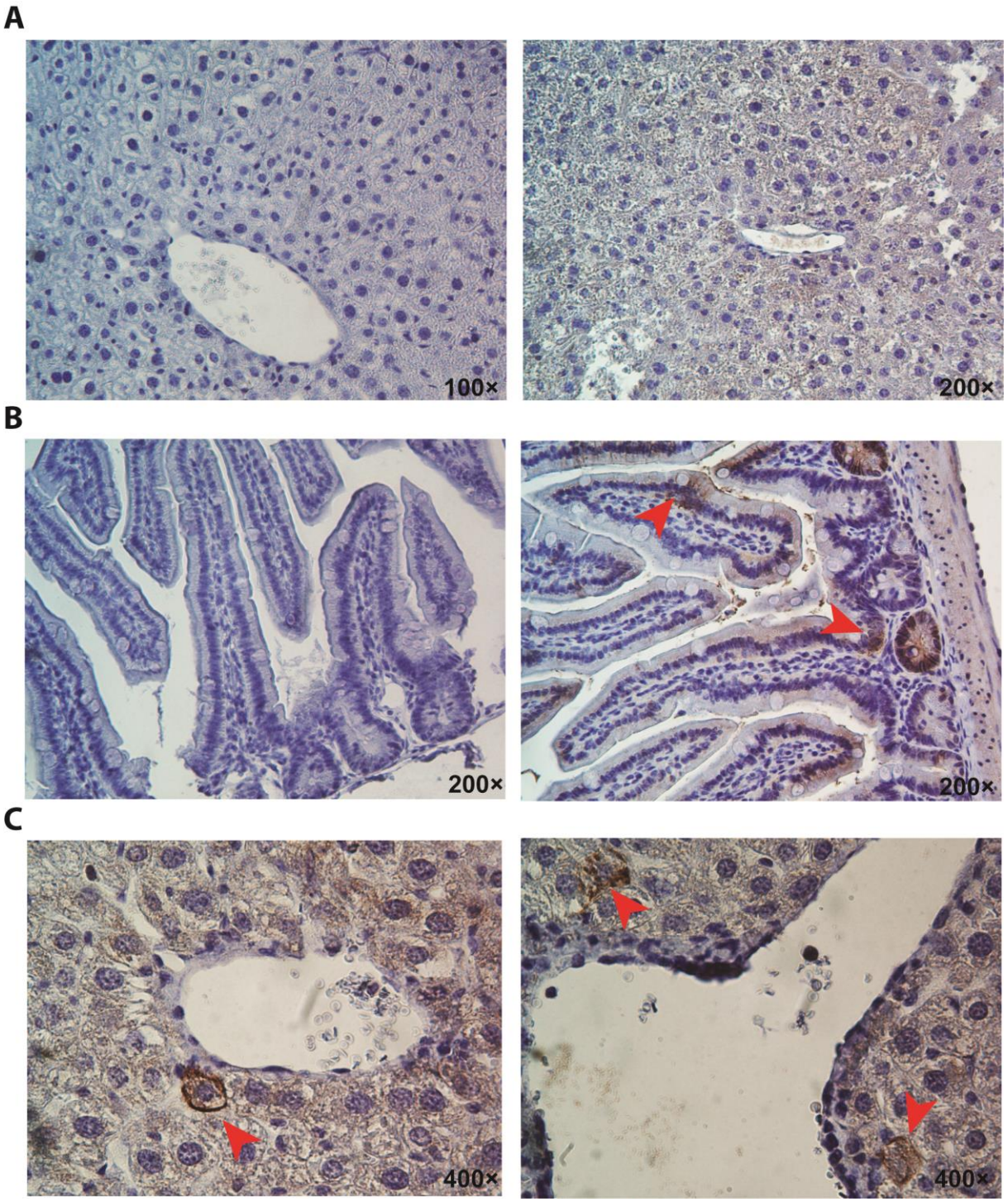
A
100×
200×
B
200×
200×
C
400×
400×

**Supplementary Figure 4.** Immunohistochemistry staining of $LGR5^+$ cells and their offspring cells which expressed membrane-targeted green fluorescent protein (mG). (*A*) Representative immunohistochemistry picture of negative control for anti-GFP staining. Without adding primary antibody: left panel; The negative sample which did not express GFP: right panel. (*B*) Representative immunohistochemistry pictures of intestinal *LGR5-mG* cells, which was stained with anti-GFP antibody. The negative sample which did not express GFP: left panel. (*C*) Representative immunohistochemistry pictures of *LGR5-mG* cells (presenting sample: acute $CCl_4$ induced liver injury, post TAM day25), which was stained with anti-GFP antibody. Red arrow: $LGR5^+$ and daughter cells.

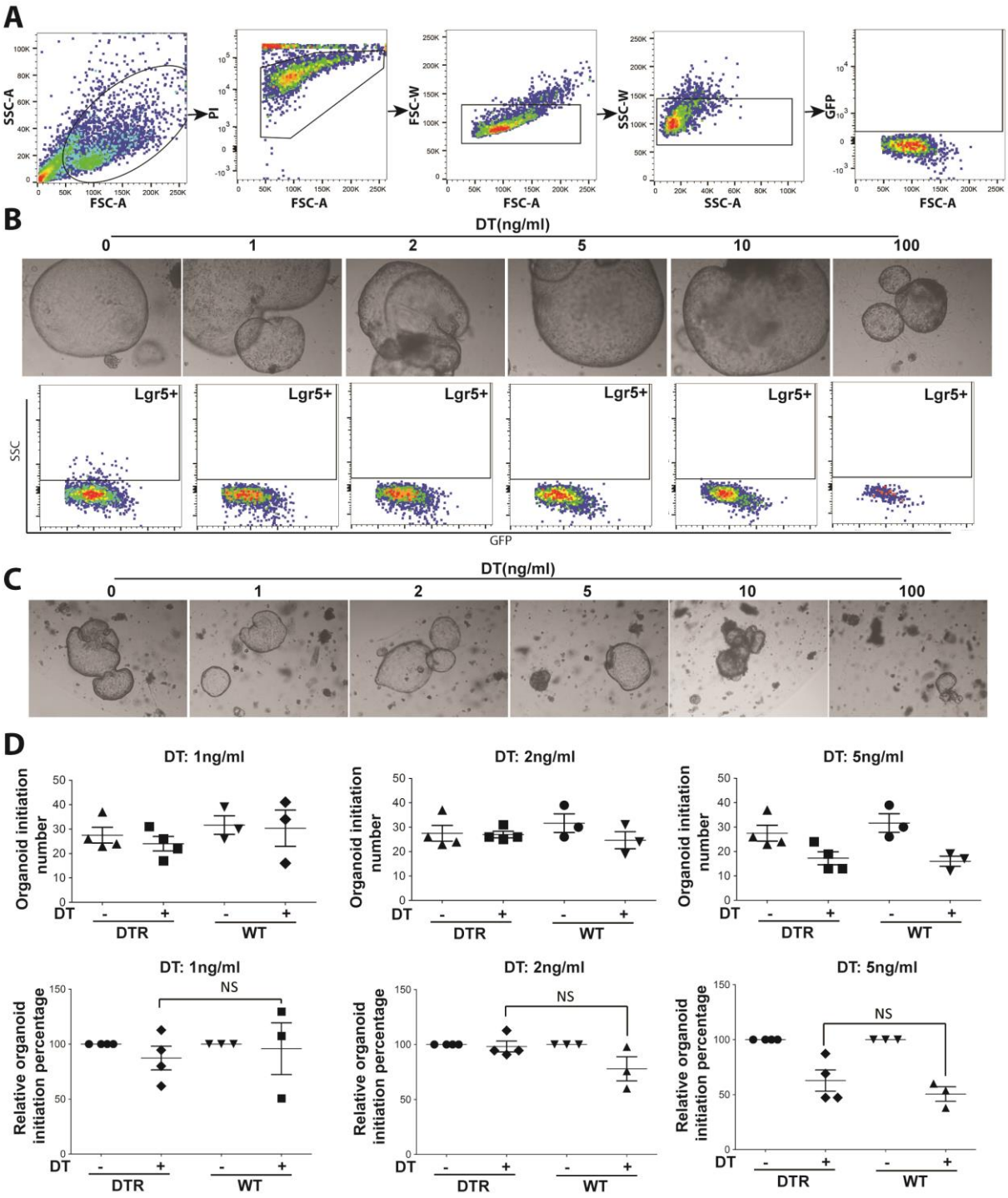
A
SSC-A
FSC-A
PI
FSC-A
FSC-W
FSC-A
SSC-W
SSC-A
GFP
FSC-A
B
DT(ng/ml)
0
1
2
5
10
100
Lgr5+
SSC
GFP
C
DT(ng/ml)
0
1
2
5
10
100
D
DT: 1ng/ml
DT: 2ng/ml
DT: 5ng/ml
Organoid initiation number
DT
DTR
WT
Relative organoid initiation percentage
NS

**Supplementary Figure 5.** DT depletion in organoids. (*A*) The FACS testing strategy of LGR5-GFP$^{+}$ cells from organoids. (*B*) Representative organoid pictures (upper panel; Original magnifications were ×40) and flow cytometry plots (lower panel) showing the organoids were treated with different concentrations of DT. Concentrations arranged from 0-100 ng/ml (n = 3). (*C*) Representative organoid pictures showing the wild type mice liver derived organoids treated with different concentrations of DT. Concentrations arranged from 0-100 ng/ml (n = 3). (*D*) The organoid initiation efficiency of organoids derived from *Lgr5-DTR-GFP* and wild type mice liver, under the treatment of different concentrations of DT. DTR: *Lgr5-DTR-GFP* mice liver derived organoids; WT: wild type mice liver derived organoid. Upper panel: the raw initiated organoid numbers. Lower panel: the relative organoid initiation efficiencies which normalized to the corresponding control (without DT treatment). NS: not significant.

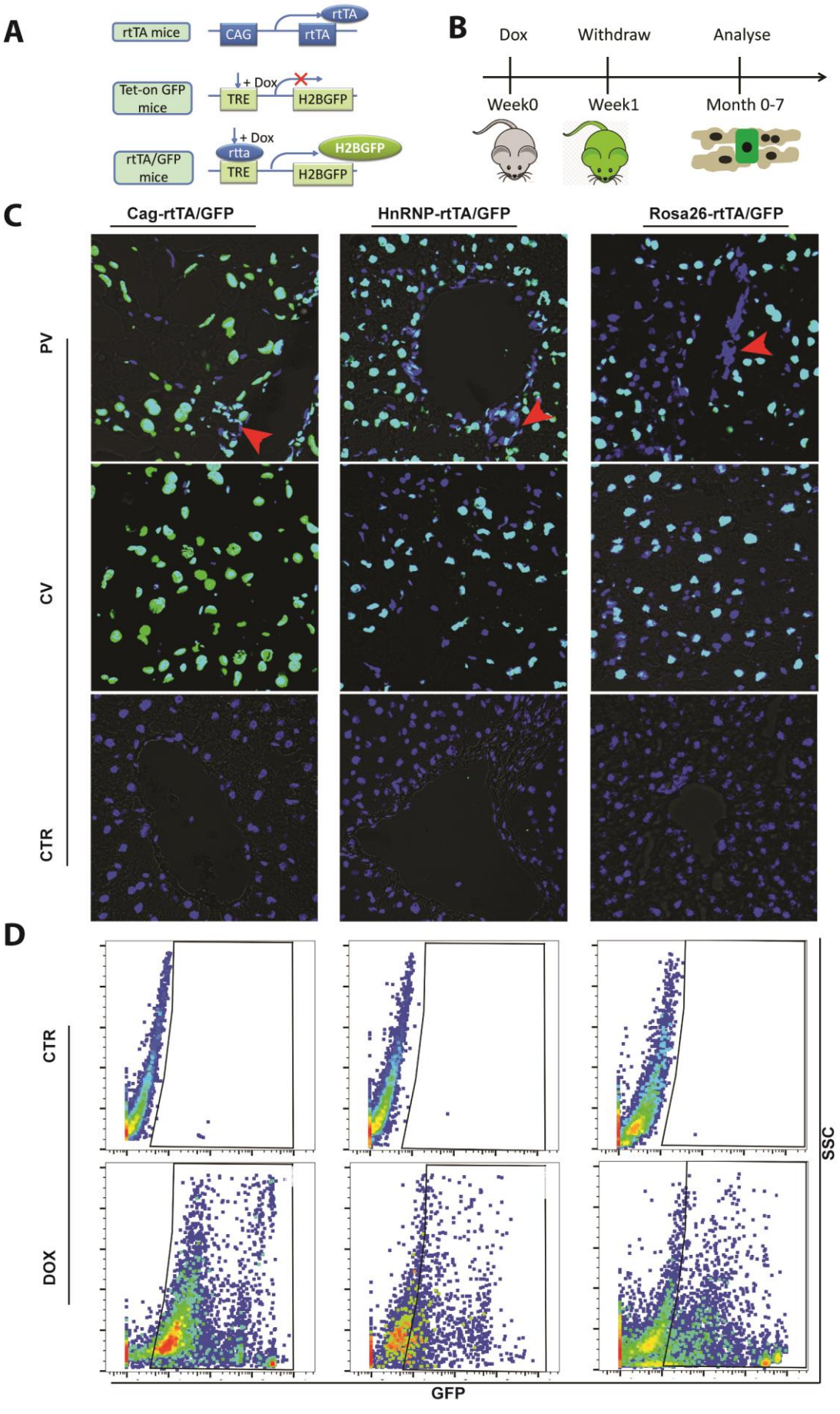
A
rtTA mice
CAG
rtTA
rtTA
Tet-on GFP mice
+ Dox
TRE
H2BGFP
rtTA/GFP mice
+ Dox
rtta
TRE
H2BGFP
H2BGFP
B
Dox
Withdraw
Analyse
Week0
Week1
Month 0-7
C
Cag-rtTA/GFP
HnRNP-rtTA/GFP
Rosa26-rtTA/GFP
PV
CV
CTR
D
CTR
DOX
SSC
GFP

**Supplementary Figure 6.** The induction efficiency of three *rtTA/GFP* transgenic mice. (*A*) Diagram representing of *rtTA/GFP* transgenic mice. (*B*) Transgenic *rtTA/GFP* mice were fed with dox water to induce H2BGFP expression for one week, then 7 month of chasing as indicated in the scheme. (*C*) Representative confocal microscopic pictures showing before/after dox induction in the liver of three *rtTA/GFP* transgenic mouse models. PV: portal vein. CV: central vein. Red arrow: bile duct structure. CTR: control. (*D*) Representative flow cytometry plots showing induction condition. SSC: side scatter. CTR: control. DOX: doxycycline induction (n = 2).

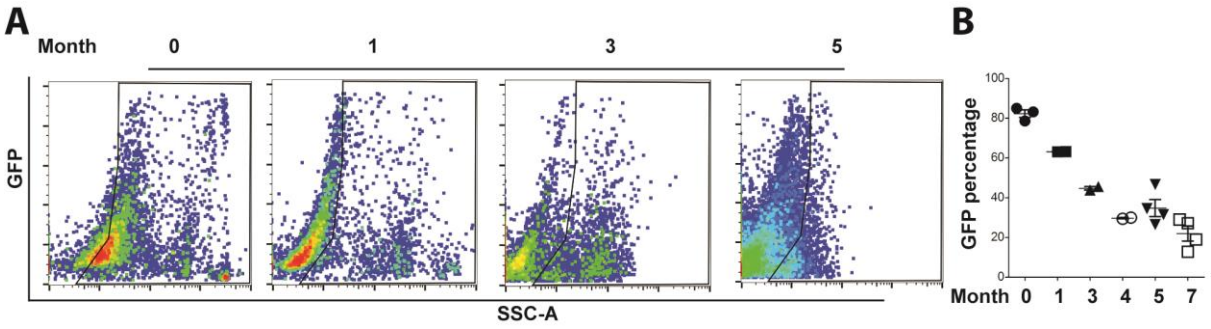


**Supplementary Figure 7.** Liver cells gradually lost GFP label during long-term fading period. (*A-B*) Representative flow cytometry plots (*A*) and absolute percentages of $GFP^+$ (*B*) showing liver cells slowly lost GFP label during long-term chasing period. SSC-A: side scatter area (Month 0: n = 3; Month 1: n = 2; Month 3: n = 2; Month 4: n = 2; Month 5: n = 4; Month 7: n = 4).

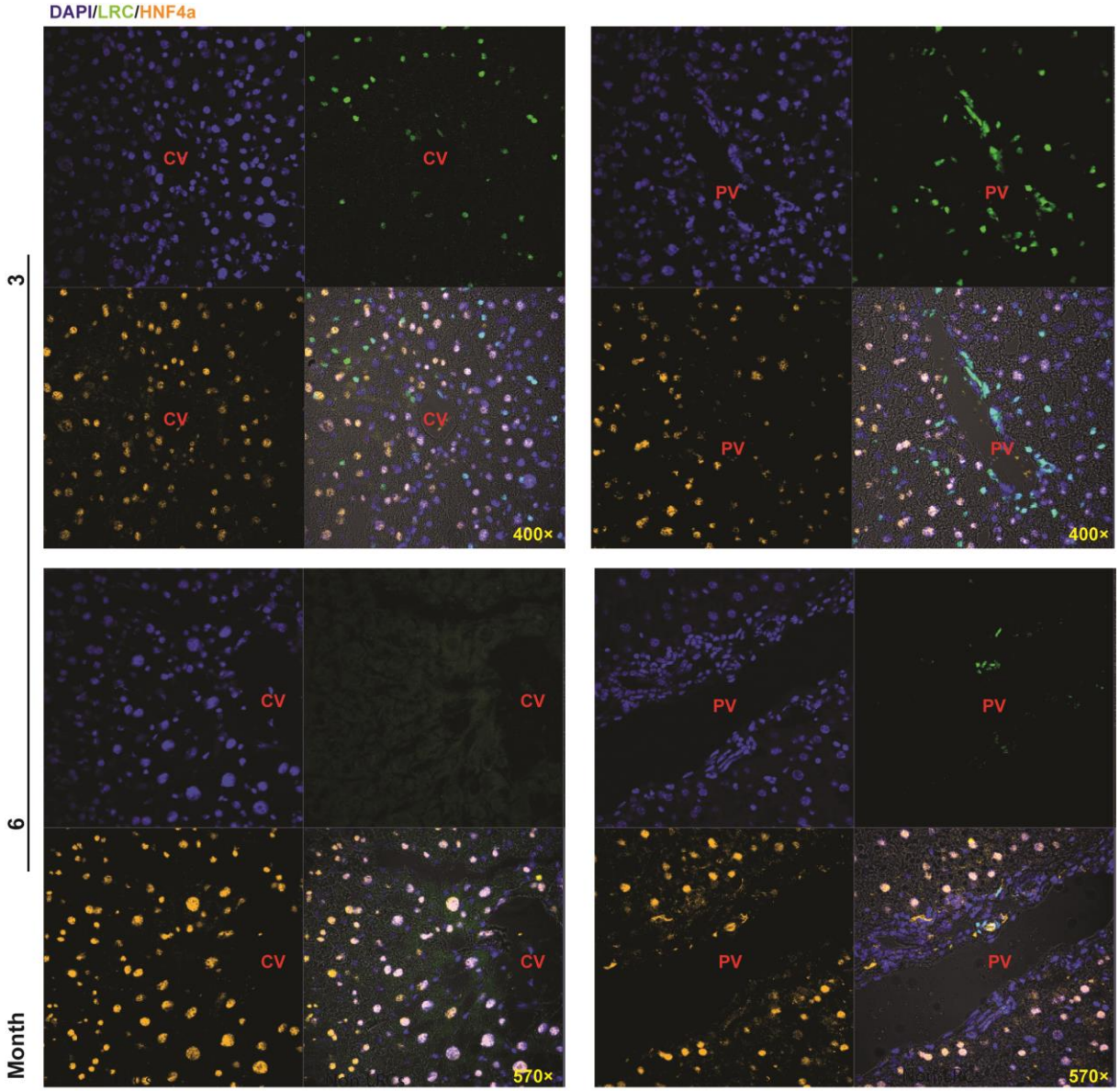


**Supplementary Figure 8.** LRCs did not express hepatocyte marker HNF4α. Representative confocal images for hepatocyte marker HNF4α expression in LRCs, month 3 LRCs (upper panel), month 6 LRCs (lower panel). HNF4α: yellow; DAPI: blue; LRCs: Green; PV: portal vein. CV: central vein.

**A**

| Homeostasis Liver (3-7 months) | Experiment 1 | | Experiment 2 | | Experiment 3 | | Experiment 4 | | Experiment 5 | |
|---|---|---|---|---|---|---|---|---|---|---|
| | LRCs | Non-LRCs | LRCs | Non-LRCs | LRCs | Non-LRCs | LRCs | Non-LRCs | LRCs | Non-LRCs |
| Cells input | 56565 | 95674 | 23374 | 36196 | 24637 | 53727 | 11845 | 39961 | 10687 | 16899 |
| Organoid number | 25 | 0 | 42 | 0 | 17 | 0 | 12 | 0 | 5 | 0 |
| Colony formation percentage | 0.044% | 0% | 0.18% | 0% | 0.069% | 0% | 0.10% | 0% | 0.05% | 0% |

**B**

| Homeostasis Bile duct (3-7 months) | Experiment 1 | | Experiment 2 | | Experiment 3 | |
|---|---|---|---|---|---|---|
| | LRCs | Non-LRCs | LRCs | Non-LRCs | LRCs | Non-LRCs |
| Cells input | 1439 | 1543 | 1449 | 1978 | 1789 | 31749 |
| Organoid number | 4 | 0 | 11 | 1 | 8 | 4 |
| Colony formation percentage | 0.28% | 0% | 0.76% | 0.05% | 0.45% | 0.01% |

**C**

| Homeostasis Liver (14-15 months) | Experiment 1 | | Experiment 2 | | Experiment 3 | | Experiment 4 | |
|---|---|---|---|---|---|---|---|---|
| | LRCs | Non-LRCs | LRCs | Non-LRCs | LRCs | Non-LRCs | LRCs | Non-LRCs |
| Cells input | 1203 | 1270 | 1312 | 3647 | 723 | 118347 | 818 | 1113 |
| Organoid number | 1 | 0 | 3 | 0 | 1 | 1 | 18 | 0 |
| Colony formation percentage | 0.08% | 0% | 0.23% | 0% | 0.14% | 0.0008 % | 2.2% | 0 |

**D**

| Homeostasis Bile duct (14-15 months) | Experiment 1 | | Experiment 2 | | Experiment 3 | | Experiment 4 | |
|---|---|---|---|---|---|---|---|---|
| | LRCs | Non-LRCs | LRCs | Non-LRCs | LRCs | Non-LRCs | LRCs | Non-LRCs |
| Cells input | 115 | 107 | 1983 | 1984 | 341 | 293 | 398 | 307 |
| Organoid number | 0 | 0 | 2 | 0 | 1 | 0 | 1 | 0 |
| Colony formation percentage | 0% | 0% | 0.1% | 0% | 0.29% | 0% | 0.25% | 0% |

**E**

| Injury Liver | Experiment 1 | | Experiment 2 | | Experiment 3 | |
|---|---|---|---|---|---|---|
| | LRCs | Non-LRCs | LRCs | Non-LRCs | LRCs | Non-LRCs |
| Cells input | 103284 | 106691 | 21960 | 33585 | 10214 | 12278 |
| Organoid number | 13 | 0 | 26 | 0 | 10 | 0 |
| Colony formation percentage | 0.013% | 0% | 0.12% | 0% | 0.10% | 0% |

**F**

| Injury Bile duct | Experiment 1 | | Experiment 2 | | Experiment 3 | |
|---|---|---|---|---|---|---|
| | LRCs | Non-LRCs | LRCs | Non-LRCs | LRCs | Non-LRCs |
| Cells input | 20059 | 14120 | 20129 | 20259 | 1164 | 20677 |
| Organoid number | 5 | 2 | 5 | 4 | 9 | 23 |
| Colony formation percentage | 0.025% | 0.014% | 0.025% | 0.020% | 0.77% | 0.11% |

**G**

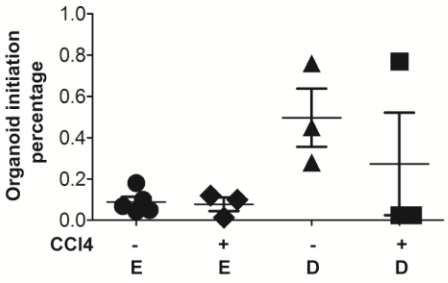


**H**

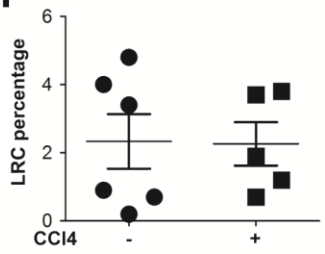

**Supplementary Figure 9.** Organoid formation of LRCs derived from homeostatic and injured mouse livers. (*A-B*) The organoid initiation efficiency of LRCs and non-LRCs from homeostatic liver (post dox induction month 3-7), isolated from the entire liver (*A*) (n = 5) or from bile duct (*B*) (n = 3). (*C-D*) The organoid initiation efficiency of LRCs and non-LRCs from homeostatic liver (post dox induction month 14-15), isolated from the entire liver (*C*) (n = 4) from bile duct (*D*) (n = 4). (*E-F*) The organoid initiation efficiency of LRCs and non-LRCs from injured liver, isolated from the entire liver (*E*) (n = 3) or from bile duct (*F*) (n = 3). (*G*) Comparison of organoid initiation efficiency between LRCs from healthy liver (month 3-7) and injured liver. E: entire liver derived LRCs; D: bile duct derived LRCs. (*H*) The percentage of LRCs within the entire cell population from both homeostatic and injured liver (NS: not significant).

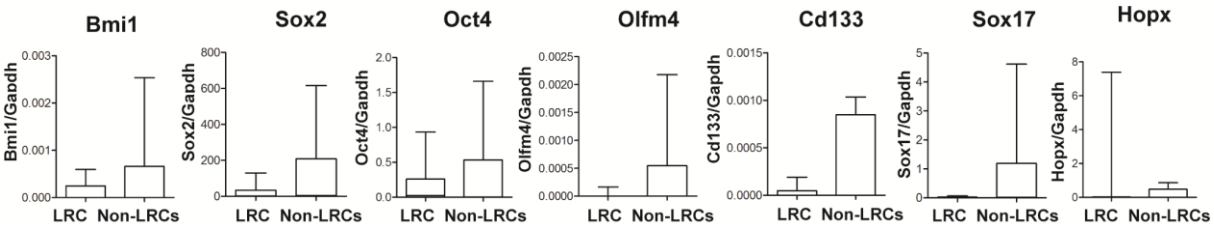


**Supplementary Figure 10.** The panel of progenitor cell markers which did not show specific enrichment. Both LRCs or non-LRCs (freshly isolated, from month 3-15) did not show enrichment for those markers, as quantified by qRT-PCR. Values were normalized against *Gapdh* expression (n = 6).

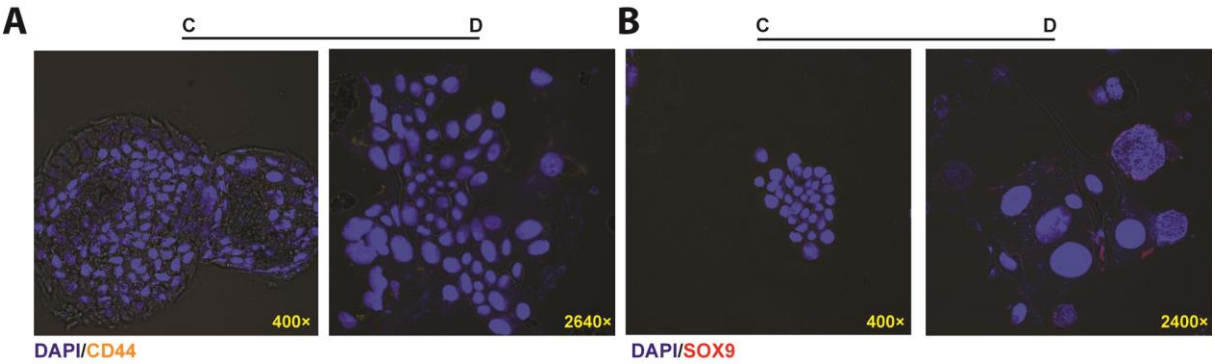


**Supplementary Figure 11.** LRCs derived organoids lost the expression of progenitor markers upon hepatocyte differentiation. (*A-B*) LRCs derived organoids lost the expression of CD44 (*A*) and SOX9 (*B*) upon differentiation. C: negative control; D: CD44/SOX9 expression upon differentiation.

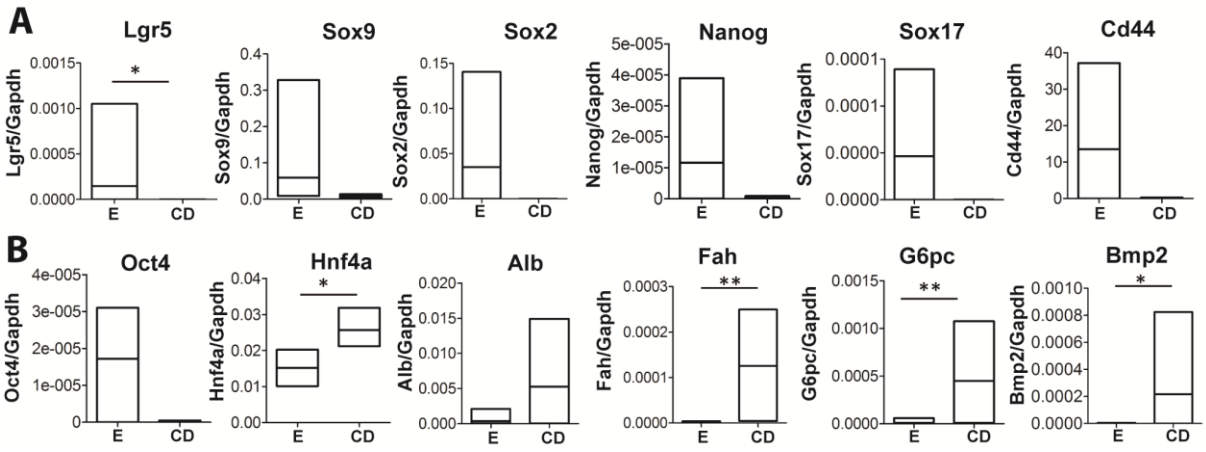


**Supplementary Figure 12.** LRCs could differentiate towards hepatocyte and cholangiocyte lineages. (*A*-*B*) Gene expression of LRCs derived organoids for progenitor (*A*), hepatocyte and maturation markers (*B*), compared between expansion and cholangiocyte directed differentiation phase. E: expansion. CD: cholangiocyte directed differentiation. Values were normalized against *Gapdh* expression (**P* < .05; ***P* < .01; n = 4).

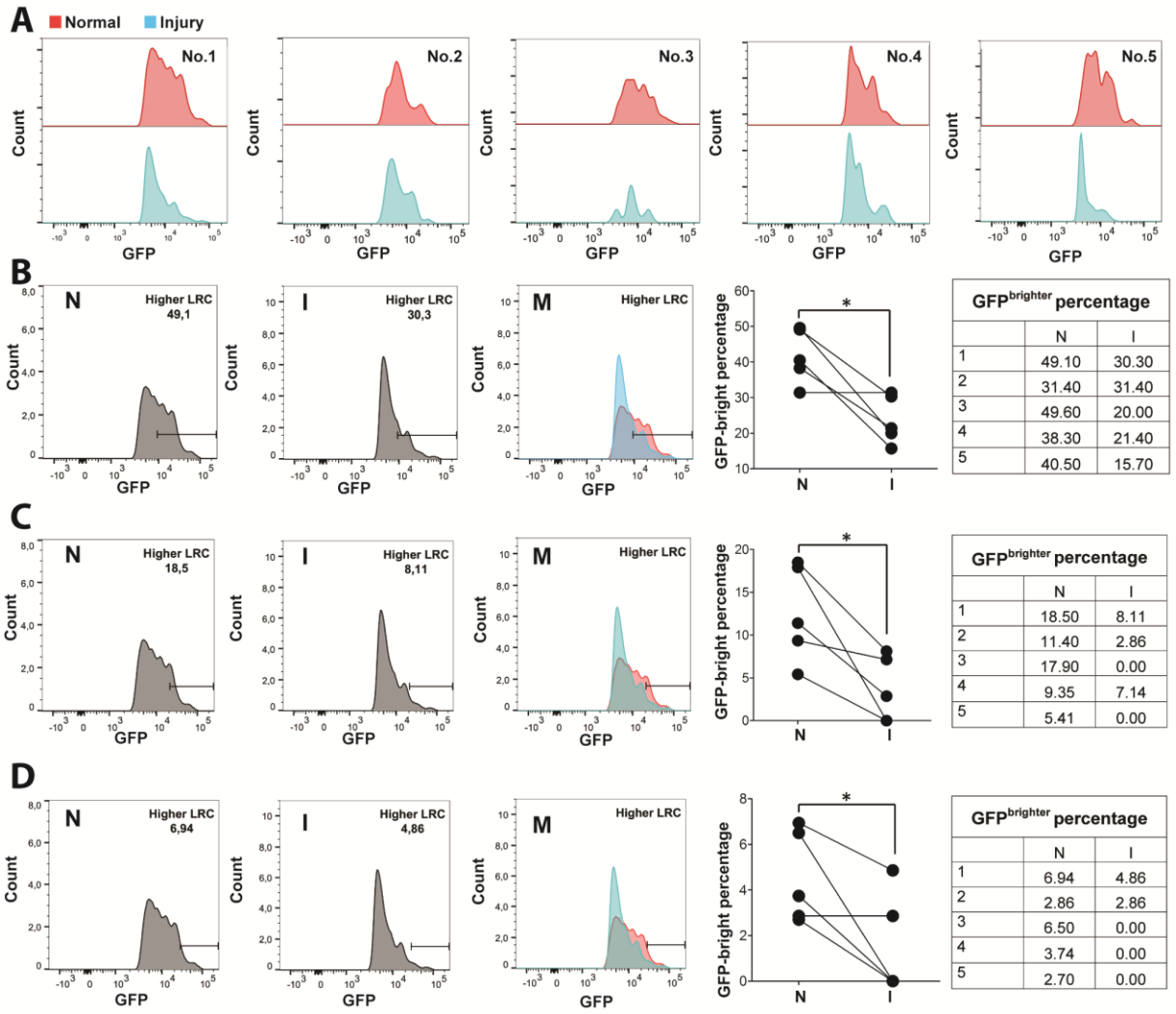


**Supplementary Figure 13.** LRCs responded to injury. (*A*) All of the five paired mice (paired mice: start/stop the dox induction in the same day; sacrifice within 1 day) showed that the LRCs shifted towards a relatively lower expression of GFP, upon 3 days of $CCl_4$ injury. (*B-D*) Representative FACS graphs (for No.1 samples, Left three figures) and absolute percentages (for all five pairs, right two figures) showing that the bright GFP population was dramatically decreased after three days of $CCl_4$ injury (*$P < .05$; n = 5). N: normal; I: injury: M: merged FACS figures from normal and injury.

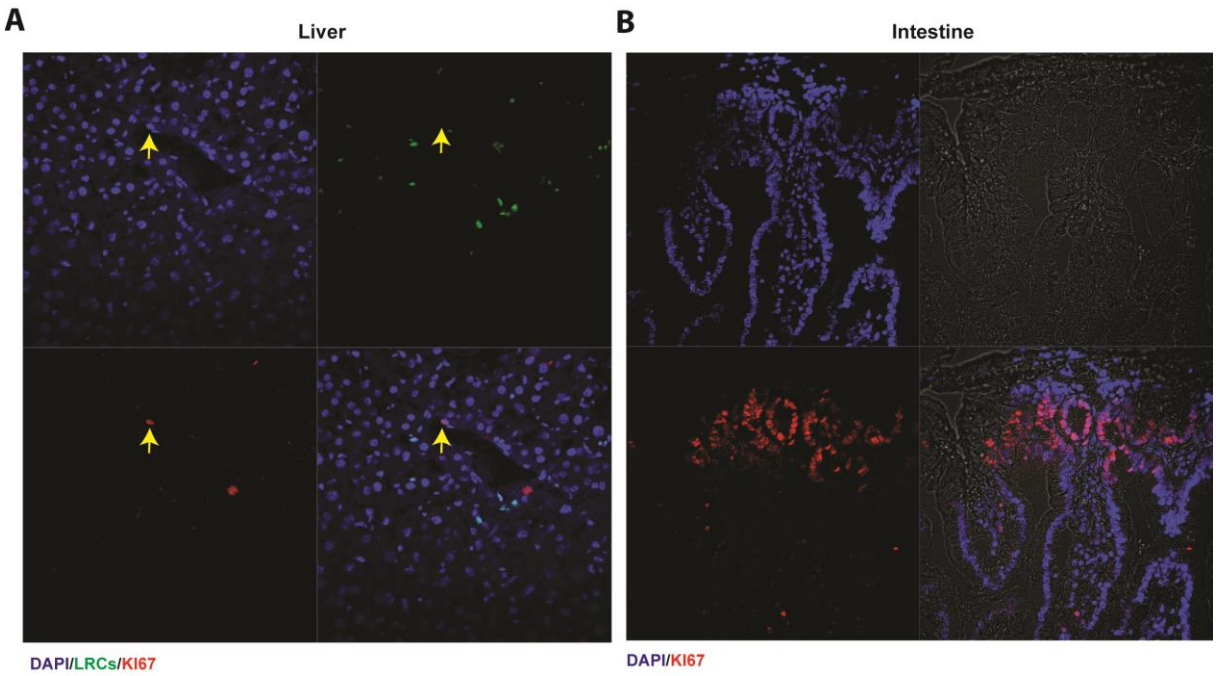


**Supplementary Figure 14.** LRCs in healthy liver did not express proliferation marker KI67. (*A*) LRCs in healthy liver did not express KI67. DAPI: Blue; LRCs: Green; KI67: Red. Yellow arrow: one non-LRC expressed KI67 protein. (*B*) Positive control for anti-KI67 staining, indicating the intestinal cells with higher index of proliferation.

**Supplementary Table 1.**

| Antibody | Antibody clone/ reference | Raised | Origin |
|---|---|---|---|
| CD45 | 56-0451-82 | Mouse | eBioscience |
| Albumin | sc46291 | Goat | STCruz |
| GFP | A-11122 | Rabbit | Invitrogen/Life Technologies |
| KI67 | ab15580 | Rabbit | Abcam |
| HNF4α | sc-8987 X | Rabbit | STCruz |
| CK19 | ab52625 | Rabbit | Abcam |
| CD44 | ab157107 | Rabbit | Abcam |
| SOX9 | AB5535 | Rabbit | Millipore |
| Alexa Fluor® 488 AffiniPure Donkey Anti-Goat IgG (H+L) | 705-545-147 | Donkey | Bio-Connect |
| Donkey anti-Rabbit IgG (H+L) Secondary Antibody, Alexa Fluor® 594 conjugate | A-21207 | Donkey | Thermo fisher |
| Donkey anti-Goat IgG (H+L) Cross-Adsorbed Secondary Antibody, Alexa Fluor 594 | A-11058 | Donkey | Thermofischer |
| Donkey anti-Goat IgG (H+L) Secondary Antibody, Alexa Fluor® 647 conjugate | A-21447 | Donkey | Life Technologies |

**Supplementary Table 2**

| Gene name | Gene Symbo | Sequence | |
|---|---|---|---|
| Leucine-rich repeat-containing G-protein coupled receptor 5 | Lgr5 | fw | CTG ACT TTG AAT GGT GCC TCG |
| | | re | ATG TCC ACT ACC GCG ATT AC |
| Albumin | Alb | fw | TCC TGA TTG CCT TTT CCC AGT ATC T |
| | | re | GCC AGT TCA CCA TAG TTT TCA CGG A |
| Hepatocyte nuclear factor 4α | Hnf4α | fw | CAG ACG TCC TCC TTT TCT TGT GAT |
| | | re | TGT TTG GTG TGA AGG TCA TGA TTA |
| Bone morphogenetic protein 2 | Bmp2 | fw | TGA GGA TTA GCA GGT CTT TG |
| | | re | CAC AAC CAT GTC CTG ATA AT |
| Peroxisome proliferator-activated receptor gamma | Pparg | fw | GCC CTT TGG TGA CTT TAT GGA |
| | | re | GCA GCA GGT TGT CTT GGA TG |
| T-box transcription factor | Tbx3 | fw | CCA CCC GTT CCT CAA TTT GAA CAG |
| | | re | CGG AAG CCA TTG ATG GTA AAG CTG |
| Glucose-6-phosphatase, catalytic subunit | G6pc | fw | TCC CCA GAA TTC TCC ACT TG |
| | | re | AAC ATC GGA GTG ACC TTT GG |
| Fumarylacetoacetase | Fah | fw | CAT GGG TCT GGG TCA AGC |
| | | re | AGG TCC CCA GGT CTC AGG |
| Cytochrome P450, family 3, subfamily a, polypeptide 11 | Cyp3a11 | fw | GAC AAA CAA GCA GGG ATG GAC |
| | | re | CCA AGC TGA TTG CTA GGA GCA |
| Antigen KI-67 | ki67 | fw | CTG CCT GCG AAG AGA GCA TC |
| | | re | AGC TCC ACT TCG CCT TTT GG |

| | | | |
|---|---|---|---|
| Antigen Cd44 | Cd44 | fw | CGT CCA ACA CCT CCC ACT AT |
| | | re | AGC CGC TGC TGA CAT CGT |
| Transcription factor SOX-9 | Sox9 | fw | CGA CTA CGC TGA CCA TCA GA |
| | | re | GAC TGG TTG TTC CCA GTG CT |
| SRY (sex determining region Y)-box 17 | Sox17 | fw | GGC GCA GCA GAA TCC AGA |
| | | re | CCA CGA CTT GCC CAG CAT |
| Antigen Cd133 | Cd133 | fw | TCT GTT CAG CAT TTC CTC AC |
| | | re | TCA GTA TCG AGA CGG GTC |
| Transcription factor Nanog | Nanog | fw | AGG GTC TGC TAC TGA GAT GCT CTG |
| | | re | CAA CCA CTG GTT TTT CTG CCA CCG |
| Octamer-binding transcription factor 4 | Oct4 | fw | CTG TAG GGA GGG CTT CGG GCA CTT |
| | | re | CTG AGG GCC AGG CAG GAG CAC GAG |
| SRY (sex determining region Y)-box 2 | Sox2 | fw | GGC AGC TAC AGC ATG ATG CAG GAG C |
| | | re | CTG GTC ATG GAG TTG TAC TGC AGG |
| Cytokeratin-19 | Ck19 | fw | GTG AAG ATC CGC GAC TGG T |
| | | re | AGG CGA GCA TTG TC AAT CTG |
| Cytokeratin 7 | Ck7 | fw | ATC CGC GAG ATC ACC ATC |
| | | re | ATG TGT CTG AGA TCT GCG ACT |
| Leucine-rich repeats and immunoglobulin-like domains protein 1 | Lrig1 | fw | AAG GGA ACT CAA CTT GGC GAG |
| | | re | ACG TGA GGC CTT CAA TCA GC |
| Telomerase reverse transcriptase | Tert | fw | GCA GGT GAA CAG CCT CCA GAC AG |
| | | re | TCC TAA CAC GCT GGT CAA AGG GAA GC |

| | | | |
|---|---|---|---|
| Oligomeric mucus/gel-forming | Muc5ac | fw | GGA CCA AGT GGT TTG ACA CTG AC |
| | | re | CCT CAT AGT TGA GGC ACA TCC CAG |
| Mucin 1, cell surface associated | Muc1 | fw | CCC CAG TTG TCT GTT GGG GTC |
| | | re | GGA TTC TAC CAC CAC GGA GCC |
| Mex-3 RNA Binding Family Member A | Mex3a | fw | ACA CCA CGG AGT GCG TTC |
| | | re | GTT GGT TTT GGC CCT CAG A |
| Polycomb complex protein BMI-1 | Bmi1 | fw | TTC ATT GAT GCC ACA ACC AT |
| | | re | CAG CAT CAG CAG AAG GAT GA |
| Homeodomain-only protein | Hopx | fw | CAT CCT TAG TCA GAC GCG CA |
| | | re | AGG CAA GCC TTC TGA CCG C |
| Olfactomedin 4 | Olfm4 | fw | TGG CCC TTG GAA GCT GTA GT |
| | | re | ACC TCC TTG GCC ATA GCG AA |

# CHAPTER 3

# Modeling liver cancer and therapy responsiveness using organoids derived from primary mouse liver tumors

Wanlu Cao[1], Meng Li[1], Yuebang Yin[1], Buyun Ma[1], Monique M.A. Verstegen[2], Jiaye Liu[1], Kan Chen[1,3], Michiel Bolkestein[2,4], Dave Sprengers[1], Luc J. W. van der Laan[2], Jaap Kwekkeboom[1], Ron Smits[1], Maikel P. Peppelenbosch[1] and Qiuwei Pan[1*]

[1]Department of Gastroenterology and Hepatology, Erasmus MC-University Medical Center, Rotterdam, The Netherlands.

[2]Department of Surgery, Erasmus MC-University Medical Center, Rotterdam, The Netherlands.

[3]College of Life Sciences, Zhejiang Sci-Tech University, Hangzhou, China.

[4]Department of Cell Biology, Erasmus MC-University Medical Center, Rotterdam, The Netherlands.

***Carcinogenesis, conditionally accepted***

## Abstract

The current understanding of cancer biology and the availability of effective treatments for cancer remain far from satisfactory. In order to facilitate cancer research, easy and robust model systems are required that resemble the architecture and physiology of the tumors in patients. Cancer research has mainly been based on the use of immortalized cancer cell lines that have been propagated in 2D culture for decades, which deviate in many aspects from the original primary tumors. The recent development of the organoid technology allowing generation of organ-buds in 3D culture from adult stem cells has endowed the possibility of establishing stable culture from primary tumors. Although culturing organoids from liver tumors is thought to be difficult, we now convincingly demonstrate the establishment of organoids from mouse primary liver tumors. We have succeeded in establishing 90 lines from 128 tumors. These organoids can be grown in long-term cultures and expand in vitro. A subset of these liver cancer organoids have the potential to initiate tumors in immunodeficient mice upon (serial) transplantation, confirming their malignant and cancer stem cell-like properties. Interestingly, a single organoid derived from a single cancer cell is able to initiate tumor in mice, indicating the enrichment of tumor-initiating cells in the organoids. Furthermore, these organoids recapitulate, to some extent, the heterogeneity of liver cancer as seen in patients, with respect to phenotype, cancer cell composition and treatment response. These model systems provide new research opportunities to advance knowledge on liver cancer (stem cell) biology, drug development and personalized medicine.

**Keywords:** Tumor organoid, Liver tumor, Anti-cancer research

# 1. Introduction

Liver cancer is one of the most common cause of cancer-related death worldwide with limited treatment options available [1]. Better understanding of the biology of liver cancer is urgently needed to facilitate the development of new therapies. However, this in turn heavily relies on the availability of easy and robust model systems that resemble the architecture and physiology of the tumors in patients. So far, the cancer research society has mainly used immortalized cancer cell lines that have been propagated in 2D culture for decades. Obviously, these cell lines behave very different from the original tumor in many aspects [2]. Primary cell culture of liver cancer cells from either human or mouse has proven to be very difficult [3]. Thus, innovative approaches enabling *in vitro* propagation of primary liver cancer cells that maximize the modeling capacity of the patient disease and treatment response will be of particular importance.

The recent development of the organoid technology has driven the stem cell research field moving forward. Organoids are initiated *in vitro* from one or a few adult stem cells of a particular tissue/organ and self-organize into 3D structures [4]. They recapitulate the tissue architecture and lineage hierarchy, allow self-renewal and expansion of the stem cell population and empower different types of experimental manipulation [5]. Many types of cancers are believed to harbor a subset of cells, often termed as tumor-initiating cells (TIC). Thus, it is conceivable that organoids could be cultured from tumor tissues, if sophisticated 3D cell culture techniques/conditions are employed. Indeed, tumor organoid models have been successfully established from primary colorectal [6], pancreas [7] and prostate cancer tissues [8]. This technology is now used to explore many aspects of cancer research, including studying oncogenic transformation, cancer stem cells, drug development and personalized treatment [9, 10]. Our study presents the successful establishment of malignant organoid models from mouse primary liver tumors and demonstrates their applications in liver cancer research.

## 2. Materials and Methods:

*2.1. Primary liver tumor model*

C57Bl6 (B6), C3H and CD1 were purchased from Charles River. And then C57Bl6 (B6) mice were further bred with C3H or CD1 into B6/C3H and B6/CD1 separately. B6, B6/C3H and B6/CD1 mice (3-4 weeks) were administrated weekly with Diethylnitrosamine (DEN) by intraperitoneal injection (i.p., 100 mg/kg) for 6-17 weeks. Mice were sacrificed 3-16 months after the last DEN injection and livers were collected for further experiments. All animal experiments were approved by the Committee on the Ethics of Animal Experiments of the Erasmus Medical Center.

*2.2. Immunohistochemistry and Immunofluorescence of tissues*

Liver or liver tumor was fixed in 4% paraformaldehyde (4°C, overnight). For immunofluorescence, samples were further dehydrated with 30% sucrose solution overnight, stored at -80°C and then sectioned at 8 μm for further analysis. For immunohistochemistry and H&E staining, materials were embedded in paraffin according to standard procedures and sectioned at 4 μm for further staining. All antibodies are listed in Supplementary Table 4.

*2.3. Immunohistochemistry and Immunofluorescence of organoids*

For immunofluorescence, cold advanced DMEM/F12 medium was used to collect the organoids. Organoids were fixed in 4% paraformaldehyde for 10 min, and centrifuged onto the slice for staining (Cytospin, 1000rpm×3min). For H&E staining and immunohistochemistry, the organoids including the matrigel were directly fixed with 4% paraformaldehyde for 30 min in room temperature, embedded in 1% agarose, further embedded in paraffin, and sectioned at 4 μm for further analysis.

*2.4. Tumor organoid culture*

Single cells were isolated from mouse liver tumor tissues using a digestion solution: Collagenase type XI (0.5 mg/ml, Sigma-Aldrich), Dispase (0.2 mg/ml, Gibco), 1% FBS in DMEM medium (Lonza) (37°C, 30min), then centrifuged (600rpm, 10min) to collect the cell

pellets. Cells were directly mixed with matrigel (BD Bioscience), seeded on 24/48 well plates and kept at 37°C for at least 30 min. After the matrigel formed a solid gel, medium was slowly added. Organoid culture medium was based on advanced DMEM/F12 (Invitrogen), which is supplemented with B27 (2% vol/vol, Invitrogen) and N2 (1% vol/vol, Invitrogen), N-acetylcysteine (1.25 µM, Sigma-Aldrich), gastrin (10 nM, Sigma-Aldrich), EGF (50 ng/ml, Peprotech), R-spondin 1 (10% vol/vol, conditioned medium produced by 293T-H-RspoI-Fc cell line), FGF10 (100 ng/ml, Peprotech), nicotinamide (10 mM, Sigma-Aldrich) and HGF (50 ng/ml, Peprotech). For the initial 3 days, the organoids also need to be supplemented with Noggin (10% vol/vol, conditioned medium produced by 293T-HA-Noggin cell line) and Wnt3a (30% vol/vol, conditioned medium produced by L-Wnt3a cell line) [4]. Medium was refreshed every 2-3 days and organoids were passaged in 1:2-1:10 split ratio once per week, or according to the growth of the organoids.

*2.5. Organoid allografting*

Cold advanced DMEM/F12 medium was used to collect the organoids. After centrifuging, organoids pellets were mixed directly with matrigel in the ratio of 1:1 with a total volume of 100-200 µl. 4-6 weeks old female NOG/JicTac (CIEA NOD.Cg-Prkdc-scid Il2rg-tm1Sug) mice were purchased from Taconic, and subcutaneously injected with the collected tumor organoids (transplanted cell number: $1\text{-}10\times10^6$). Tumor formation was monitored weekly and mice were sacrificed to harvest tumor after visualizing the tumor (the tumor diameter reached approx.1 cm). Tumor tissues were stored or cultured as described above.

*2.6. Single organoid formation assay and allograft assay*

Cold medium was used to collect the organoids, and organoids were digested into single cells. FACS sorter (BD FACSAriaTM II) was used to isolate the single living cells. Propidiumiodide (PI) staining was used to exclude dead cells. FSC-Width with FSC-Area and then SSC-Width with SSC-Area gates were used to select the single cells. After mixing one single cell with matrigel, a droplet with in total volume of 5 µl was seeded in a well of 96-well plate for organoid initiation. After 1-3 weeks, single organoids were formed. Cold medium was used to collect the single organoids. After removing the supernatant, matrigel was mixed with the organoid pellet and transplanted subcutaneously into the NOG mice directly. Tumor formation was monitored as described above.

*2.7. Metabolic activity analysis of organoids*

Different organoid lines were seeded separately in a 24/48-well plate. Sorafenib (1 µM, 10 µM) or Regorafenib (1 µM, 10 µM) was added to the organoid culture since the initial day or post-initiation day 3, respectively. Drugs were refreshed every 2 days. At the day 7, organoids were incubated with Alamar Blue (Invitrogen, 1:20 in DMEM) for four hours, and then medium was collected for analysis of the metabolic activity of the cells, which is an indirect measure of living cells. Absorbance was determined by using fluorescence plate reader (CytoFluor® Series 4000, Perseptive Biosystems) at the excitation of 530/25nm and emission of 590/35. Each treatment condition was repeated for four times and matrigel only was used as blank control.

*2.8. qRT–PCR*

We performed the qRT–PCR as described previously [11]. In short, Machery-NucleoSpin RNA II kit (Bioké) was used to extract RNA from organoids. Glyceraldehyde 3-phosphate dehydrogenase (*Gapdh*) gene was used as a reference. All primers are listed in Supplementary Table 5.

*2.9. Statistical Analysis*

Prism software (GraphPad Software) was used for all statistical analysis. We used Mann-Whitney U-test and differences were considered significant at a p value less than 0.05. More details are described in the supplementary materials and methods.

## 3. Results:

*3.1. Successful culture of organoids from mouse primary liver tumors*

Diethylnitrosamine (DEN) is widely used as a carcinogen in experimental animal models, in particular for inducing liver tumors in mice. Similar to the gender disparity in patients,

DEN also preferentially induce liver tumors in male mice [12]. Thus, we have mainly used male mice (53 male; 3 female) to induce liver tumor by DEN. The livers were harvested for organoid culture (Fig. 1A: the upper panel). The numbers of visible tumors vary among the harvested mouse livers, ranging from zero to multiple tumors per liver (Supplementary Fig. S1). In total, we obtained 128 individual tumors from these mice, which were subjected to organoid culture. In general, small organoids could be visualized since post day 2-7 and passage was required around 7-14 days. We have succeeded in establishing organoid culture from 90 out of the 128 tumors, representing an efficiency of 70.3% (Supplementary Table S1). Among the 38 tumors that failed to establish organoid culture, 12 samples did initiate organoids but stopped proliferation at an early stage; whereas many of the other tumors had extensive necrosis and did not initiate any organoid from the start.

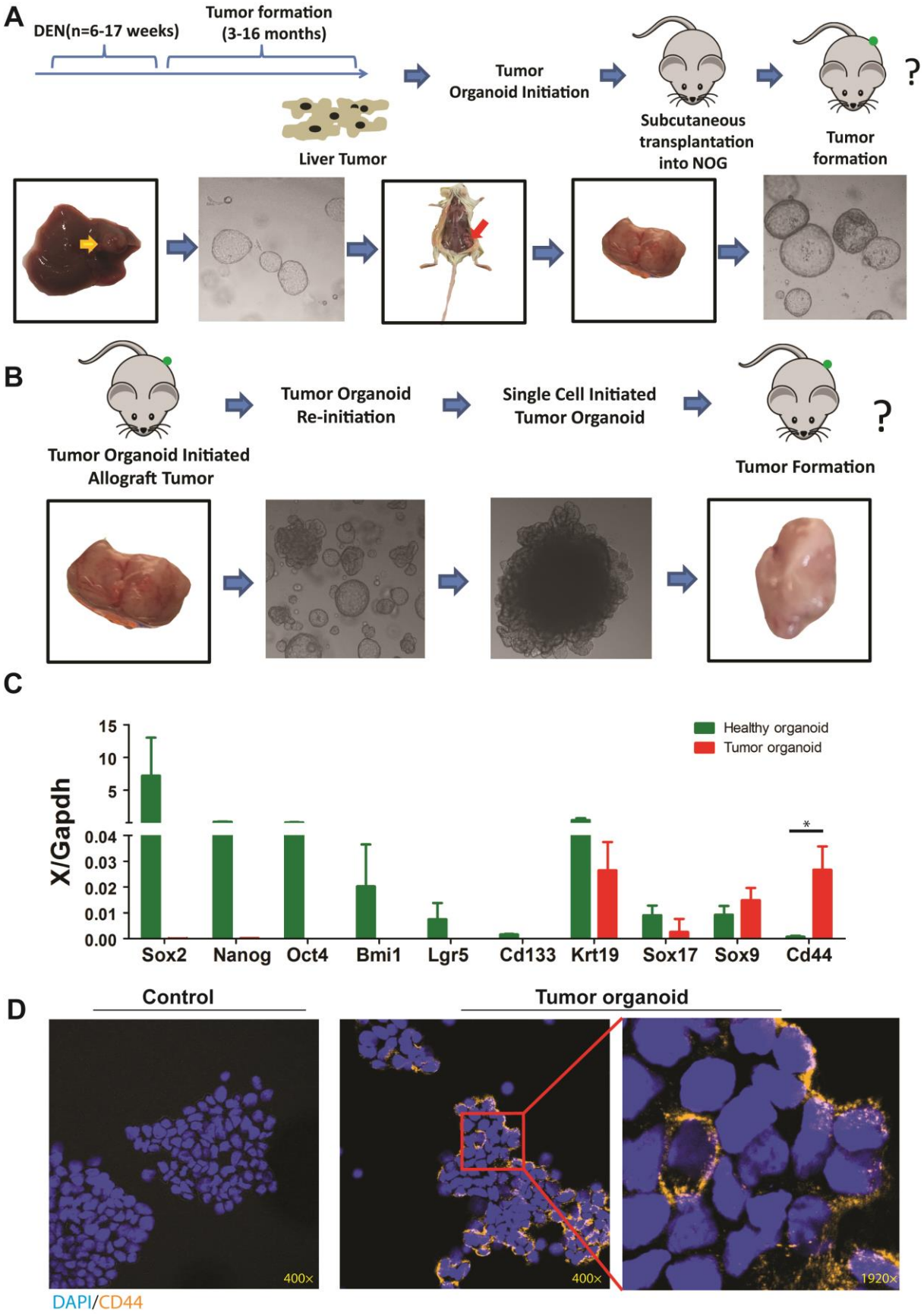


**Fig. 1. Establishment of long-term cultures of primary mouse liver tumor organoids and their further characterization** (A) The upper panel: An outline of the experimental strategy used to establish primary tumor organoid; The lower panel: Representative pictures showing tumor

organoids cultured from mouse primary liver tumors, and the formation of allograft tumor in the NOG mice. The allograft tumors can again be cultured into tumor organoids . (B) The upper panel: An outline of the experimental strategy used to investigate a single tumor organoid; The lower panel: Representative pictures showing that allograft tumor can again initiate tumor organoids . A single cell isolated from the tumor organoid can initiate a single organoid and then initiate tumor growth in NOG mice. (C) The expression profile of progenitor markers of tumor organoids, compared to healthy liver organoids (n=3). (D) Representative immunofluorescence pictures showing the expression of CD44 in tumor organoids.

The successfully established lines could be maintained and propagated in 3D culture for at least 5 months (the maximum time period tested so far), by passaging in the ratio of 1:2-1:4 for every 7 days. We further demonstrated that these tumor-derived organoids can be frozen, stored and re-cultured again without affecting their growth rate. With respect to the morphology, we (Supplementary Fig. S2A) and others [4] have observed that organoids derived from the healthy liver have a uniform, bubble-like structure. In contrast, organoids derived from liver tumors presented diverse morphologies, ranging from bubble-like to condensed and flower-like, as well as an irregular sheet-like structure (Supplementary Fig. S2B-D). Interestingly, some cultures contained a mixture of organoids with different morphology (Supplementary Fig. S3A), which may reflect the heterogeneity of cell types within the tumors.

### *3.2. Tumorigenicity of expanded organoids in immunodeficient mice*

To functionally assess whether these tumor-derived organoids are malignant, we performed the allograft assay in NOG immunodeficient mice as described previously [13]. We have subcutaneously engrafted all the established 90 organoid lines and assessed their tumor formation ability *in vivo*. Within 4-10 weeks, 16 out of 90 (18%) lines initiated tumor formation in NOG mice (Fig. 1A: the lower panel and Table 1: the upper panel).

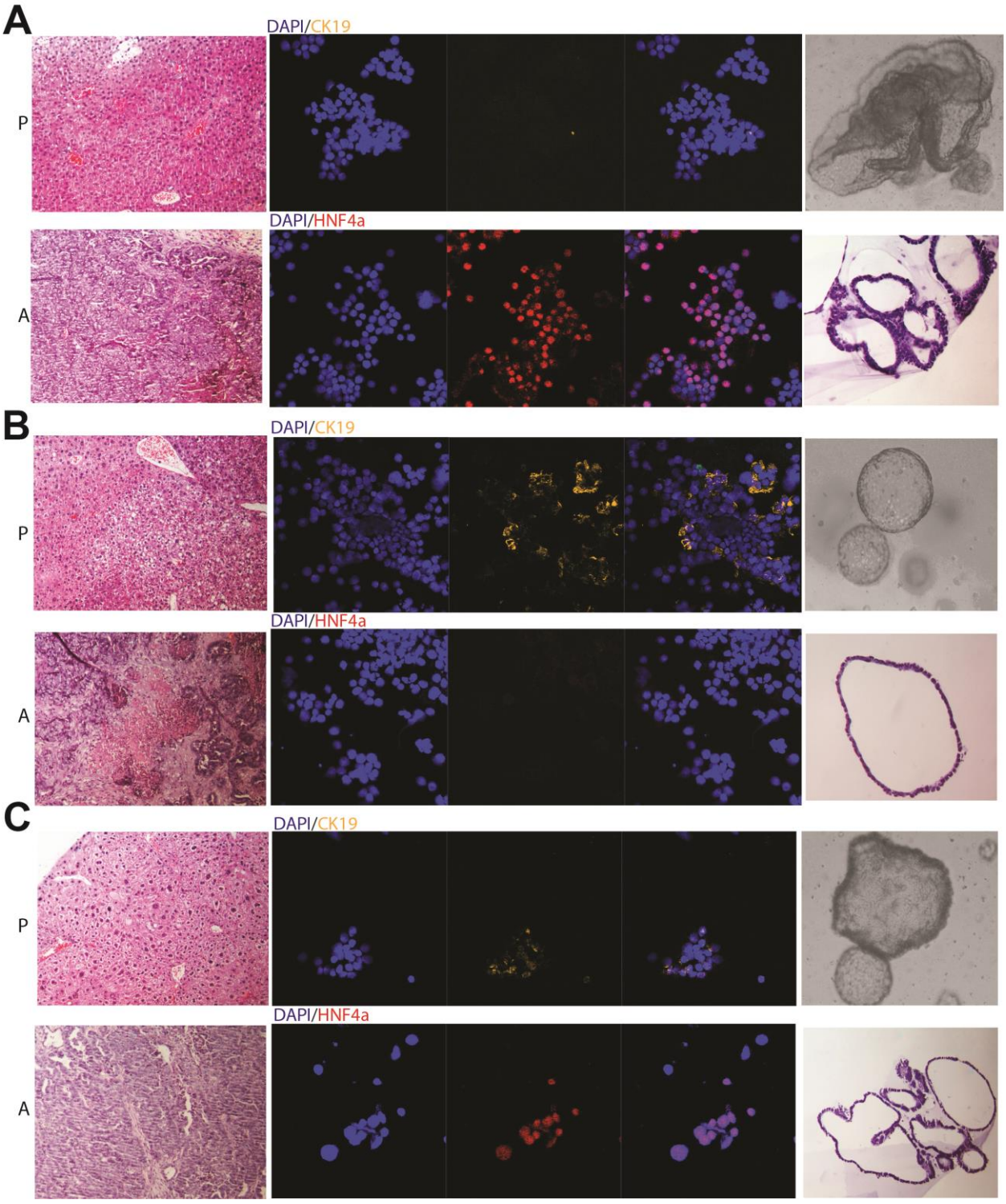


**Fig. 2. Liver tumor organoids express hepatocyte and cholangiocyte markers** (A-C) Representative pictures showing the organoid lines that mainly express the hepatocyte marker HNF4α (A, n=1), the cholangiocyte marker CK19 (B, n=4) and both (C, n=3), and the corresponding H&E staining for the primary tumor (P) and its corresponding allograft tumor (A) and the organoids.

Organoids could be cultured again from these allograft tumors (Fig. 1A: the lower panel). These tumor organoids have to be passaged every 5 days in the ratio of 1:5-1:10, indicating an increased speed of growth. Importantly, when engrafting into NOG mice,

these organoids are capable to readily initiate tumors again (Table 1: the middle panel). These results firmly demonstrated that those liver tumor derived organoids are malignant and tumorigenic with self-renewal capability.

| Tumor Organoid Lines | | | | |
|---|---|---|---|---|
| | Organoid Code | Primary Tumor Harvesting Time(Month) | Mice Background | Allograft Tumor Harvesting Time(Day) |
| 1 | PT12 | 14 | B6/CD1 | 24 |
| 2 | PT18 | 13 | B6 | 58 |
| 3 | PT20 | 16 | B6/CD1 | 41 |
| 4 | PT22 | 9 | B6 | 58 |
| 5 | PT23 | 5 | B6/C3H | 58 |
| 6 | PT26 | 9 | B6 | 58 |
| 7 | PT28 | 13 | B6 | 58 |
| 8 | PT61 | 14 | B6 | 36 |
| 9 | PT71 | 15 | B6 | 22 |
| 10 | PT72 | 7 | B6/C3H | 22 |
| 11 | PT81 | 15 | B6 | 66 |
| 12 | PT85 | 7 | B6/C3H | 40 |
| 13 | PT86 | 8 | B6/C3H | 40 |
| 14 | PT102 | 14 | B6/CD1 | 33 |
| 15 | PT104 | 13 | B6 | 33 |
| 16 | PT105 | 13 | B6 | 33 |

| Tumor Re-initiation From Allograft Tumor Derived Organoids | | |
|---|---|---|
| | Organoid Code | 2nd Allograft Tumor Harvesting Time (Day) |
| 1 | AT65 | 28 |
| 2 | AT66 | 28 |
| 3 | AT83 | 42 |
| 4 | AT84 | 42 |

| Tumor Initiation Of Single Organoids | | |
|---|---|---|
| | Organoid Code | 2nd Allograft Tumor Harvesting Time (Day) |
| 1 | AT50 | 14 |
| 2 | AT53 | 22 |
| 3 | AT54 | 22 |

**Table 1. Liver tumor organoids can initiate tumors.** The upper panel: The primary tumor organoid lines which formed tumor in the NOG mice, and the corresponding information of tumor harvesting time and mouse strain; The middle panel: Tumor organoids derived from the allograft (1st allograft) can re-initiate tumor again (2nd allograft) in the NOG mice; The lower panel: The corresponding tumor harvesting time of single cell formed organoid derived allograft tumors.

*3.3. A single organoid derived from a single cancer cell is able to initiate tumor formation in mice*

To further consolidate the ability to initiate tumor growth of the organoids, we performed an organoid formation assay with isolated single cells. We found that isolated single cells from the tumor organoids can efficiently re-initiate organoids (Fig. 1B). More importantly, subcutaneous transplantation of a single tumor organoid derived from a single cell into immunodeficient NOG mice rapidly initiated tumor around two weeks, confirming their malignant property (Fig. 1B and Table 1: the lower panel). Furthermore, organoids can be re-cultured from those allograft tumors and exhibited progressive expansion for over 4 months. These results indicate that 3D tumor organoid system enriches the cells with the capacity of tumor initiating.

Classically, stem cell markers have been widely used to identify potential TIC, although it is an ever debating issue of defining qualified TIC markers [14]. Based on previous studies [14, 15], we have profiled a panel of potential TIC markers, in comparison with liver organoids from normal liver stem cells. We found that liver tumor organoids have lower gene expression of *Sox2*, *Sox17*, *Nanog*, *Oct4*, *Krt19*, *Bmi1*, *Lgr5* and *Cd133,* relatively higher expression of *Sox9* and significantly upregulation of *Cd44*. The expression of CD44 at protein level was confirmed by immunofluorescent staining (all positive in tested 8 lines), indicating that tumor organoids have a different expression profile of these putative markers compared to the normal stem cell pool (Fig. 1C-D).

### *3.4. Tumor organoids express cholangiocyte and/or hepatocyte markers*

In patients, primary liver cancer has been traditionally classified into three main types based on the tumor cell type. These are hepatocellular carcinoma (HCC), cholangiocarcinoma (CC) and hepatocellular-cholangiocarcinoma (CHC). Although it remains a challenge to differentiate these types, hepatocyte (e.g. AFP, HNF4α) or/and cholangiocyte (e.g. CEA, CK19, C-KIT) markers are often used as one of the approaches to distinguish these types of liver cancer [16]. In this respect, we have characterized the established tumor organoids by staining with hepatocyte (HNF4α) and cholangiocyte (CK19) markers, respectively. We found a distinct variation among different lines of established tumor organoids. Some with a subset of cells express HNF4α (Fig. 2A), some express CK19 (Fig. 2B), and others express both markers (Fig. 2C). In contrast, organoids derived from normal liver stem cells often do not express these lineage markers, especially HNF4α (Supplementary Fig. S4). These data indicate a distinct phenotype of tumor compared to normal organoids, and may recapitulate the heterogeneity of liver cancer

types in patients to some extent. Of note, given that the etiology of liver cancer is diverse, DEN induced liver tumors in mice do not fully represent liver cancer in patients [12].

*3.5. Assessment of anti-cancer drugs in the tumor organoid model*

Current treatment options, in particular for advanced liver cancer, are very limited. Sorafenib is the only FDA-approved first-line systemic therapy for patients with advanced HCC, with improvement of patient survival for only 3 months [1]. Regorafenib is now emerging as a potential second-line therapy for HCC patients [17]. To explore the potential of using liver tumor organoid models for future drug development, we assessed the feasibility by testing the effects of Sorafenib and Regorafenib.

We used organoid lines established from eight allograft tumors. We evaluated the effects on tumor organoid initiation by treatment with the drugs in the early phase of seeding the cells; while the effects on organoid growth were determined by starting the treatment at day 3 when the organoids are already formed.

Overall, these two targeted therapies dose-dependently inhibited the numbers of organoids formed and the growth of the organoids (Fig. 3, Supplementary Table S2 and S3). However, we also observed clear variations of the responsiveness among these organoids. For instance, organoid initiation of AT72 is sensitive to Sorafenib but less to Regorafenib; whereas initiation of AT71 is moderately suppressed by both Sorafenib and Regorafenib treatment. AT65 is more sensitive to early treatment; whereas both AT71 and AT85 better responded to Sorafenib when treatment was applied after organoids had already formed. Taken together, these results reflect the heterogeneity of individual lines as well as the differences in responsiveness between treatments at different stages of organoid growth.

**Fig. 3. Reaction of tumor organoids in response to treatment with the targeted therapeutics Sorafenib or Regorafenib** (A-B) Eight tumor organoid lines were analyzed here: AT65, AT66, AT71, AT72, AT83, AT84, AT85 and AT86. At day 7, the Alamar blue assay was used to measure the proliferation of organoids. Organoid number was counted to determine the initiation ability. The effects on organoid initiation were evaluated by adding the drugs immediately after seeding the cells. The effects on organoid growth were evaluated by adding the drugs 3 days after seeding the cells when the organoids had already formed ($P$<0.05, n=4). (C) Representative pictures taken at day 7, showing that tumor organoids respond differently to the treatment ($P$<0.05, n=4).

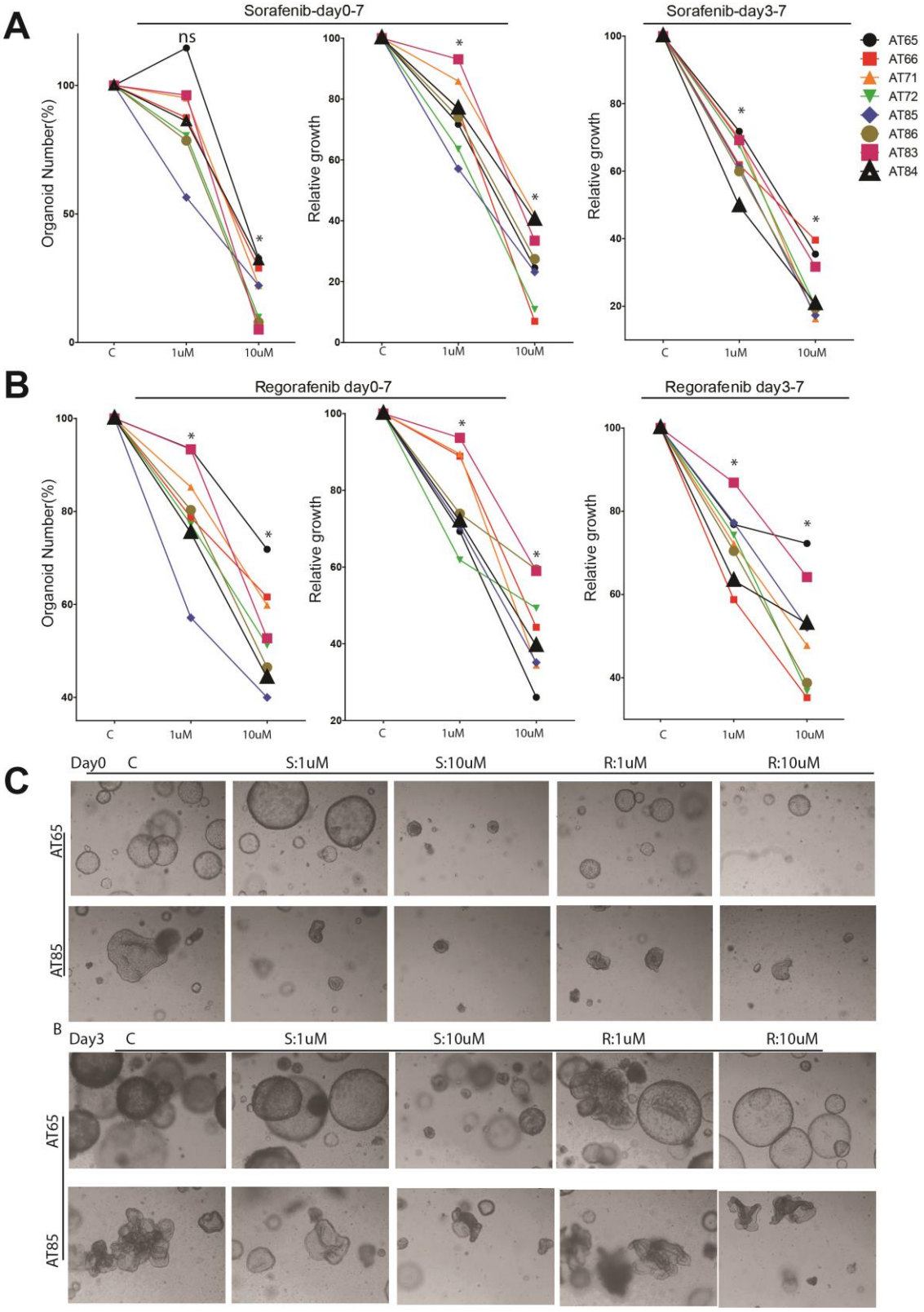
A
Sorafenib-day0-7
Sorafenib-day3-7
ns
Organoid Number(%)
Relative growth
C
1uM
10uM
AT65
AT66
AT71
AT72
AT85
AT86
AT83
AT84
B
Regorafenib day0-7
Regorafenib day3-7
C
Day0
S:1uM
S:10uM
R:1uM
R:10uM
AT65
AT85
Day3

## 4. Discussion

This study has demonstrated the establishment of organoids from primary mouse liver tumors. These organoids can be expanded in long-term cultures and initiate tumors in immunodeficient mice. Importantly, these organoids recapitulate, to some extent, the heterogeneity of liver cancer as seen in patients, with respect to phenotype, cancer cell composition and treatment response.

Classically, the investigation of liver cancer is based on *in vitro* cell lines, which have the following limitations: 1) limited number of established cell lines; 2) low efficiency of establishing new lines from primary tissues; 3) only aggressive tumors have high change to establish *in vitro* culture successfully [18]. Thus, the majority of primary tissue (>90%) cannot be successfully culture *in vitro*, especially the benign or less aggressive tumors, which also should be further investigated [18].Apart from the traditional cell line culture models, several other methods have also been explored to model liver cancer *in vitro*. The rotating wall vessel bioreactor has been used to culture HCC cell lines. This system was further used to co-culture the liver tumor cells with colon carcinoma cells to form liver-tumor hybrid, as a model to mimic liver metastasis [19]. In addition, 2D or 3D spheroid culture has been applied to culture HCC cell lines [20, 21]. However, the majority of those *in vitro* systems involve immortalized cell lines, rather than primary tissue.

We here adopted a matrigel-based 3D organoid culture system. This model allows investigation of healthy adult stem cells, as well as various types of diseases, in particular cancer. Successful examples have been reported in establishing organoids from colon [6], pancreas [7] and prostate tumor tissues [8]. Here we reported that we have succeeded in establishing 90 lines from 128 liver tumors. These organoids are capable of long-term culture and expansion *in vitro*. They are capable of initiating tumors in immunodeficient mice upon (serial) transplantation, confirming their tumorigenic, malignant and self-renewal properties. We also observed different morphology in established tumor organoids. The diversity of morphology has previously also been observed in other types of tumor organoids, such as those derived from colorectal [6], pancreatic [7] and prostate [8] cancer.

Our results also support the notion that liver tumors contain TIC, and organoids may represent an innovative model system for studying these cancer cells. TIC is a rare cancer cell population, but is thought to be the engine of tumor formation, relapse, metastasis and chemo-resistance in many cancer types [14], including in liver cancer [22]. We envision that these tumor organoid models have potential to circumvent a major bottleneck in the

TIC field as these cells are usually not able to be cultured *in vitro*. The current research is largely based on phenotypic description and tumor formation assays in immunodeficient mice [22]. Sophisticated *in vitro* culture of liver tumor organoids that are capable of long-term propagation *ex vivo*, as demonstrated in our study, provides a unique tool for the research field to advance in-depth research of liver TIC.

We further reveal the heterogeneity of individual lines as well as the differences in responsiveness between treatments at different stages of organoid growth. This provides proof-of-concept that organoids have the potential to be used as an *in vitro* model to study anti-cancer drug development in general, as well as for personalized medicine in cancer treatment in particular. Furthermore, TIC have been proposed as attractive anti-cancer targets and recent studies have demonstrated the possibility and efficacy of targeting TIC in animal models [23]. We believe that tumor organoid models have particular advantages as a platform for facilitating the development of TIC targeted therapies, given that these cells can be *ex vivo* cultured from primary tumor tissues [24].

The organoid model system may well provide enormous opportunities for advancing research on liver cancer/stem cell biology, drug development and personalized medicine. Of note, organoid systems do not mutually exclude the use of the classical cancer cell lines, but in fact can complement each other. Finally, more efforts are urgently required to establish robust organoid models from patient liver tumors.

## 6. Statement of authors contributions

W.C., M.P.P., and Q.P. designed research; M.L; Y.Y, B.M, M.M.A.V, J.L, L.V.D.L and J.L, K.C, M.B, D.S, J.K, R.S contributed new reagents/analytic tools; W.C. and Q. P. performed research and analyzed data; W.C, M.M.A.V, M.B, D.S, J.K, R.S, M.P.P., and Q.P writing, review, and/or revision of the manuscript:


## 7. Funding:

This work was supported by the Daniel den Hoed Foundation for a Centennial Award fellowship (to Q. Pan) and a KWF Young Investigator Grant 10140 (to Q. Pan), and the China Scholarship Council for funding PhD fellowships to W. Cao (201307060013), Y. Yin (201307720045), M Li (201506100033), B Ma (201508330291) and J Liu (201606240079).

## 8. Acknowledgments:

We thank S.A. van der Heide-Mulder, R. Lieshout, K.F. Meijsen and S. Mancham for technical assistance.

# Supplementary data for:

## Modeling liver cancer and therapy responsiveness using organoids derived from primary mouse liver tumors

**Table of contents**

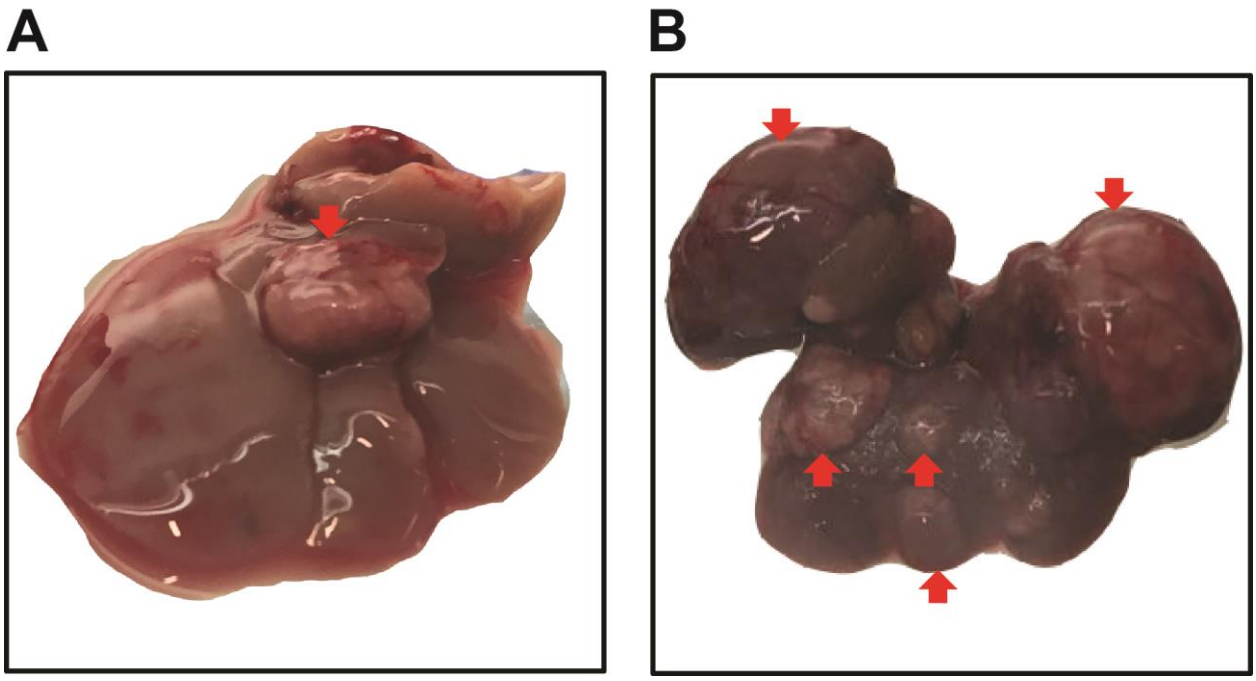


**Supplementary Fig. 1. Examples of primary liver tumor** (A) liver with one visible tumor. (B) liver with more than one tumor. The red arrow depicts the location of tumors.

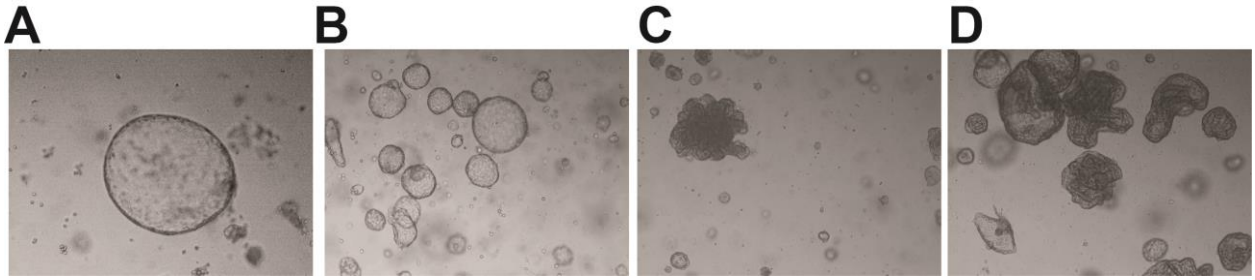


**Supplementary Fig. 2. Morphology of tumor organoids** (A) Example of normal liver organoids. (B-D) The tumor organoids with different morphological aspects.

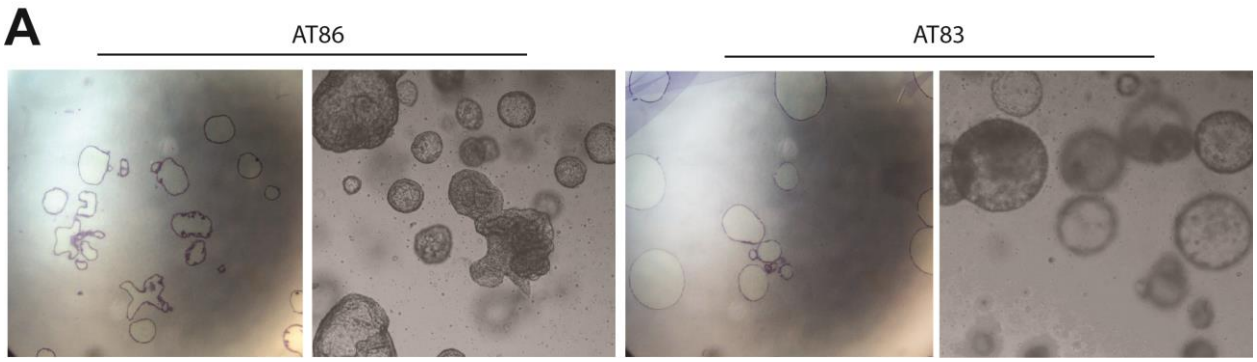


**Supplementary Fig. 3. Tumor organoids show mixed or uniform morphology.** AT86 show mixed morphology and AT83 show uniform morphology (Left: H&E staining, 25×; Right: bright view, 100×).

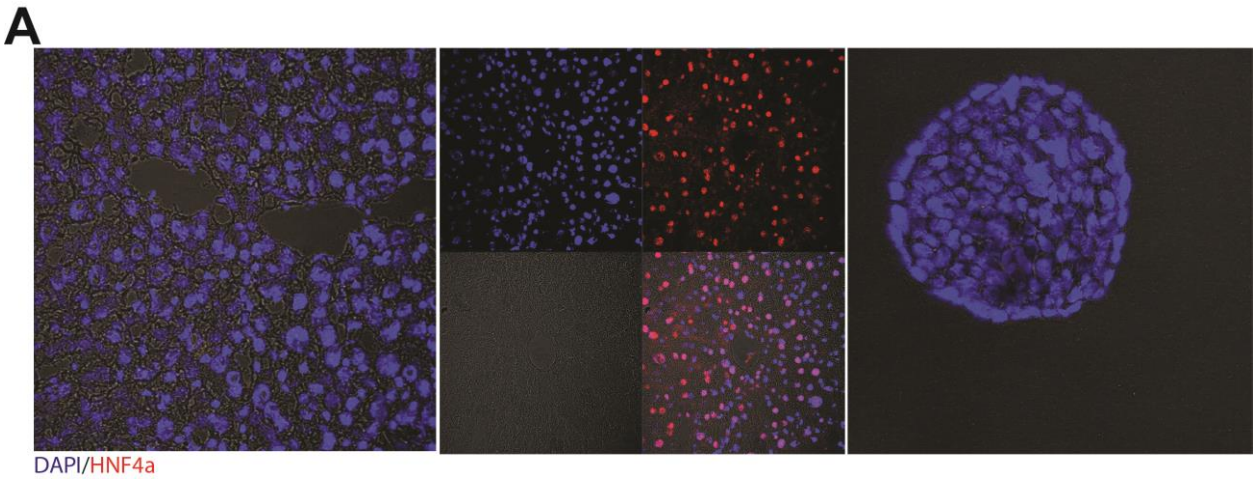


**Supplementary Fig. 4. The normal organoid do not express HNF4α.** Left panel: negative control for the antibody; Middle panel: healthy liver tissue expresses HNF4α; Right panel: the healthy organoids do not express HNF4α (40×).

| | Organoid Code | Mice Background | M/F | Primary Tumor Harvesting Time(Month) | | Organoid Code | Mice Background | M/F | Primary Tumor Harvesting Time(Month) |
|---|---|---|---|---|---|---|---|---|---|
| 1 | PT1 | B6 | M | 7 | 46 | PT52 | B6/CD1 | M | 14 |
| 2 | PT2 | B6/CD1 | M | 7 | 47 | PT57 | B6 | M | 10 |
| 3 | PT3 | B6/CD1 | M | 7 | 48 | PT59 | B6/CD1 | M | 14 |
| 4 | PT6 | B6 | M | 7 | 49 | PT61 | B6 | M | 14 |
| 5 | PT7 | B6 | M | 7 | 50 | PT62 | B6/CD1 | M | 15 |
| 6 | PT8 | B6 | M | 7 | 51 | PT63 | B6/C3H | M | 8 |
| 7 | PT9 | B6 | M | 7 | 52 | PT68 | B6 | M | 8 |
| 8 | PT10 | B6 | M | 13 | 53 | PT69 | B6 | M | 8 |
| 9 | PT11 | B6 | M | 12 | 54 | PT70 | B6 | M | 8 |
| 10 | PT12 | B6/CD1 | M | 14 | 55 | PT71 | B6 | M | 15 |
| 11 | PT13 | B6/CD1 | F | 12 | 56 | PT72 | B6/C3H | M | 7 |
| 12 | PT14 | B6/CD1 | M | 12 | 57 | PT77 | B6/CD1 | M | 14 |
| 13 | PT15 | B6/CD1 | F | 12 | 58 | PT78 | B6 | M | 8 |
| 14 | PT16 | B6 | M | 13 | 59 | PT79 | B6/C3H | M | 8 |
| 15 | PT17 | B6 | M | 10 | 60 | PT80 | B6/C3H | M | 7 |
| 16 | PT18 | B6 | M | 13 | 61 | PT81 | B6 | M | 15 |
| 17 | PT19 | B6 | M | 9 | 62 | PT82 | B6/C3H | M | 7 |
| 18 | PT20 | B6/CD1 | M | 16 | 63 | PT85 | B6/C3H | M | 7 |
| 19 | PT21 | B6/CD1 | M | 16 | 64 | PT86 | B6/C3H | M | 8 |
| 20 | PT22 | B6 | M | 9 | 65 | PT87 | B6 | M | 15 |
| 21 | PT23 | B6/C3H | M | 5 | 66 | PT88 | B6/C3H | M | 8 |
| 22 | PT24 | B6 | M | 7 | 67 | PT89 | B6 | M | 15 |
| 23 | PT25 | B6/CD1 | M | 15 | 68 | PT90 | B6 | M | 15 |
| 24 | PT26 | B6 | M | 9 | 69 | PT92 | B6/CD1 | M | 15 |
| 25 | PT27 | B6 | M | 13 | 70 | PT91 | B6 | M | 15 |
| 26 | PT28 | B6 | M | 13 | 71 | PT93 | B6/CD1 | M | 15 |
| 27 | PT29 | B6 | M | 9 | 72 | PT94 | B6 | M | 15 |
| 28 | PT30 | B6 | M | 9 | 73 | PT96 | B6 | M | 15 |
| 29 | PT31 | B6 | M | 9 | 74 | PT97 | B6 | M | 15 |
| 30 | PT32 | B6 | M | 14 | 75 | PT98 | B6 | M | 15 |
| 31 | PT35 | B6 | M | 13 | 76 | PT99 | B6 | M | 15 |
| 32 | PT36 | B6 | M | 12 | 77 | PT100 | B6/C3H | M | 8 |
| 33 | PT37 | B6 | M | 13 | 78 | PT101 | B6/C3H | M | 8 |
| 34 | PT38 | B6 | M | 6 | 79 | PT102 | B6/CD1 | M | 14 |
| 35 | PT39 | B6/C3H | M | 3 | 80 | PT103 | B6 | M | 13 |
| 36 | PT40 | B6 | F | 15 | 81 | PT104 | B6 | M | 13 |
| 37 | PT41 | B6 | M | 9 | 82 | PT105 | B6 | M | 13 |
| 38 | PT42 | B6 | M | 13 | 83 | PT107 | B6 | M | 15 |
| 39 | PT43 | B6 | M | 13 | 84 | PT108 | B6/CD1 | M | 15 |
| 40 | PT44 | B6 | M | 13 | 85 | PT109 | B6/CD1 | M | 15 |
| 41 | PT45 | B6 | M | 13 | 86 | PT110 | B6/CD1 | M | 16 |
| 42 | PT46 | B6 | M | 13 | 87 | PT111 | B6/C3H | M | 7 |
| 43 | PT47 | B6 | M | 16 | 88 | PT112 | B6 | M | 15 |
| 44 | PT49 | B6 | M | 13 | 89 | PT113 | B6/CD1 | M | 15 |
| 45 | PT51 | B6 | M | 14 | 90 | PT115 | B6 | M | 15 |

**Supplementary Table 1. Tumor organoid lines.** All the 90 tumor organoid lines, for the genetic background, gender and primary tumor formation time (counted since the time of first Den injection until the time to sacrifice the mice).

| Proliferation | AT65 | AT66 | AT71 | AT72 | AT85 | AT86 | AT83 | AT84 |
|---|---|---|---|---|---|---|---|---|
| Sorafenib,10μM, Initiation | ↓↓↓ | ↓↓↓ | ↓ | ↓↓↓ | ↓↓ | ↓↓ | ↓↓ | ↓↓ |
| Sorafenib, 10μM, Post Day3 | ↓↓ | ↓↓ | ↓↓ | ↓↓↓ | ↓↓↓ | ↓↓↓ | ↓↓ | ↓↓↓ |
| Regorafenib, 10μM, Initiation | ↓↓↓ | ↓↓ | ↓↓ | ↓ | ↓↓ | ↓ | ↓ | ↓↓ |
| Regorafenib, 10μM, Post Day3 | ↓ | ↓ | ↓ | ↓↓ | ↓ | ↓↓ | ↓ | ↓ |

**Supplementary Table 2. Tumor organoids respond differently to drugs.** Inhibition of growth in response to drug treatment is depicted relative to the untreated group and divided in three categories: weak inhibition (100%-60%, ↓), moderate inhibition (60%-40%, ↓ ↓) and strong inhibition (40%-0%, ↓ ↓ ↓).

| Organoid number | AT65 | AT66 | AT71 | AT72 | AT85 | AT86 | AT83 | AT84 |
|---|---|---|---|---|---|---|---|---|
| Sorafenib, 10μM , Initiation | ↓↓↓ | ↓↓↓ | ↓↓↓ | ↓↓↓ | ↓↓↓ | ↓↓↓ | ↓↓↓ | ↓↓↓ |
| Regorafenib, 10μM, Initiation | ↓ | ↓ | ↓ | ↓ | ↓↓ | ↓↓ | ↓ | ↓↓ |

**Supplementary Table 3. Tumor organoids respond differently to the drug.** For the inhibition of the organoid initiation, response to the drug was exhibited by the relative initiated organoid number compared to the drug-untreated group and also divided into three categories: weak inhibition (100%-50%, ↓), moderate inhibition (50%-20%, ↓ ↓) and strong inhibition (20%-0%, ↓ ↓ ↓).

| Antibody | Antibody clone/ reference | Raised | Origin |
|---|---|---|---|
| HNF4α | sc-8987 X | Rabbit | STCruz |
| CK19 | ab52625 | Rabbit | Abcam |
| CD44 | ab157107 | Rabbit | Abcam |
| Donkey anti-Rabbit IgG (H+L) Secondary Antibody, Alexa Fluor® 594 conjugate | A-21207 | Donkey | Thermo fisher |

**Supplementary Table 4. The antibodies employed in this study**

| Gene name | Gene Symbol | Sequence | |
|---|---|---|---|
| Leucine-rich repeat-containing G-protein coupled receptor 5 | *Lgr5* | fw | CTG ACT TTG AAT GGT GCC TCG |
| | | re | ATG TCC ACT ACC GCG ATT AC |
| Antigen Cd44 | *Cd44* | fw | CGT CCA ACA CCT CCC ACT AT |
| | | re | AGC CGC TGC TGA CAT CGT |
| Transcription factor SOX-9 | *Sox9* | fw | CGA CTA CGC TGA CCA TCA GA |
| | | re | GAC TGG TTG TTC CCA GTG CT |
| SRY (sex determining region Y)-box 17 | *Sox17* | fw | GGC GCA GCA GAA TCC AGA |
| | | re | CCA CGA CTT GCC CAG CAT |
| Antigen Cd133 | *Cd133* | fw | TCT GTT CAG CAT TTC CTC AC |
| | | re | TCA GTA TCG AGA CGG GTC |
| Transcription factor Nanog | *Nanog* | fw | AGG GTC TGC TAC TGA GAT GCT CTG |
| | | re | CAA CCA CTG GTT TTT CTG CCA CCG |
| Octamer-binding transcription factor 4 | *Oct4* | fw | CTG TAG GGA GGG CTT CGG GCA CTT |
| | | re | CTG AGG GCC AGG CAG GAG CAC GAG |
| SRY (sex determining region Y)-box 2 | *Sox2* | fw | GGC AGC TAC AGC ATG ATG CAG GAG C |
| | | re | CTG GTC ATG GAG TTG TAC TGC AGG |
| Cytokeratin-19 | *Krt19* | fw | GTG AAG ATC CGC GAC TGG T |
| | | re | AGG CGA GCA TTG TC AAT CTG |
| Polycomb complex protein | *Bmi1* | fw | TTC ATT GAT GCC ACA ACC AT |
| | | re | CAG CAT CAG CAG AAG GAT GA |

**Supplementary Table 5. The primers employed in this study**

# Reference:


1. Llovet JM, Ricci S, Mazzaferro V, et al. Sorafenib in advanced hepatocellular carcinoma. N Engl J Med 2008;359:378-90.

2. Voskoglou-Nomikos T, Pater JL, Seymour L. Clinical predictive value of the in vitro cell line, human xenograft, and mouse allograft preclinical cancer models. Clin Cancer Res 2003;9:4227-39.

3. Llovet JM, Zucman-Rossi J, Pikarsky E, et al. Hepatocellular carcinoma. Nat Rev Dis Primers 2016;2:16018.

4. Huch M, Dorrell C, Boj SF, et al. In vitro expansion of single Lgr5+ liver stem cells induced by Wnt-driven regeneration. Nature 2013;494:247-50.

5. Bredenoord AL, Clevers H, Knoblich JA. Human tissues in a dish: The research and ethical implications of organoid technology. Science 2017;355.

6. van de Wetering M, Francies HE, Francis JM, et al. Prospective derivation of a living organoid biobank of colorectal cancer patients. Cell 2015;161:933-45.

7. Huang L, Holtzinger A, Jagan I, et al. Ductal pancreatic cancer modeling and drug screening using human pluripotent stem cell- and patient-derived tumor organoids. Nat Med 2015;21:1364-71.

8. Gao D, Vela I, Sboner A, et al. Organoid cultures derived from patients with advanced prostate cancer. Cell 2014;159:176-87.

9. Schutte M, Risch T, Abdavi-Azar N, et al. Molecular dissection of colorectal cancer in pre-clinical models identifies biomarkers predicting sensitivity to EGFR inhibitors. Nat Commun 2017;8:14262.

10. Tetteh PW, Basak O, Farin HF, et al. Replacement of Lost Lgr5-Positive Stem Cells through Plasticity of Their Enterocyte-Lineage Daughters. Cell Stem Cell 2016;18:203-13.

11. Zhou X, Wang Y, Metselaar HJ, et al. Rapamycin and everolimus facilitate hepatitis E virus replication: revealing a basal defense mechanism of PI3K-PKB-mTOR pathway. J Hepatol 2014;61:746-54.

12. He L, Tian DA, Li PY, et al. Mouse models of liver cancer: Progress and recommendations. Oncotarget 2015;6:23306-22.

13. Pan Q, Fouraschen SM, de Ruiter PE, et al. Detection of spontaneous tumorigenic transformation during culture expansion of human mesenchymal stromal cells. Exp Biol Med (Maywood) 2014;239:105-15.

14. Peitzsch C, Tyutyunnykova A, Pantel K, et al. Cancer stem cells: The root of tumor recurrence and metastases. Semin Cancer Biol 2017.

15. La Porta CA, Zapperi S. Complexity in cancer stem cells and tumor evolution: Toward precision medicine. Semin Cancer Biol 2017.

16. Kim H, Park C, Han KH, et al. Primary liver carcinoma of intermediate (hepatocyte-cholangiocyte) phenotype. J Hepatol 2004;40:298-304.

17. Bruix J, Tak WY, Gasbarrini A, et al. Regorafenib as second-line therapy for intermediate or advanced hepatocellular carcinoma: multicentre, open-label, phase II safety study. Eur J Cancer 2013;49:3412-9.

18. Lin ZY, Wu CC, Chuang YH, et al. Clinical utility of a simple primary culture method in hepatocellular carcinoma patients. J Gastroenterol Hepatol 2015;30:352-7.

19. Skardal A, Devarasetty M, Rodman C, et al. Liver-Tumor Hybrid Organoids for Modeling Tumor Growth and Drug Response In Vitro. Ann Biomed Eng 2015;43:2361-73.

20. Mori R, Sakai Y, Nakazawa K. Micropatterned organoid culture of rat hepatocytes and HepG2 cells. J Biosci Bioeng 2008;106:237-42.

21. Takai A, Fako V, Dang H, et al. Three-dimensional Organotypic Culture Models of Human Hepatocellular Carcinoma. Sci Rep 2016;6:21174.

22. Yamashita T, Wang XW. Cancer stem cells in the development of liver cancer. J Clin Invest 2013;123:1911-8.

23. Junttila MR, Mao W, Wang X, et al. Targeting LGR5+ cells with an antibody-drug conjugate for the treatment of colon cancer. Sci Transl Med 2015;7:314ra186.

24. Shimokawa M, Ohta Y, Nishikori S, et al. Visualization and targeting of LGR5(+) human colon cancer stem cells. Nature 2017;545:187-192.

# CHAPTER 4

## LGR5 marks tumor initiating cells and represents a new therapeutic target in liver cancer

Wanlu Cao[1], Meng Li[1], Jiaye Liu[1], Buyun Ma[1], Kan Chen[1], Wenshi Wang[1], Michiel Bolkestein[2,3], Luc J. W. van der Laan[3], Dave Sprengers[1], Jaap Kwekkeboom[1], Ron Smits[1], Maikel P. Peppelenbosch[1] and Qiuwei Pan[1]

[1]Department of Gastroenterology and Hepatology, Erasmus MC-University Medical Center, Rotterdam, The Netherlands.

[2]Department of Cell Biology, Erasmus MC-University Medical Center, Rotterdam, The Netherlands.

[3]Department of Surgery, Erasmus MC-University Medical Center, Rotterdam, The Netherlands.

## Abstract:

**Background & Aims**: Leucine-rich repeat-containing G-protein coupled receptor 5 (Lgr5) is a recently identified marker for a liver stem cell population. However, the existence and function of LGR5 cells in liver cancer has not been demonstrated. Here we investigate the role of hepatic LGR5-expressing cells in liver tumors.

**Methods:** A LGR5-promotor driven diphtheria toxin (DT) receptor knock-in mice model with a GFP reporter were used. Carbon tetrachloride ($CCL_4$) was used to induce chronic liver injury and diethylnitrosamine (DEN) was used to induce primary liver tumors in mice.

**Results:** We observed that the carcinogen DEN induces a liver LGR5-positive stem cell compartment. In thus-induced hepatic tumors, the percentage of LGR5 cells is significantly higher as compared to tumor adjacent tissue (n=28, P< .05, 3-fold higher), and this even more apparent when compared to tissue of $CCl_4$-induced chronic injury (n=28, P<0. 001, 52-fold higher). Tumor organoids generated by *ex vivo* culturing of primary mouse liver tumor contain an LGR5-expressing cell population. Subcutaneous transplantation of these tumor organoids into immunodeficient NOG mice results in solid tumors, which retain a LGR5 positive compartment. Isolation and culturing of single $LGR5^+$ cell from primary mouse tumor initiated tumor organoids, and transplantation of these organoids into NOG mice formed tumor again. Thus, these cells have cancer initiating/stem cell-like properties. Importantly, LGR5 cancer cells are resistant to therapeutic agents and specific depletion of these cells impedes the growth of liver tumors *in vivo*.

**Conclusion:** Hepatic LGR5 stem cells contribute to DEN-induced liver carcinogenesis and LGR5 marks tumor initiating cells. Thus targeting LGR5-positive cells appears promising as an anti-cancer strategy in the liver.

**Keyword:** LGR5, Tumor stem cell, Tumor organoid, Liver tumor

## Introduction

The key concept of cancer stem cell theory is that tumor contains a hierarchical structure with different functional populations of cells [1]. The bulk of a tumor consists of cancer stem cells as well as rapidly proliferating cells. Cancer stem cells are responsible for tumor initiation and fueling the growth of tumor continually, as well as responsible for the local tumor recurrence and distant metastasis. Rapidly proliferating cell are responsible for enlarging the volume of the tumor and are thought to be derived from the tumor stem cell pool.

Classically, the identification of cancer stem cells is based on the following features: 1) strong self-renewal capability; 2) differentiation into different types of cells; 3) resistance to treatment. Those are also the key features of normal stem cells. Thus, normal stem cell/embryonic stem cell markers are widely used to identify cancer stem cells [2]. LGR5 (leucine-rich repeat-containing G protein-coupled receptor 5) is a well-characterized stem cell marker in several organs, including the intestine, the colon and the liver [3-5]. In the colon and the intestine, the LGR5 stem cell pool regularly proliferates to compensate for the loss of functional cells. Interestingly, LGR5 stem cells from colon/intestine are already reported to participate in the tumor formation and progression, acting as cancer stem cell/ tumor initiating cells [6-8]. In adenoma as well as malignant carcinoma, LGR5 cells account consistently for a ratio of 10%-25% [6, 9]. Considering the notion that cancer stem cells are relatively resistant to the regular treatment, the development of new treatment targeting cancer stem cells is attractive. It has been reported that elimination of colorectal cancer LGR5 cells can delay the growth of the colon cancer, without major impact on the function of normal LGR5 stem cells [7].

In contrast to the colon/intestine, liver LGR5 cells are not present in normal liver homeostasis, but emerge upon liver injury. Thus, liver LGR5 cells are classified as an injury response stem cell population [10]. However, the existence and function of LGR5 cells in liver cancer remain largely elusive. Thus, this study aims to investigate whether liver LGR5 cells participate in tumor formation and progression, and whether represent as a therapeutic target for treating liver cancer.

## Materials and Methods

### *Primary liver tumor model*

*Lgr5-DTR-GFP* transgenic mice (kindly provided by Genentech) specifically co-express the diphtheria toxin (DT) receptor (DTR) and Green florescent protein (GFP) under the control of the *Lgr5* promotor [11]. Thus, $LGR5^+$ cells will be identified by GFP, and $LGR5\text{-}GFP^+$ cells can be specifically depleted by DT administration. *Lgr5-DTR-GFP* transgenic mice (3-4 weeks) were administrated with Diethylnitrosamine (DEN) by intraperitoneal injection (i.p., 100 mg/kg) weekly for 6-17 weeks. Mice were sacrificed 3-16 months after the last DEN injection and livers/tumors were collected for further experiments. All animal experiments were approved by the Committee on the Ethics of Animal Experiments of the Erasmus Medical Center.

### *Tumor Organoid Culture*

Digestion solution II (37°C, 30 min, 500 µg/ml of collagenase type XI, 200 µg/ml of Dnase-1, 1% FBS in DMEM medium) was used to digest liver or tumor tissues into single cell suspension. Single cell suspension was directly mixed with matrigel and then used for culturing, or further sorted for further experiments. Sorted cells were also mixed with matrigel and seeded for organoid initiation. Cells were cultured in organoid culture medium as previously published [10, 12]. For the first 8-12 days, the organoids were supplemented with 10 µM Y-27632 (Sigma-Aldrich), Noggin and Wnt3a conditioned medium. Medium was refreshed every 2 days and passage was performed in split ratios of 1:2-1:15 weekly.

### *Histology, Immunohistochemistry and Immunofluorescence*

Liver or tumor was fixed in 4% paraformaldehyde (PFA) overnight at 4°C. For immunofluorescence, samples were further dehydrated with 30% sucrose (Sigma-Aldrich, 4°C, overnight), stored at -80°C and then sectioned at 8 µm for further analysis. Images were acquired with a Zeiss LSM510META confocal microscope. For histology and immunohistochemistry, materials were dehydrated with 70% ethanol, embedded with paraffin, sectioned at 4 µm for staining. Images were acquired with a Zeiss Axioskop 20 microscope. All antibodies are listed in Supplementary Table 1.

### *Organoid allografting*

Cold advanced DMEM/F12 medium was used to collect the organoids. After centrifuging, supernatant was discarded and organoids pellets were mixed directly with matrigel in the ratio of 1:1 with a total volume of 200 µl. 4-6 weeks old female NOG/JicTac (CIEA NOD.Cg-Prkdc-scid Il2rg-tm1Sug) mice or nude mice (NMRI:BomTac- Nude) were purchased from Taconic, and subcutaneously injected with the collected tumor organoids. Tumor dimensions were measured using calipers and tumor volume was calculated as 0.523× length× width× width [7]. Tumor formation was monitored every other day and mice were sacrificed to harvest tumor after the tumor diameter reached approx.2 cm. Tumor tissues were stored or cultured as described above.

***Diphtheria Toxin-mediated Cell Ablation***

To ablate $LGR5^+$ cells in organoids, DT (1-10 ng/ml) was added to organoid expansion/initiation medium, followed by further analysis [12]. For *in vivo* ablation, DT was administrated via intraperitoneal injection every other day (50 µg per kg). If mice suffer from weight loss⩾10%,compared to the previous injection, the injection was omitted.

***FACS Analysis***

For FACS analysis, single cells derived from liver and organoids were suspended in DMEM plus 2% FBS. Cell suspensions were analyzed using a BD FACSCalibur or BD FACSAria™ II. For FACS sort, a BD FACSAria™ II cell sorter was used to isolate the target cell population. Propidium iodide (PI) staining was performed to exclude dead cells and CD45 staining was adopted for excluding leucocytes.

***Metabolic activity analysis of organoids***

Different organoid lines were seeded separately in a 24/48-well plate. Sorafenib (10 µM) or 5-FU (10 µM) was added to the organoid culture since the initial day or post-initiation day 3, respectively. Drugs were refreshed every other day. At the day 6-7, organoids were incubated with Alamar Blue (Invitrogen, 1:20 in DMEM) for four hours (37°C), and then medium was collected for analysis of the metabolic activity of the cells. Absorbance was determined by using fluorescence plate reader (CytoFluor® Series 4000, Perseptive Biosystems) at the excitation of 530/25nm and emission of 590/35. Each treatment

condition was repeated for four times and matrigel with medium only was used as a blank control.

***Statistical Analysis***.

Prism software (GraphPad Software) was used for all statistical analysis. For statistical significance of the differences between the means of groups, we used a Mann-Whitney U-test. Differences were considered significant at a *P* value less than 0.05.

## Results

### *DEN-induced primary liver tumors contain LGR5 expressing cells*

Employing *Lgr5-DTR-GFP* knock-in mice (Figure 1A), we first confirmed that LGR5$^+$ cells (GFP expressing cells) are absent in the healthy liver. We then induced primary liver tumors by repeated administration of carcinogen compound DEN (Figure 1B). We observed that single/repeated administration of DEN triggered the emergence of LGR5-GFP$^+$ cells in the liver within a short period (mean ± SEM, 1 × DEN: 0.025 ± 0.05%, n = 3) (Supplementary Figure 1A-B). After 4-14 months of tumor formation, we found that LGR5 expressing cells remained stably present in the liver tumor, as well as in tumor surrounding tissues (Figure 1C). Liver tumors (7.3 ± 1.7%, N=58) have significantly higher percentage of LGR5-GFP$^+$ cells compared to tumor surrounding tissues (2.4 ± 1.1%, N=29). Compared to the liver injured with single/repeated $CCl_4$ and livers in physiological homeostatis, the DEN-treated livers have significantly upregulated percentages of LGR5 cells (Figure 1D). We observed that the percentages of LGR5-GFP$^+$ cells within liver tumor varied from 0.081% up to 55.6% (Supplementary Figure 1C-D). The expression level of tumor LGR5 also showed different levels of upregulation compared to injury induced LGR5 expressing cells (Figure 1E). Both anti-GFP immunohistochemistry and immunofluorescence depended on the GFP expression both confirmed the expression of LGR5-GFP (IF: Figure 1F; IHC: Supplementary Figure 1E-F). We also observed different types of localization of LGR5-GFP$^+$ cells (IF: Figure 1F; IHC: Supplementary Figure 1E-F). After co-staining with hepatocyte marker (HNF4α) or cholangiocyte marker (CK19) respectively by immunofluorescence, we found that LGR5-GFP$^+$ cells can express hepatocyte or cholangiocyte markers (Figure 1G-H). Thus, these data demonstrated that LGR5$^+$ cells are present in DEN induced primary murine liver tumors.

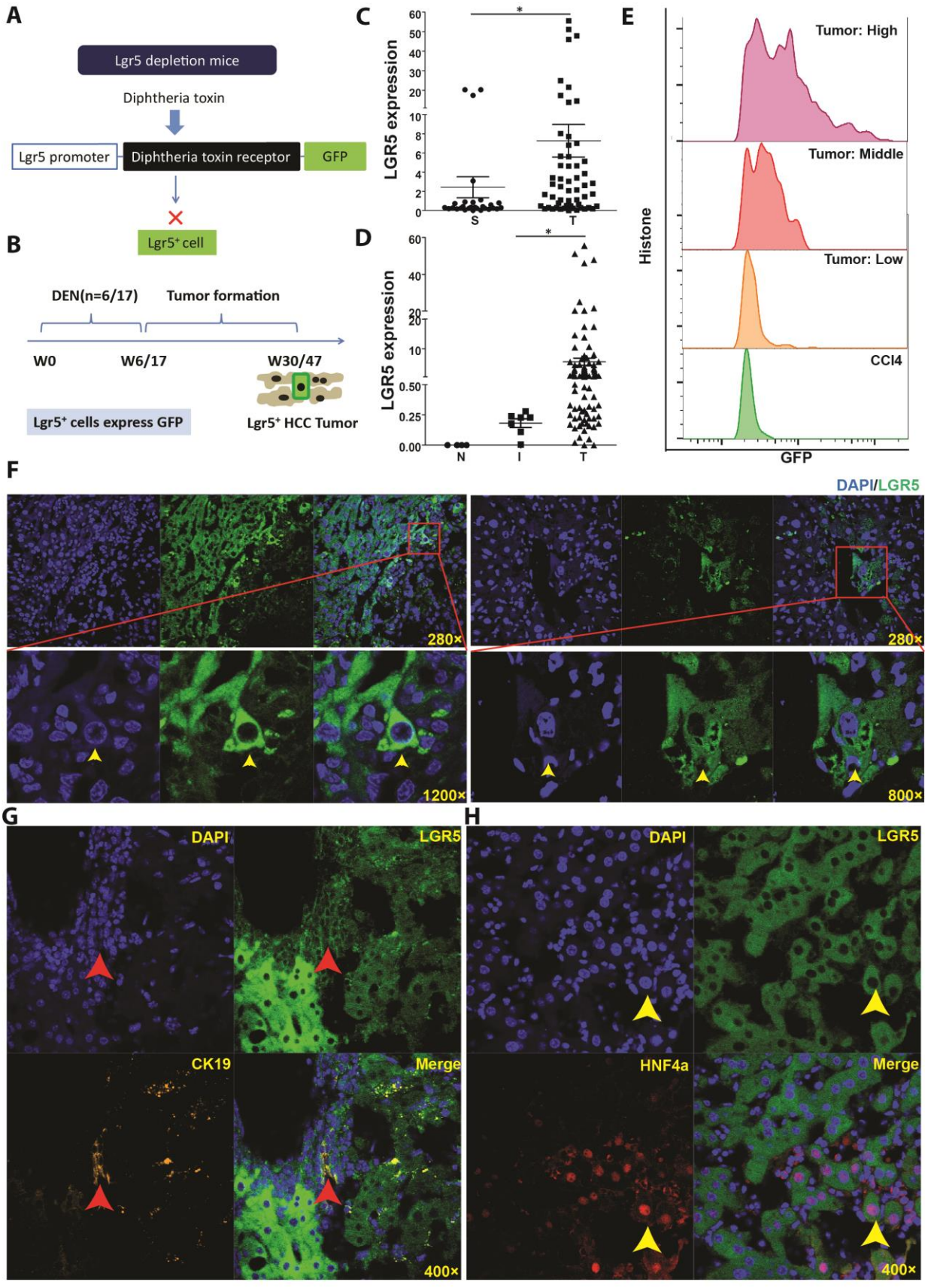


**Figure 1:** LGR5 expressing cells are present in the DEN-induced primary liver tumors. (A) A schematic of the *Lgr5-DTR-GFP* transgenic mouse model used. (B) An outline of the experimental strategy used. (C) LGR5$^{+}$ cells showed significant upregulation in liver tumor, compared to tumor surrounding tissue (*$P$ < .05). S: tumor surrounding tissues; T: tumors. (D) LGR5$^{+}$ cells showed

significant upregulation in DEN induced liver, compared to healthy liver and $CCL_4$ induced injured liver (*$P$ < .05). N: normal liver; I: $CCL_4$ injured liver; T: DEN induced liver. (E) Liver tumor $LGR5^+$ cells showed enhanced fluorescence intensity compared to healthy liver $LGR5^+$ cells. (F) Representative pictures showing LGR5 cells existed in liver tumors, which indicated by anti-GFP immunofluorescence staining; Yellow arrow: $LGR5^+$ cell. DAPI: blue. (G) Representative confocal images for the expression of hepatocyte-specific marker (HNF4α, red) and cholangiocyte marker (CK19, yellow) in LGR5-GFP expressing cells.

### *Allograft liver tumors sustain LGR5 cells*

To further characterize the LGR5 expressing compartment in liver tumor, we established organoid cultures from primary liver tumors. After tumor formation, murine liver tissues were collected and cultured with matrigel in a 3D system (Supplementary Figure 2A). In total, 66 organoid strains were obtained from 37 independent livers. The successfully established lines could be maintained and propagated in 3D culture for at least 5 months (the maximum time period tested so far), by passaging in the ratio of 1:2-1:4 for every 7 days. With respect to the morphology, organoids derived from liver tumors presented diverse aspects, ranging from a normal outlook, to bubble-like (Supplementary Figure 2C), condensed (Supplementary Figure 2D), and flower-like, irregular sheet-like structures (Supplementary Figure 2E).

**Figure 2:** Allograft liver tumors sustain the expression of LGR5. (A) The expression of LGR5 in allograft tumor and the corresponding primary tumor. (B) The distribution of LGR5 expression percentages in allograft tumors and the corresponding primary tumors. (C) Representative pictures showing LGR5 cells existed in allograft liver tumors, which indicated by anti-GFP immunohistochemistry staining. $LGR5^+$ cell: Brown; DAPI: blue. (D-E) Representative pictures showing the organoid lines that mainly express the hepatocyte marker HNF4α (D) and the cholangiocyte marker CK19 (E). (F-G) Representative pictures showing the HCC (F) and CC (G) organoid lines.

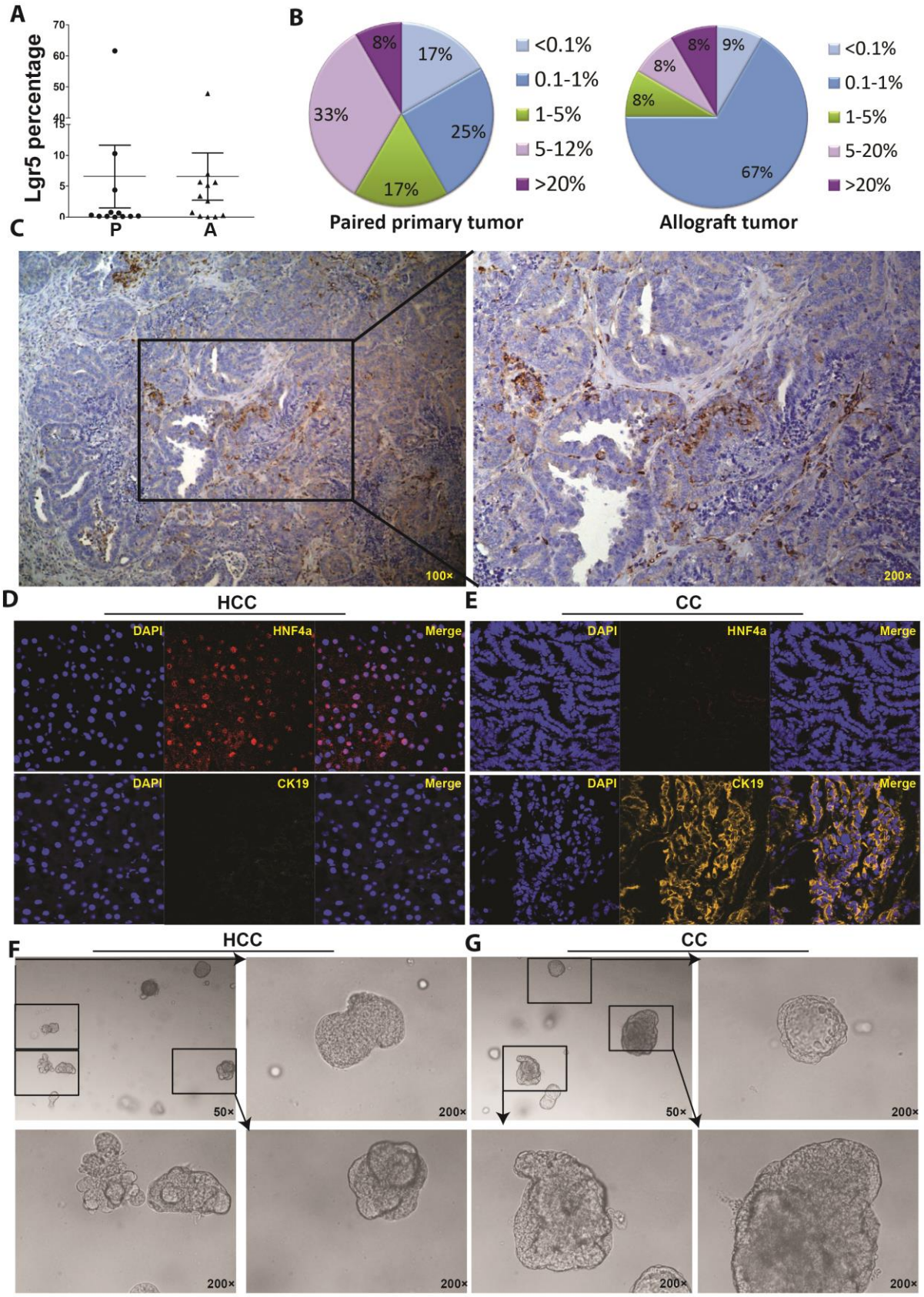


To further confirm that these organoid strains were indeed malignant, we transplanted the organoid into immunodeficient NOG mice (Supplementary Figure 2A). After 1-6 months of tumor formation, 12 out of 66 strains of the organoid formed tumor (18.2%). We

further collected the allograft tumors and checked the Lgr5 expression by FACS machine. The FACS results indicated that the expression of LGR5 is retained in the allograft tumors (Figure 2A-C). We also collected the allograft tumor and cultured these into organoids again. After 1-3 days of culturing, small organoids could be observed and passaging was performed every 4-7 days, in a ratio of 1:4-1:20. We further stained these allograft tumor-initiating organoids with CK19 and HNF4α respectively, to establish whether these organoids are of a cholangiocyte carcinoma (CC) or a hepatocellular carcinoma (HCC)-like phenotype (Supplementary Figure 2F). Among these tumor initiating organoid strains, 2 out of 12 were HCC-like; 10 out of 12 were CC/CHC-like. This CK19 and HNF4α staining of the corresponding allograft tumors also further confirmed the tumor type (Figure 2D). The expression of LGR5 is maintained in the organoid cultures (Supplementary Figure 2G). In conjunction these results indicate that LGR5 cells are constitutively present in allograft liver tumors.

## *Single LGR5 cells from liver tumor have a relative large organoid initiating ability*

To functionally characterize LGR5 liver tumor cells, we carried out an organoid initiation assay, that measures the clonogenic ability of single LGR5 expressing cells. By using FACS, LGR5-GFP$^{+}$ and LGR5-GFP$^{-}$ cells were sorted from liver tumors, and cultured in 3D matrigel (Figure 3A and Supplementary Figure 3A). After 2-3 weeks of organoid formation, we observed that LGR5-GFP$^{+}$ cells can form organoids and have a larger organoid forming ability compared to LGR5-GFP$^{-}$ cells (LGR5$^{+}$: 1.9 ± 0.7% Vs. LGR5$^{-}$: 0.1 ± 0.1%, N=25) (Figure 3B-C).

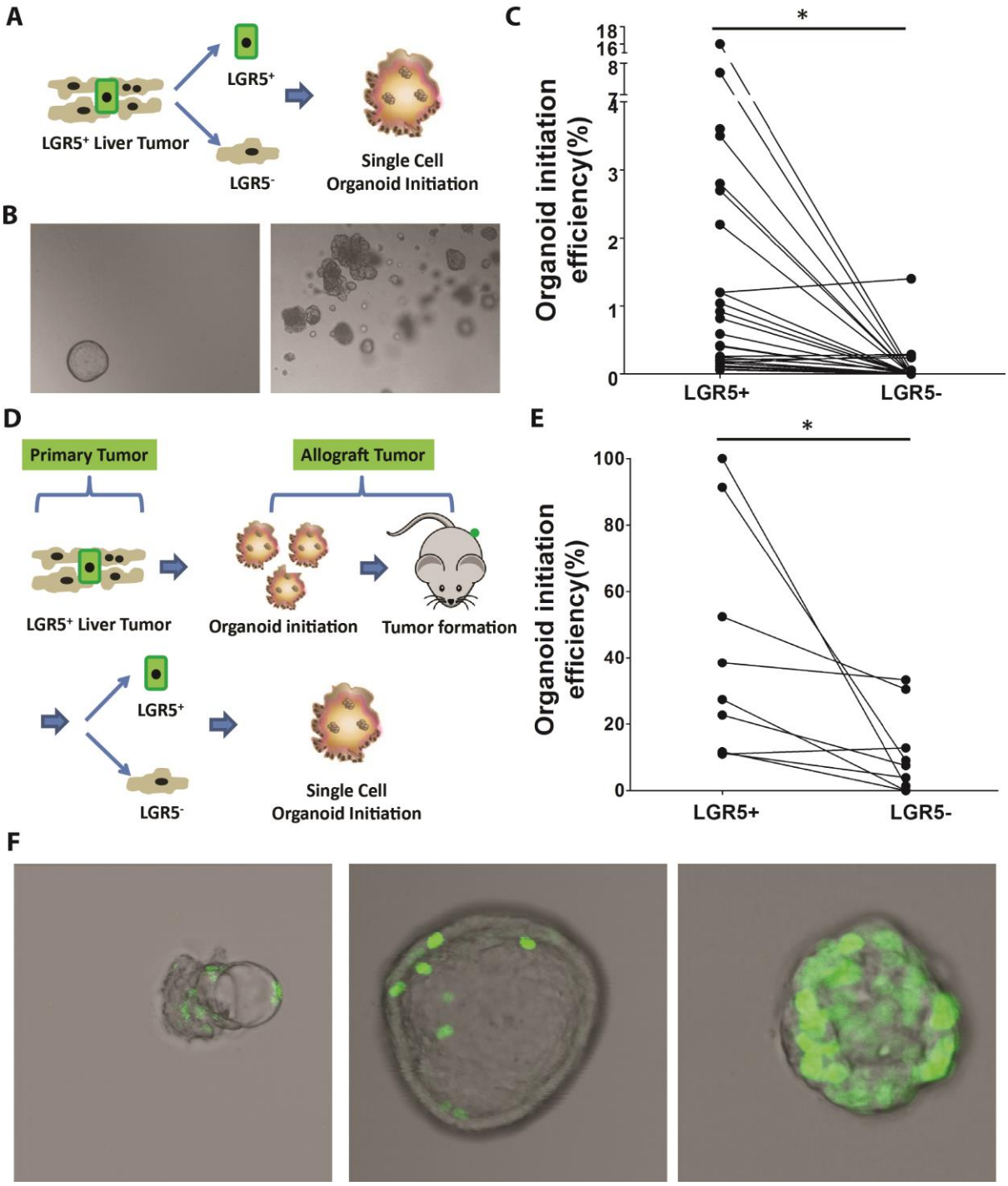


**Figure 3:** Single LGR5 cells have strong organoid initiation ability *in vitro*. (A) An outline of the experimental strategy used. (B) Representative pictures showing single LGR5$^+$ cells initiated organoids from CC (Left) and HCC (Right) tumors. (C) The organoid initiation efficiency of LGR5-GFP$^+$ and LGR5-GFP$^-$, isolated from primary liver tumor (*$P$ < .05). (D) An outline of the experimental strategy used. (E) The organoid initiation efficiency of LGR5-GFP$^+$ and LGR5-GFP$^-$, isolated from allograft liver tumor (*$P$ < .05). (F) Representative pictures showing that single LGR5$^+$ cells can initiate organoids which can give birth to both LGR5$^+$ and LGR5$^-$ offspring.

We also performed this organoid initiation assay on allograft tumors (Figure 3D). The LGR5-GFP$^+$ cells derived from allograft tumors also have more organoid initiating ability as compared to LGR5-GFP$^-$ cells (LGR5$^+$: 40.5 ± 10.2% Vs. LGR5$^-$: 10.9 ± 4.2%, N=10 (Figure 3E-F). These single LGR5-GFP$^+$ cells-initiated organoids maintained a LGR5

positive compartment, but also gave birth to LGR5 negative offspring,indicating a possible hierarchical structure (Figure 3F). Thus, these results indicate that $LGR5^+$ cells have larger organoid forming ability when compared to the $LGR5^-$ pool of cells.

## *$LGR5^+$ cells can initiate tumors in vivo*

To further investigate the tumor initiating ability of $LGR5^+$ tumor cells, we performed an *in vivo* tumor formation assay. Upon isolation by FACS, we transplanted the same number of $LGR5^+$ and $LGR5^-$ cells directly into the NOG mice (Figure 4A). After 1-6 month of tumor formation, we observed that $LGR5^+$ showed stronger tumor initiating capacity as compared to $LGR5^-$ cells (n = 3, Figure 4B). We further harvested these tumors and tested the LGR5 expression using GFP expression as a surrogate by FACS. We found that the $LGR5^+$ cells initiated tumors that contained both an $LGR5^+$ and $LGR5^-$ population (Figure 4C and H). Anti-GFP immunohistochemistry and immunofluorescence also showed the existence of LGR5 positive cells, as well as the LGR5 negative cells, in $LGR5^+$ cells initiated tumors (Figure 4I-J). Thus, these results indicated that LGR5-expressing cells have more tumor initiating capacity as compared to $LGR5^-$ cells.

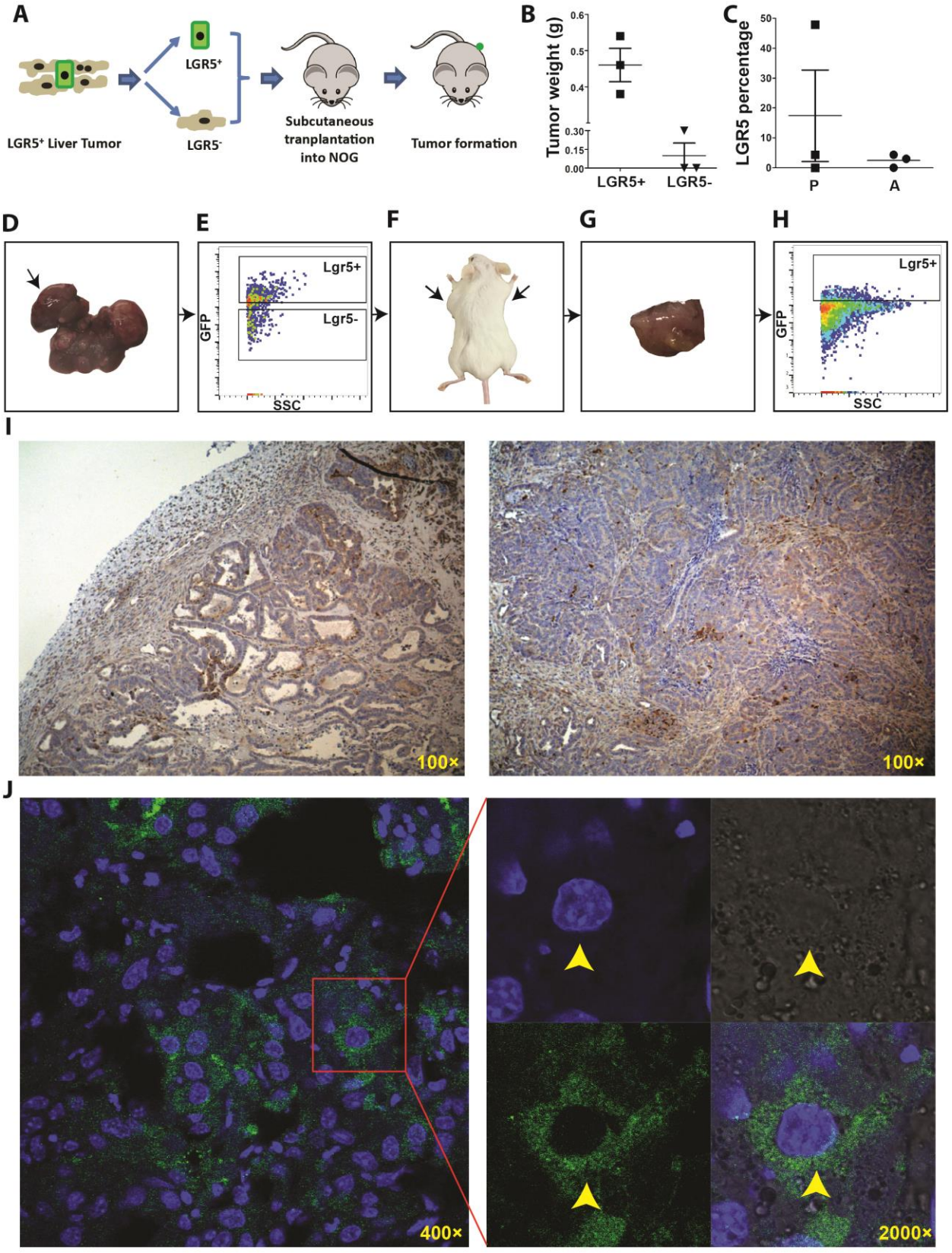


**Figure 4**: LGR5$^{+}$ cells can initiate tumors *in vivo*. (A) The outline of the experimental strategy used. (B) The exact weight of tumors initiated by LGR5$^{+}$ and LGR5$^{-}$ cells. (C) The LGR5 expression in single LGR5$^{+}$ cells initiated allograft tumors and corresponding primary tumors. (D-H) Representative pictures showing that LGR5-GFP$^{+}$ and LGR5-GFP$^{-}$ cells (E) were both isolated from DEN-induced primary liver tumor (E). An LGR5-GFP$^{+}$ cell-initiated allograft tumor after five months (F-G). The initiated allograft tumor sustained LGR5 expression (H). (I-J) Representative

immunohistochemistry (I) and immunofluorescence (J) pictures showing the presence of LGR5 in sorted LGR5$^+$ cells in an allograft tumor, employing anti-GFP staining as a surrogate marker; Yellow arrow: LGR5$^+$ cell; DAPI: blue; Green: LGR5$^+$ cell.`

## *LGR5 expressing cells are more resistant to treatment.*

Tumor initiating/stem cells are thought to be relatively resistant to treatment. Currently, the only FDA-approved drug for treating HCC is Sorafenib. Thus, we first investigate how LGR5$^+$ liver tumor cells respond to Sorafenib (Figure 5A). Considering that primary tumor organoid strains may contain untransformed cells as well, we employed for these experiments the allograft tumor strains which have confirmed malignant potential. We observed that the treatment of Sorafenib increased the relative size of the LGR5 positive compartment (Figure 5B-D). An even more profound increase of LRG5 cells was observed under treatment with the chemotherapeutic agent, 5-FU (Figure 5A) (Figure 5C-D). We then further evaluated how LGR5$^+$ liver tumor cells respond to treatment *in vivo* (Figure 5E). Similar results were observed (Figure 5F). Thus, LGR5-expressing cells from liver tumors are relatively resistant to treatment.

## *Targeting LGR5 inhibits the growth of tumor organoids*

To explore the therapeutic potential of targeting LGR5 cells in liver cancer, we first investigated whether specific depletion of LGR5 will influence organoid expansion *in vitro*. Because the *Lgr5-DTR-GFP* mice co-express DTR, LGR5-GFP$^+$ cells can be specifically depleted by DT administration (Figure 6A). In agreement with our previous research, 1 -10 ng/ml of DT can deplete the LGR5 in the healthy organoid culture with a high efficiency [12]. Thus, we adopted a similar strategy of DT treatment of tumor organoids to study the effects of depletion of LGR5 cells on organoid growth. To this end, we evaluated the effects on organoid initiation and expansion through treating with DT at initiating the culture or at post passage day 3. Interestingly, we observed that the depletion of LGR5-expressing cells inhibited the growth of the tumor organoids and that these effects correlated to the initial relative size of the LGR5$^+$ compartment. Cultures of organoid strains with higher percentages of LGR5 cells were relatively more sensitive to the DT (Figure 6D and F). In contrast, the initiation and expansion of organoid strains with relatively lower percentages of LGR5 cells were not significantly affected by DT treatment (Figure 6E and G). As a control: DT treatment did not influence the initiation and

expansion of the wide type tumor organoids (Figure 6C). Thus, these results revealed that depletion of LGR5 cells inhibited tumor organoid formation and growth.

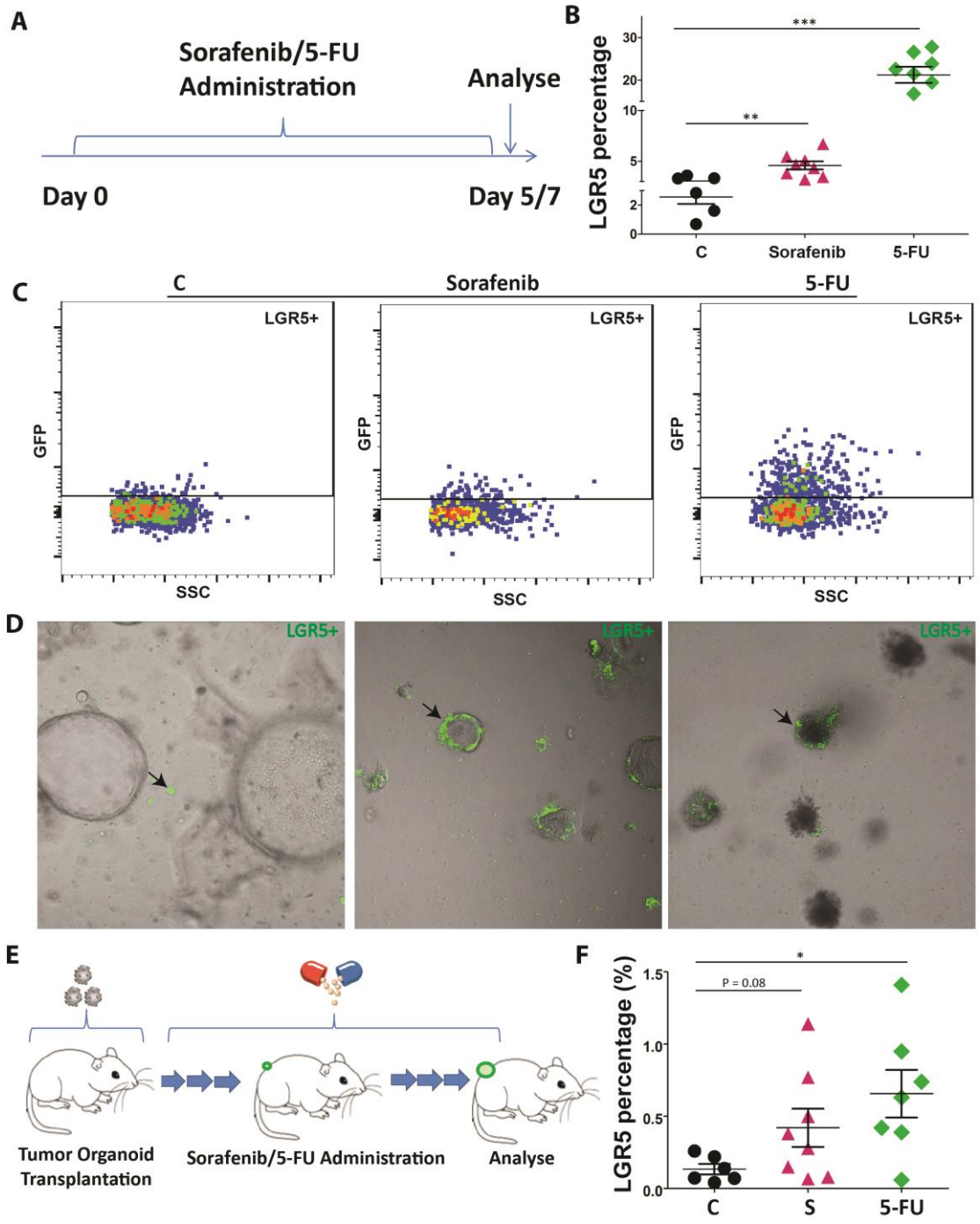


**Figure 5**: LGR5 expressing cells are more resistant to treatment. (A) An outline of the experimental strategy used to investigate how Lgr5 expressing cells respond to treatment *in vitro*. (B) LGR5-GFP$^+$ cells become significantly more frequent upon administration of Sorafenib and 5-FU. **P< 0.01, ***P< 0.001. (C-D) Representative FACS plots (C) and confocal pictures (D) indicating that LGR5-GFP$^+$ cells were upregulated upon administration of Sorafenib and 5-FU. (E) An outline of the experimental strategy used to investigate how Lgr5 expressing cells respond to treatment *in vivo*. (F) LGR5-GFP$^+$ cells become more frequent upon administration of Sorafenib and 5-FU *in vivo*. *P< 0.01.

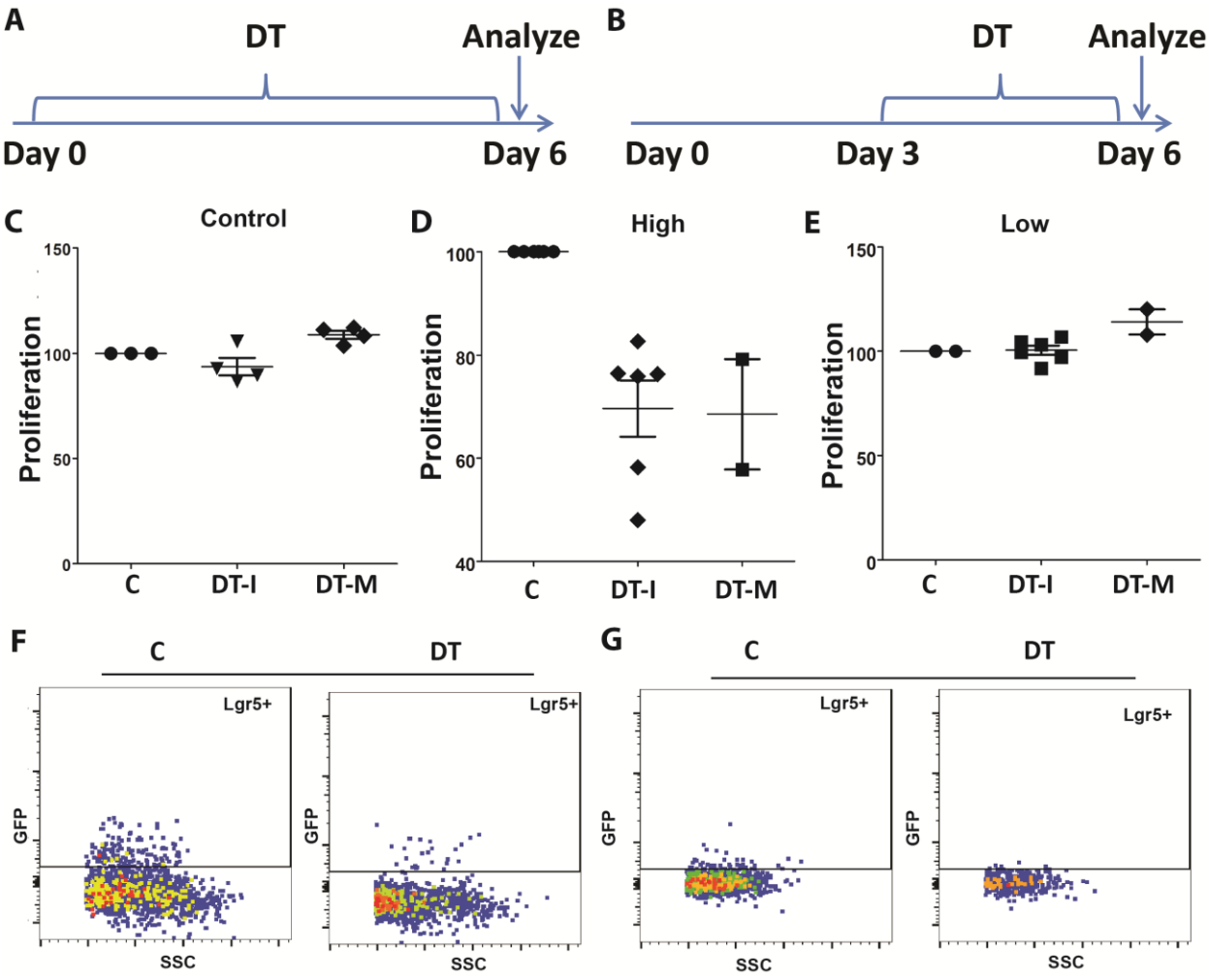


**Figure 6:** Targeting LGR5 cells can inhibit the growth of tumor organoids in an effect that correlates to the initial size of the LGR5$^+$ compartment. (A-B) The outlines of the experimental strategies used. (C) The response of wide type tumor organoids to DT administration. The Alamar blue assay was used to measure the proliferation of organoids. (D) The response of *Lgr5-DTR-GFP* mice derived tumor organoids to DT administrations, which initially have high LGR5 expression. DT-I: DT administration at the start of the experiment; DT-M: DT administration initiated at half of the observation time; C: control organoid without adding DT. (E) The response of *Lgr5-DTR-GFP* mice derived tumor organoid to DT administration, which initially have relatively low LGR5 expression. DT-I: DT administration initiated at the start of the experiment; DT-M: DT administration initiated at half of the observation time; C: control organoids without adding DT. (F-G) Representative FACS plots showing that LGR5-GFP$^+$ cells are depleted by DT administration, for high LGR5 expression organoid strains (F) and low LGR5 expression organoid strains (G).

## *Targeting LGR5$^+$ cells inhibits tumor growth in vivo.*

We next assessed the potential of targeting LGR5 cancer cells *in vivo*. Upon transplanting tumor organoids into immunodeficient mice, we first evaluated the effect of DT treatment after formation of visible tumors (Supplementary Figure 4A). We found that the depletion of LGR5 cells inhibited the growth of tumors, but the effect was moderate (Supplementary Figure 4B-C). In contrast, administration of DT directly following transplantation of tumor

organoids (Figure 7A) effectively delayed tumor formation and inhibited their growth (Figure 7B). After 10-16 days, tumors were collected and further analyzed by FACS. We confirmed the LGR5-depleted tumors were indeed smaller compared to the control group (Figure C and D) and that LGR5 cells were depleted in the tumors by the DT treatment (Figure 7E). When the DT administration strategy was tested on wild type tumor organoids, no significant inhibition of growth was observed (Supplementary Figure 5A-C). These results demonstrated that $LGR5^+$ cells are very important in the tumor initiation phase and ablation of $LGR5^+$ cells inhibits the growth of tumors *in vivo*. We further investigated the possibility of combination therapy. We observed that the 5-FU&DT co-treatment can significantly inhibit tumor growth, compared to any single-agent treatment (Figure 8A-D).

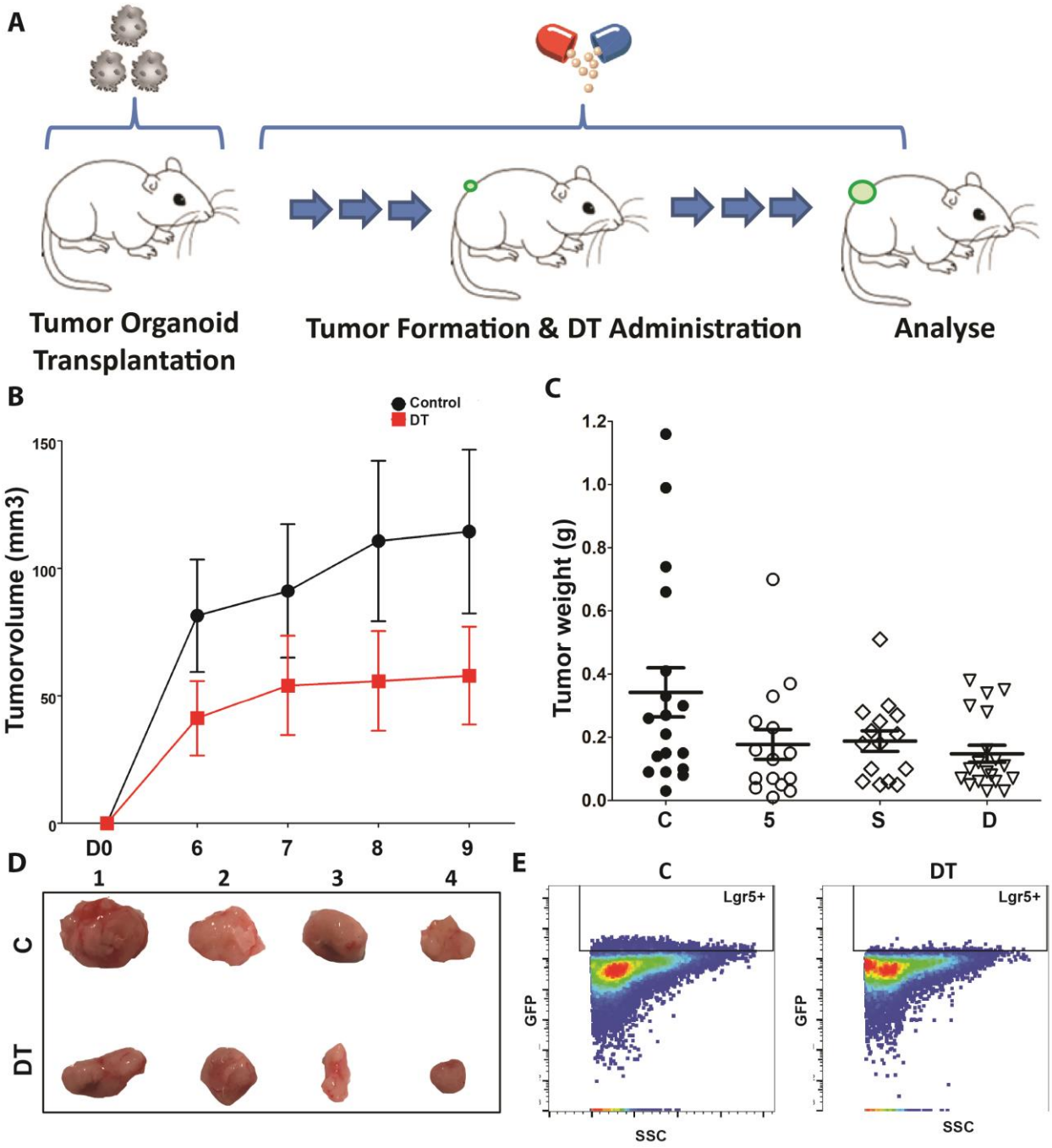


**Figure 7**: Targeting LGR5$^{+}$ cells can inhibit tumor growth *in vivo*. (A) The outline of the experimental strategy used. (B) Representative pictures showing tumor volumes of control group and the DT-administrated group. (C) The exact weights of tumors of the control (C), 5-Fu- (5), Sorafenib- (S) and DT- (D) challenged groups, at the day of mice sacrifice. (D) Representative pictures showing the morphological aspect of tumors of the control group and the DT-administrated group, from the day of mice sacrifice. (E) Representative FACS plots showing that LGR5$^{+}$ cells were depleted by DT administration.

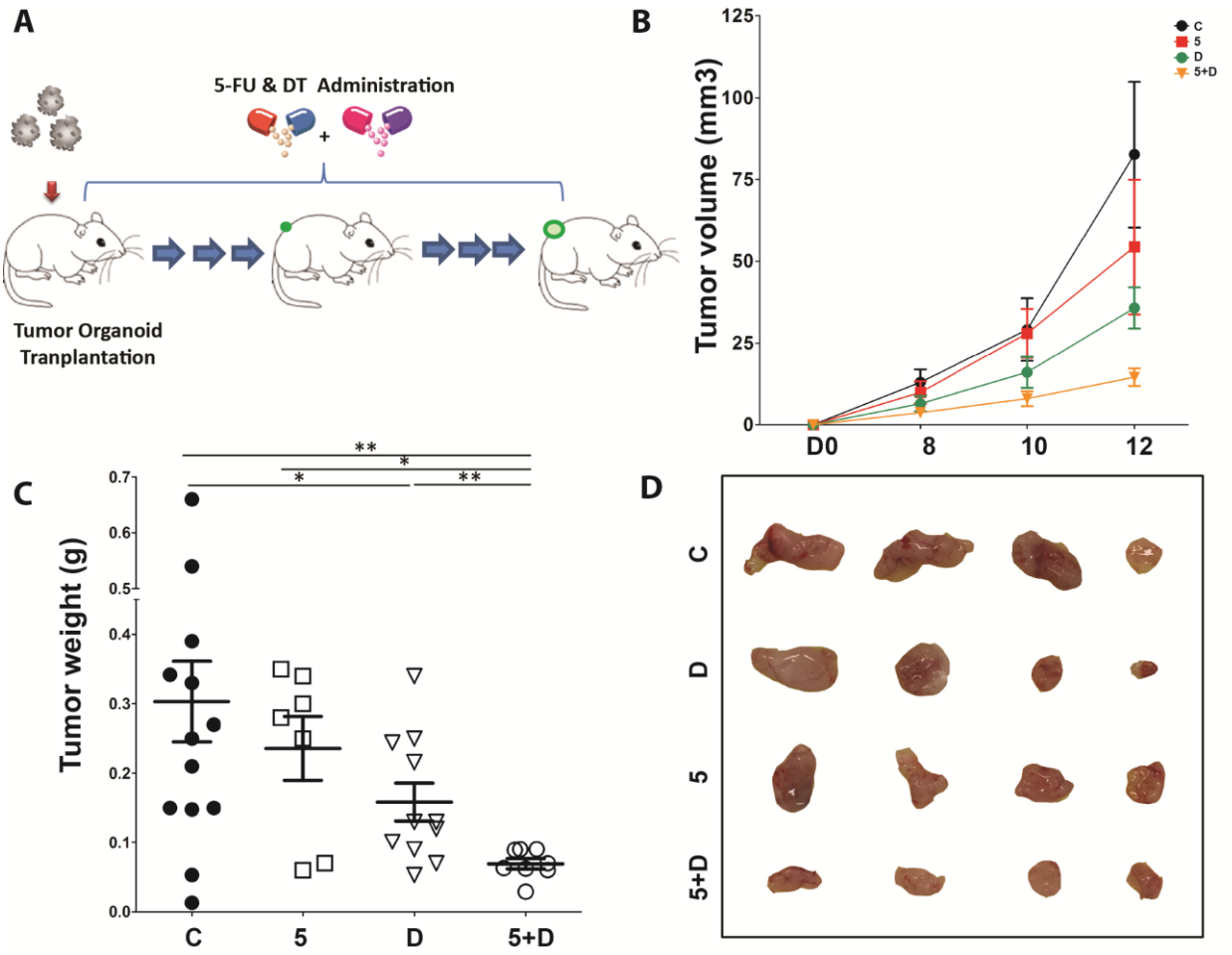


**Figure 8**: Combination therapy can significantly inhibit tumor growth. (A) The outline of the experimental strategy used. (B) Representative tumor growth curves showing tumor volumes of the control, the 5-FU, the DT and the 5-FU & DT co-treatment group. C: control group; 5: 5-FU-administrated group; D: DT-administrated group; 5+D: 5-FU & DT co-treatment group. (C) The exact weights of tumors from the control, the 5-FU, the DT and the 5-FU & DT co-treatment group, at the day of mice sacrifice. *P< 0.05, **P< 0.01. (D) Representative pictures showing the photos of tumors from different groups.

## Discussion

This study has demonstrated that LGR5 expressing cells are present in DEN-induced liver tumors and represent the cancer stem/tumor initiating cell population. We observedd that these cells have more organoid initiating capacity *in vitro* and more tumor initiating capacity *in vivo*. Interestingly, we found that depletion of LGR5 cells can impede the growth of liver tumors.

Although LGR5 has been reported to mark injury response stem cells in the liver [10, 12], the presence and function of these cells in liver cancer remains largely unknown. Overexpression of LGR5 has been reported in patient HCC, and these cells appear especially enriched in β-catenin-mutated liver tumors [13]. However, those observations are based on mRNA expression only, due to the lack of reliable anti-LGR5 antibodies. Thus, an strong point of the present study is the use transgenic mice which can efficiently label the LGR5 expressing cells with GFP and can conditionally ablate LGR5-expressing cells with DT-DTR system [11]. This model allows the identification and direct visualization of LGR5 expressing cells based on the GFP, as well as isolation of LGR5-GFP$^+$ cells for further functional analyses and detailed characterization.

In intestinal adenomas, LGR5 marks 5-10% of the cells and these appear to sustain the growth of established adenomas [9]. Here we demonstrate that similar to colon/intestinal cancer, LGR5-expresing cells are present in DEN induced primary liver tumors. The percentage of LGR5-GFP$^+$ cells within the liver tumors varied from 0.1% up to 55% (7.3 ± 1.7%, N=58). In colon cancer, the percentage of LGR5 tumor initiating cells has been reported to be associated with different backgrounds of the tumors, and especially with the accumulation of certain oncogenic mutations [6]. Thus, the large variation of LGR5-GFP$^+$ cells within liver tumors is conceivably related to the different types of oncogenic mutations, which deserves further investigation.

Targeting cancer stem cells is thought to be an important strategy for effective anti-cancer therapy. The reason is that cancer stem cells appear highly tumorigenic, therapy resistant and can differentiate into different types of tumor cells [14]. Here we also show that the depletion of LGR5 cells can postpone the fast growth phase of the liver tumors following transplantation. However, if the depletion starts after the tumor formation has been initiated, inhibition is very limited. The possible reason could be that the LGR5$^+$ cells represent a very low percentage in well-established tumors, only around 1%. However, if the depletion started at an early stage of tumor initiation, the inhibition achieved is more

significant. As is also widely accepted, we feel that the xenograft/allograft tumor assay is most reminiscent to cancer metastasis [1]. Thus, our results indicated that the LGR5 tumor stem cells play clinically a more important function when initiating new tumors. This result is consistent with earlier findings in colorectal cancer, where results with $LGR5^+$ cells are interpreted to be especially relevant for understanding metastasis [6]. Those results, in conjunction with the data presented here, may hint that the cancer stem cell targeted therapy could be very effective, when applied after surgical resection in preventing tumor recurrence.

Several pharmaceutical companies are investigating therapies aimed at eliminating the cancer stem cell population. The main strategies include: 1) using antibody-drug conjugates to ablate cancer stem cells [7]; 2) targeting quiescent cancer stem cells [15]; 3) inhibiting key pathway with special relevance for cancer stem cell physiology [14]. However, the de-differentiation of LGR5 negative to LGR5 positive cells has been postulated to limit the potential efficacy of targeting LGR5 for treating colorectal cancer [6]. Thus, combination therapies are probably necessary to exert optimal therapeutic effects. With the intention to support expansion of the stem cell pool, Cetuximab has been used to increase the size of the LGR5-positive compartment. Then, the ablation of cancer stem cells is executed in effort to treat the tumor. This combination therapy has stronger effect on the tumor regression than either treatment alone [8]. We here also illustrated the possibility of combination therapy in treating liver cancer by 5-FU and DT co-treatment (Figure 8A-D). Thus, it is important to further identify new therapies or combined treatments which can both kill the cancer stem cells and prevent the tumor re-growth.

In summary, our study illustrated the existence of LGR5 cells in liver tumors and functionally proved that LGR5 represented as a liver tumor initiating cell population. The depletion of LGR5 can inhibit the growth of tumor *in vivo*. It will be of particular interest to further study targeting LGR5 tumor initiating cell based treatment.

**Supplementary data for:**

# LGR5 marks tumor initiating cells and represents a new therapeutic target in liver cancer

## Table of contents

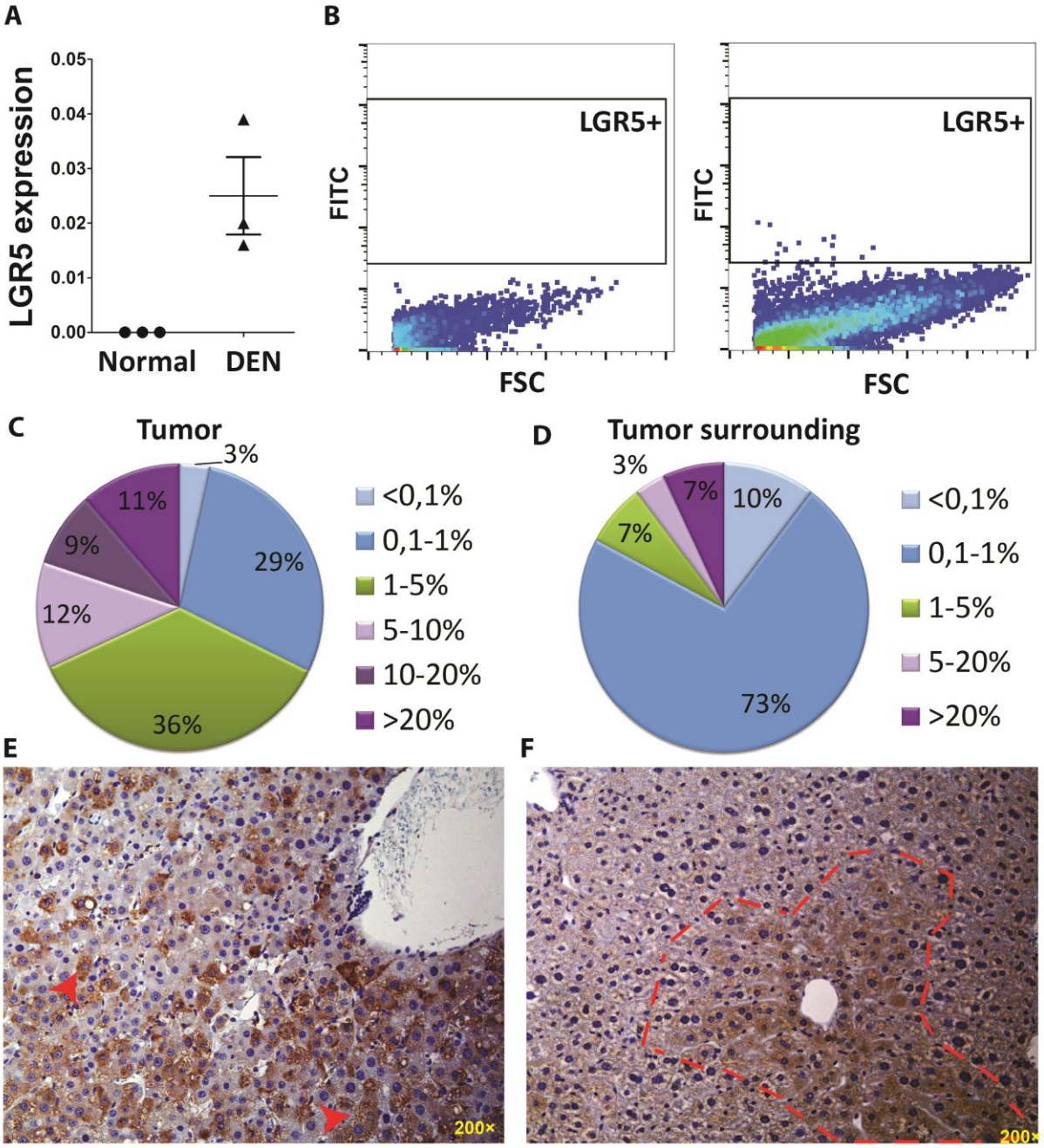


**Supplementary Figure 1**: LGR5 expressing cells present in the DEN-induced primary liver tumors. (A) LGR5$^+$ cells present in the liver immediately following DEN administration. (B) Representative FACS plots showing that LGR5$^+$ cells are present in the liver upon DEN administration. (C) The distribution of the percentages of LGR5$^+$ cells within in liver tumors. (D) The distribution of the percentage of LGR5$^+$ cells within in liver tumor surrounding tissues. (E-F) Representative immunohistochemistry pictures showing the different distribution pattern of LGR5$^+$ cells in liver tumor, as assessed by anti-GFP immunohistochemistry staining; LGR5$^+$ cell: brown; Nuclei: blue.

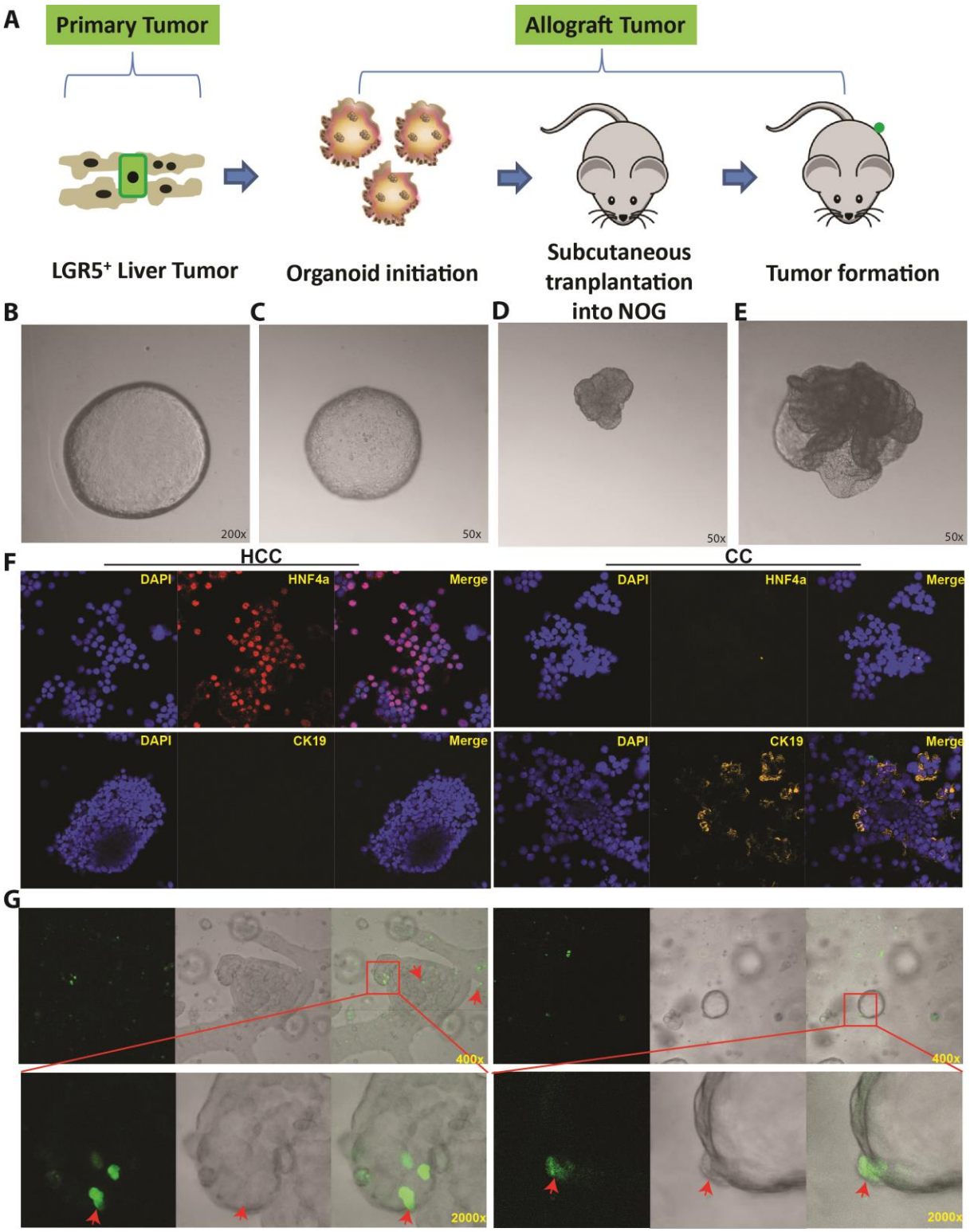


**Supplementary Figure 2:** Allograft liver tumors sustain the expression of LGR5 expressing cells. (A) The outline of the experimental strategy used. (B) Representative picture showing the morphology of a normal liver organoid. (C-E) Representative pictures showing the different morphologies observed in liver tumor organoids. (F) Representative confocal images for the expression of hepatocyte-specific marker (HNF4α, red) and cholangiocyte marker (CK19, yellow) in tumor organoids. (G) Representative confocal images showing the expression of LGR5-GFP in tumor organoids

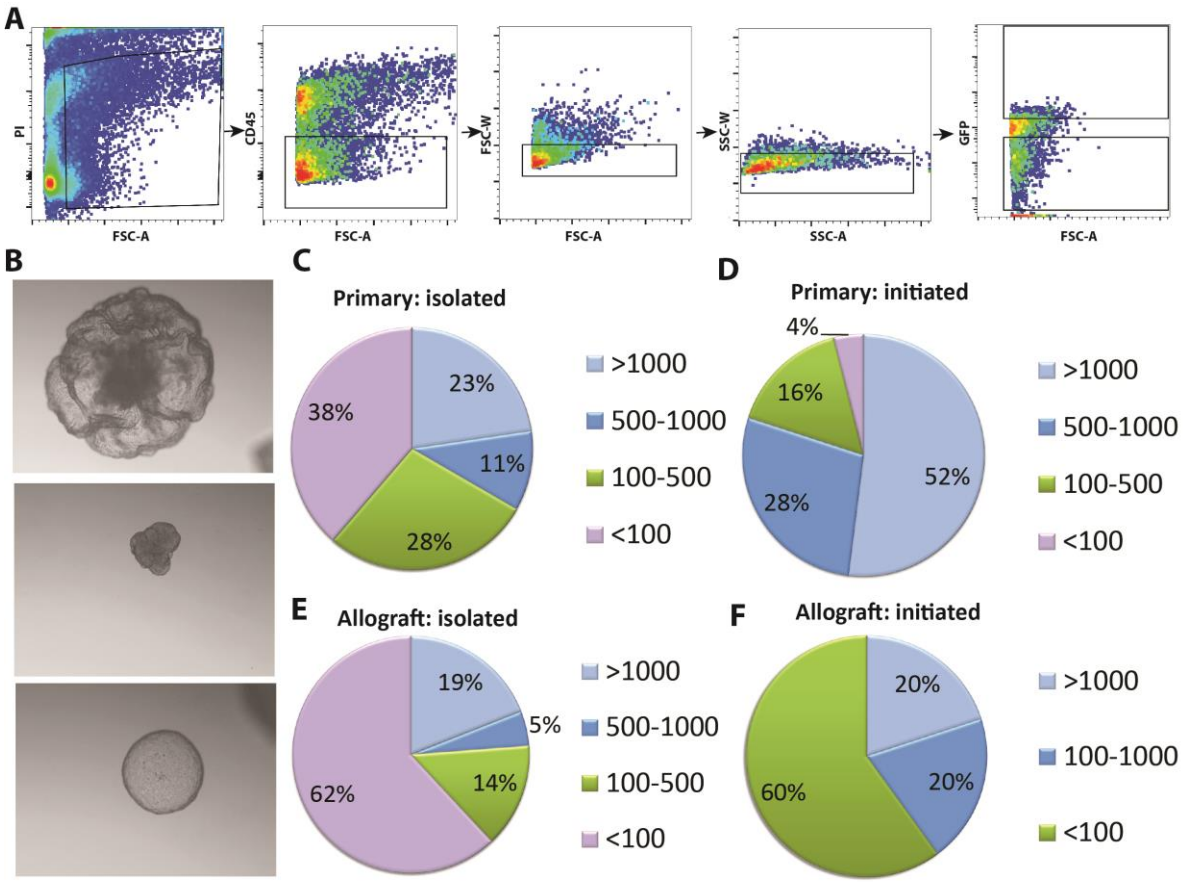


.

**Supplementary Figure 3:** Single LGR5 cells have a relatively strong organoid initiating ability *in vitro*. (A) The FACS testing/sorting strategy of LGR5-GFP$^{+}$ and LGR5-GFP$^{-}$ cells from liver/organoids. (B) Representative pictures showing organoids derived from single LGR5$^{+}$ cells isolated from allograft tumors. (C) The distribution of the percentage of LGR5$^{+}$ cells isolated from primary liver tumors. (D) The cell number distribution for the sorted LGR5$^{+}$ cells which can initiate organoids, employing primary tumors as source material. (E) The distribution of the percentages observed of LGR5$^{+}$ cells as isolated from allograft liver tumors. (F) The cell number distribution of sorted LGR5$^{+}$ cells that can initiate organoids, employing allograft tumors as source material.

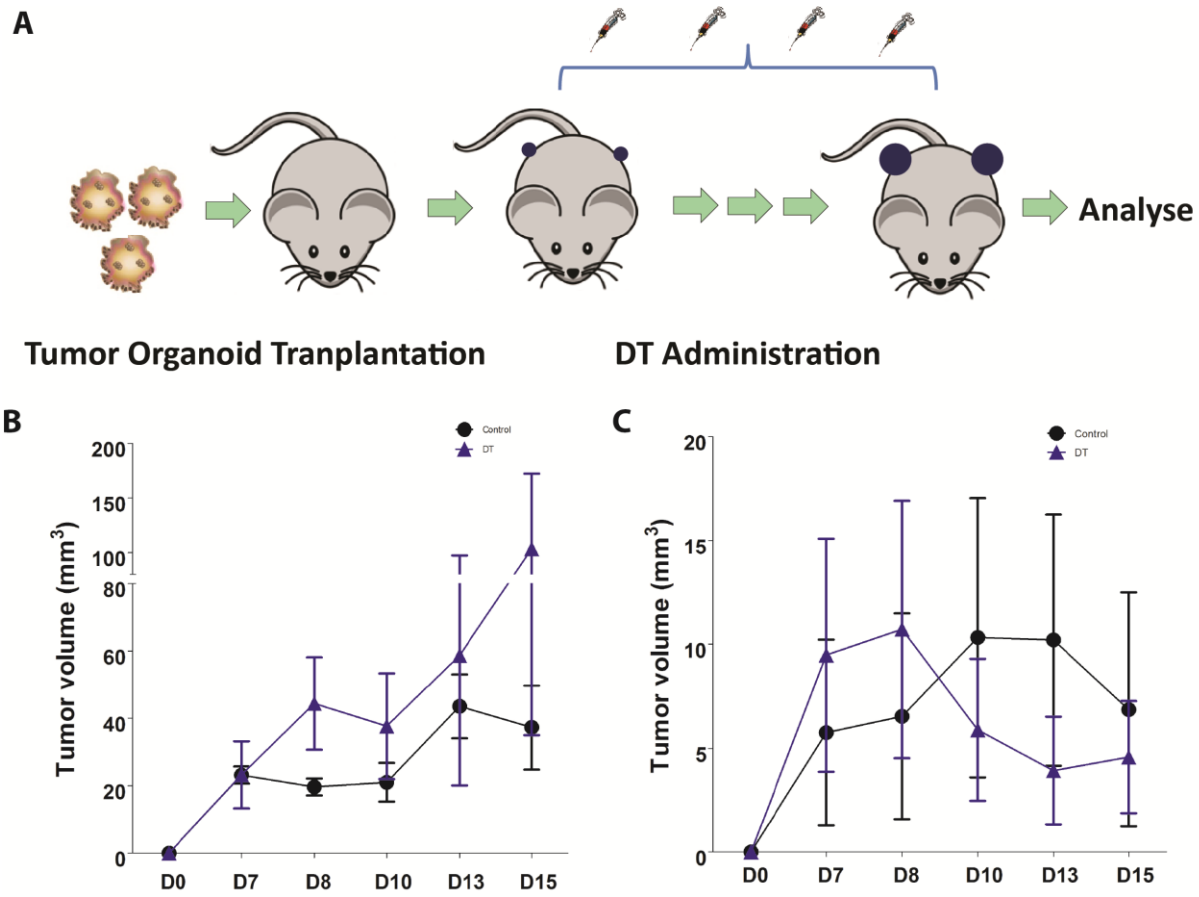


**Supplementary Figure 4:** Targeting LGR5$^{+}$ cells can inhibit tumor growth *in vivo*. (A) The outline of the experimental strategy used. (B-C) Representative tumor growth curve showing t the tumor volumes of control group and DT-challenged group in which DT treatment commenced at day 8.

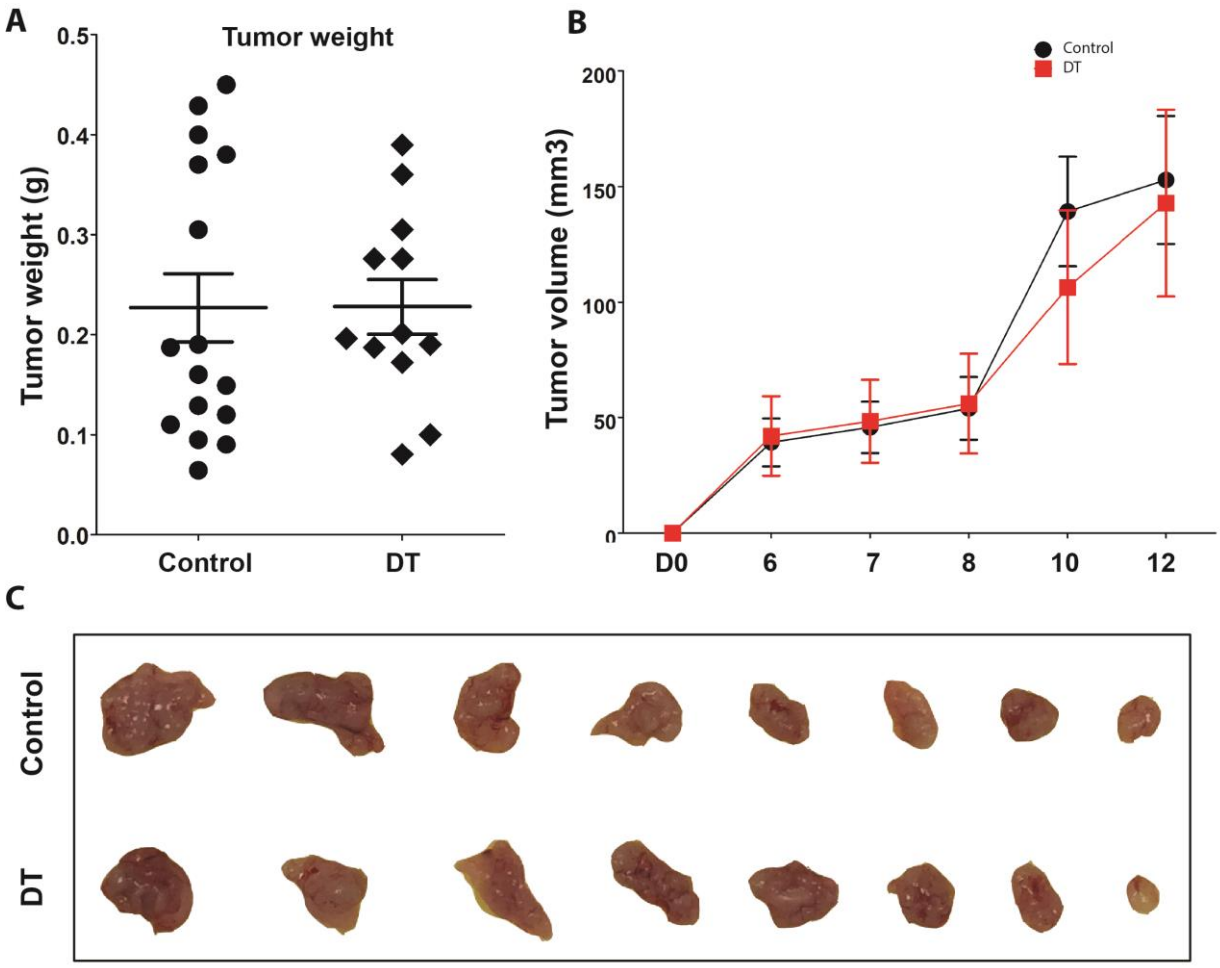


**Supplementary Figure 5:** DT administration did not have a significant influence on wild type tumor organoid-derived tumors. (A) The exact tumor weights of control tumors derived from wild type tumor organoid and DT treated group. (B) The tumor growth curve for the control and the DT treated group. (C) Representative picture showing the tumors from the control and the DT treated group.

**Supplementary Table 1.**

| **Antibody** | **Antibody clone/ reference** | **Raised** | **Origin** |
|---|---|---|---|
| CD45 | 56-0451-82 | Mouse | eBioscience |
| GFP | A-11122 | Rabbit | Invitrogen/Life Technologies |
| HNF4α | sc-8987 X | Rabbit | STCruz |
| CK19 | ab52625 | Rabbit | Abcam |
| Alexa Fluor® 488 AffiniPure Donkey Anti-Goat IgG (H+L) | 705-545-147 | Donkey | Bio-Connect |
| Donkey anti-Rabbit IgG (H+L) Secondary Antibody, Alexa Fluor® 594 conjugate | A-21207 | Donkey | Thermo fisher |
| Donkey anti-Goat IgG (H+L) Cross-Adsorbed Secondary Antibody, Alexa Fluor 594 | A-11058 | Donkey | Thermofischer |
| Donkey anti-Goat IgG (H+L) Secondary Antibody, Alexa Fluor® 647 conjugate | A-21447 | Donkey | Life Technologies |

## References:


1. Clevers H. The cancer stem cell: premises, promises and challenges. Nat Med 2011;17:313-9.
2. Ebben JD, Treisman DM, Zorniak M, et al. The cancer stem cell paradigm: a new understanding of tumor development and treatment. Expert Opin Ther Targets 2010;14:621-32.
3. Barker N, van Es JH, Kuipers J, et al. Identification of stem cells in small intestine and colon by marker gene Lgr5. Nature 2007;449:1003-7.
4. Boddupally K, Wang G, Chen Y, et al. Lgr5 Marks Neural Crest Derived Multipotent Oral Stromal Stem Cells. Stem Cells 2016;34:720-31.
5. Haegebarth A, Clevers H. Wnt signaling, lgr5, and stem cells in the intestine and skin. Am J Pathol 2009;174:715-21.
6. de Sousa e Melo F, Kurtova AV, Harnoss JM, et al. A distinct role for Lgr5+ stem cells in primary and metastatic colon cancer. Nature 2017;543:676-680.
7. Junttila MR, Mao W, Wang X, et al. Targeting LGR5+ cells with an antibody-drug conjugate for the treatment of colon cancer. Sci Transl Med 2015;7:314ra186.
8. Shimokawa M, Ohta Y, Nishikori S, et al. Visualization and targeting of LGR5+ human colon cancer stem cells. Nature 2017;545:187-192.
9. Schepers AG, Snippert HJ, Stange DE, et al. Lineage tracing reveals Lgr5+ stem cell activity in mouse intestinal adenomas. Science 2012;337:730-5.
10. Huch M, Dorrell C, Boj SF, et al. In vitro expansion of single Lgr5+ liver stem cells induced by Wnt-driven regeneration. Nature 2013;494:247-50.
11. Tian H, Biehs B, Warming S, et al. A reserve stem cell population in small intestine renders Lgr5-positive cells dispensable. Nature 2011;478:255-9.
12. Cao W, Chen K, Bolkestein M, et al. Dynamics of Proliferative and Quiescent Stem Cells in Liver Homeostasis and Injury. Gastroenterology 2017;153:1133-1147.
13. Yamamoto Y, Sakamoto M, Fujii G, et al. Overexpression of orphan G-protein-coupled receptor, Gpr49, in human hepatocellular carcinomas with beta-catenin mutations. Hepatology 2003;37:528-33.
14. Batlle E, Clevers H. Cancer stem cells revisited. Nat Med 2017;23:1124-1134.
15. Pascual G, Avgustinova A, Mejetta S, et al. Targeting metastasis-initiating cells through the fatty acid receptor CD36. Nature 2017;541:41-45.

# CHAPTER 5

# Differential sensitivities of fast- and slow-cycling cancer cells to inosine monophosphate dehydrogenase 2 inhibition by mycophenolic acid

Kan Chen[1,2#], Wanlu Cao[1#], Juan Li[1], Dave Sprengers[1], Pratika Y. Hernanda[3], Xiangdong Kong[2], Luc J. W. van der Laan[4], Kwan Man[5], Jaap Kwekkeboom[1], Herold J. Metselaar[1], Maikel P. Peppelenbosch[1], Qiuwei Pan[1]

[1]Department of Gastroenterology and Hepatology, Erasmus MC Cancer Institute, Erasmus University Medical Center, Rotterdam, The Netherlands.
[2]Bio-X Center, College of Life Sciences, Zhejiang Sci-Tech University, Hangzhou, China.
[3]Laboratory of Medical Genetics, Biomolecular Research Centre, Wijaya Kusuma University, Surabaya, Indonesia.
[4]Department of Surgery, Erasmus University Medical Center, Rotterdam, The Netherlands.
[5]Department of Surgery, Hong Kong University, Hong Kong, China.

***Molecular Medicine, 21:792-802, 2015***

## Abstract

As uncontrolled cell proliferation requires nucleotide biosynthesis, inhibiting enzymes that mediate nucleotide biosynthesis constitutes a rational approach to the management of oncological diseases. In practice, however, results of this strategy are mixed and thus elucidation of the mechanisms by which cancer cells evade the effect of nucleotide biosynthesis restriction is urgently needed. Here we explored the notion that intrinsic differences in cancer cell cycle velocity are important in the resistance towards inhibition of inosine monophosphate dehydrogenase (IMPDH) by mycophenolic acid (MPA). In short-term experiments, MPA treatment of fast-growing cancer cells effectively elicited G0/G1 arrest and provoked apoptosis thus inhibiting cell proliferation and colony formation. Forced expression of a mutated IMPDH2, lacking a binding site for MPA but retaining enzymatic activity, resulted in complete resistance of cancer cells to MPA. In nude mice subcutaneously engrafted with HeLa cells, MPA moderately delayed tumor formation by inhibiting cell proliferation and inducing apoptosis. Importantly, we developed a lentiviral vector-based Tet-on label-retaining system that enables to identify, isolate and functionally characterize slow-cycling or so-called label-retaining cells (LRCs) *in vitro* and *in vivo*. We surprisingly found the presence of LRCs in fast-growing tumors. LRCs were superior in colony formation, tumor initiation and resistance to MPA as compared to fast-cycling cells. Thus, the slow-cycling compartment of cancer seems predominantly responsible for resistance to MPA.

## Introduction

Uncontrolled cell proliferation resulting from cell cycling deregulation is a hallmark of cancer. Although aggressive cancers are diverse and heterogeneous, they almost universally contain a fast-cycling compartment that can rapidly complete a cell cycle, and these cells are primarily responsible for the increase in tumor mass [1]. This impressive proliferative capacity is, however, dependent on adequate supply of nucleotides. Cellular nucleotide synthesis is biochemically complex, but requires various enzymes that can be clinically targeted, including Inosine monophosphate dehydrogenase (IMPDH), which is a rate-limiting enzyme in *de novo* synthesis of guanine. The enzymatic activity of IMPDH is composed of two separate isoforms, type 1 and 2 [2]. The IMPDH2 isoform is associated with aggressive cancerous disease in experimental cancer [3-6], and related to poor survival in osteosarcoma patients [7]. Mycophenolic acid (MPA) acts as a nonnucleoside, noncompetitive, reversible inhibitor of IMPDH with 5-fold higher potency of inhibiting IMPDH2 than IMPDH1. It has been reported to be able to inhibit cancer cell proliferation and induce apoptosis in several experimental models of human solid tumors and hematological malignancies by depleting guanine nucleotide pools [5, 8-10].

In the last decade, interest into the importance of cell cycle velocity heterogeneity of cancers has increased. Although it was initially thought that cancer cells universally cycle and grow faster than normal cells, recently a slow-cycling (largely quiescent) compartment has been identified in many tumors, which does not divide frequently but with the capacity to generate progeny that can repopulate the fast cycling compartment [11]. Functionally, these slow-cycling cancer cells appear to be associated with capacity to generate new metastases while having superior resistance to therapy [12]. Technically, these slow-cycling cells are identified by their capacity to retain a pulse label as faster cycling cells lose the pulse label at cell division. Thus these cells are indicated with the term label-retaining cells (LRCs) [13].

In this study, we aim to develop a lentiviral vector-based Tet-on label-retaining system that enables to identify slow-cycling cancer cells *in vivo,* which can be subsequently isolated for functional characterization. We exploit this system to investigate the different sensitivity between fast and slow-cycling cancer cells to IMPDH2 inhibition by MPA.

## Materials and Methods

## Reagents

Stocks of MPA (AMRESCO LLC, USA) were dissolved in dimethyl sulfoxide (DMSO) (Sigma-Aldrich, St Louis, MO). Doxycycline, Collagenase IV and DNase were purchased from Sigma-Aldrich Corporation. Antibodies against IMPDH2, p-Histone3 and Cleaved caspase3 were purchased from Abcam Company, Millipore Corporation and Cell Signaling Technology, respectively.

## Cell culture

To investigate the effects of MPA on cancer cells, 7 different cancer cell lines derived from various tumor types were cultured. Human hepatoma cell lines HepG2 and HuH7, colon adenocarcinoma cell line Caco2, the epithelioid cervix carcinoma cell line HeLa and ovary adenocarcinoma cell line SKOV-3 were grown in Dulbecco's modified Eagle's medium (DMEM) (GIBCO Life Technologies). Pancreatic cancer cell lines BxPC3 and PANC-1 were cultured with RPMI-1640. Both of the mediums were supplemented with 10% (v/v) fetal bovine serum (FBS) (Hyclone Technologies), 100 units/mL of penicillin and 100 µg/mL of streptomycin. All the cells were incubated at 37℃ in a humidified atmosphere containing 5% $CO_2$. All the cell lines were confirmed with mycoplasma free and their STR genotyping were analyzed at the Department of Pathology, Erasmus Medical Center Rotterdam (Supplementary table. 1).

## Lentiviral vector-based Tet-on label-retaining system

Lentiviral backbone plasmids pLV.EX3D/EF1A-rtTA(M2)-dsRed-Express2 and pLV.EX2D/TRE-eGFP were used to pack third generation lentiviral vectors (Supplementary Figure S1A). HeLa cells were transduced with both vectors to generate a system (HeLa tet-on) that can express a histone 2B-green fluorescent fusion protein (Histone-GFP) upon induction by doxycycline. GFP expression *in vitro* was analyzed from week 0 to week 3 by flow cytometry analysis (FACS) and confocal microscope (Zeiss LSM 510) (Supplementary Figure S1B and S1C). ZenlightEdition software was used to analyze confocal microscope images. Cells that maintained GFP expression over this period of time were identified as LRCs.

For identification of LRCs *in vivo*, female NOG mice at the age of 8-10 weeks were purchased from Taconic Biosciences (Denmark). Animal experiment was performed with the approval of the institutional animal ethics committee (Dier Experimenten Commissie, Erasmus MC). Mice were breed in Special Pathogen Free (SPF) environment during the whole experimental period. Mice were injected subcutaneously with $5\times10^6$ HeLa tet-on cells. After engraftment (10-15 days), water containing 1 mg/mL doxycycline and 5% sucrose has been given for 5 days. Mice were sacrificed at different time points after withdrawal of doxycycline. A proportion of harvested tumor samples was fixed with 4% paraformaldehyde and embedded in paraffin for subsequent immunohistochemistry. While the remaining tumor tissue was dissociated with 5 mg/mL collagenase IV and 2 mg/mL DNase at 37℃ for 30min to obtain single cell suspension. Cells were further sorted as singlets for separation into Non-LRCs ($GFP^{low}$dsRed) and LRCs ($GFP^{high}$dsRed) by FACS sorter (Supplementary Figure S2). Non-LRCs and LRCs were injected subcutaneously into mice (either 1,000 cells or 10,000 cells *per* injection as appropriate) on four sites in the mice. At the same time, two populations of sorted cells were plated for colony formation unit assay (CFU) (treated with or without MPA).

## Colony formation assay

Cells were harvested and suspended in culture medium, yields were quantified through counting and plated in 6-well plates (500 cells/well), and then treated with serial dilutions of MPA (1, 2, 3, 4 and 5 μg/mL). The control group was supplemented with equal volume of PBS. For the cells derived from xenograft tumour, cells were seeded into 12-well collagen coating plates and cultured in medium with or without MPA (10 μg/mL). Formed colonies were fixed by 70% ethanol and counterstained with haematoxylin & eosin after two weeks. Colony numbers were counted and their sizes were measured microscopically through digital image analysis.

## MTT assay

Cells were seeded in 96-well plate, at a concentration of $5\times10^3$ cells/well in 100 μL medium. Cells were incubated overnight to attach to the bottom of the wells, and then treated with serials dilutions of MPA (1, 5, 10, 15, 20, 25 and 30 μg/mL). Cell viability was analyzed by adding 5 mg/mL MTT (Sigma-Aldrich, St Louis, MO) and 150 μL DMSO. Absorbance was determined using Enzyme mark instrument at the wavelength of 490 nm.

## Analysis of cell cycle

Cells ($5\times10^5$/well) were plated in six-well plates and allowed to attach overnight, followed by application of MPA at the concentrations of 5, 10, 15, 20 and 25 µg/mL for 48 h. Vehicle control was performed through the addition of an equal volume of PBS. After 48 h, control and treated cells were trypsinized and washed with PBS and then fixed in cold 70% ethanol overnight at 4℃. The cells were washed twice with PBS and incubated with 20 µg/mL RNase at 37℃ for 30 min, and then with 50 µg/mL Propidium Iodide (PI) at 4℃ for 30 min. The samples were analyzed immediately by FACS. Cell cycle was analyzed by ModFit LT 3.0 software.

## Analysis of cell apoptosis

Cell apoptosis analysis was performed by staining cells with Annexin V-FITC and PI. Cells ($5\times10^5$/well) were seeded into six-well plates and incubated at 37℃ in 5% $CO_2$ for overnight, then serials dilutions of MPA (5, 10, 15, 20 and 25 µg/mL) were added; whereas for vehicle control, an equal volume of PBS was used. After 48 h, all of the cells were trypsinized and resuspended in Annexin-binding buffer, and stained with Alexa Fluor 488 AnnexinV and PI at room temperature for 15 min. Detection of apoptosis was performed by FACS.

## Xenograft assays in nude mice

The xenograft tumor model was performed using nude mice in accordance with current prescribed guidelines and under a protocol approved by the Institutional Animal Care and Use Committee of Hangzhou Normal University, China. Mice were breed in SPF environment during the whole experimental period. Mice were all female and 4-6 weeks of age at the time of inoculation, and were subcutaneously inoculated with $5X10^6$ of HeLa cells. After 20 hours, mice were divided into 3 groups and were treated with different doses of MPA or PBS (240 mg/kg body weight, n = 10; 60 mg/kg body weight, n = 11 and PBS, n = 10) [2]. MPA was injected via the intraperitoneal (IP) route for 20 consecutive days. Tumor formation was monitored through palpation. At day 30 post-engraftment, mice were sacrificed and tumors were harvested and macroscopically analyzed. Tumor tissues were fixed with 4% paraformaldehyde and embedded in paraffin for evaluation by histology or immunohistochemistry.

## Immunohistochemistry

Paraffin embedded tumor tissue slides were deparaffined in xylene, rehydrated in graded alcohols, and rinsed in PBS supplemented with 0.05% Tween 20. Slides were boiled in citrate acid buffer (pH 6.0) for 10 min to retrieve antigen. A 3% $H_2O_2$ for 20 min at room temperature treatment was used to block endogenous peroxidase activity. The slides were incubated in 5% milk-containing blocking solution followed by overnight incubation with either a rabbit monoclonal antibody against IMPDH2, a rabbit polyclonal antibody against p-Histone H3 or a rabbit polyclonal antibody against cleaved caspase 3, used at a final dilution of 1:500, 1:1000, 1:3000 respectively and then counterstained with hematoxylin according to routine procedures. As a negative control, the primary antibody was omitted; positive controls were taken from other slides that had been successfully stained before. IMPDH2, phosphor-Histone H3 and cleaved caspase 3 staining were scored by two independent expert observers. The numbers of mitotic cells and cleaved caspase 3 positive cells were counted in 10 high-power fields. Median numbers of positive cells in each of the 10 fields were calculated for each sample of the different groups using a semi-quantitative assessment. Three categories were used to evaluate the percentages of apoptotic cells: < 10% mild; 10% - 50% moderate; > 50% high. The intensity of IMPDH2 staining was presented by categories: + weak; ++ moderate; +++ strong.

## Statistical analysis

Statistical analysis was performed by using the nonparametric Mann-Whitney test for paired or non-paired data, or the paired T-test using GraphPad InStat software as appropriate. A P value < 0.05 was considered statistically significant.

## Results

## MPA is very effective for inhibiting cancer cell proliferation in fast-growing cell lines

A first indication as to how MPA effects on cancer cells relate to cell cycle velocity comes from experiments in which we investigated the effects of MPA on cell proliferation and colony-forming potential of different cancer cell lines. To this end, 7 different cancer cell lines derived from various tumor types were compared. Growth curves show substantial

variation in the proliferation rate and colony-forming potential of these cell lines; with in general HeLa and Caco2 showing more aggressive behavior as compared to the other cell lines (Figure 1). Challenge with MPA inhibited both cell proliferation and colony unit-forming potential of cancer cell lines, but strikingly fast-growing cell lines are more effected by MPA treatment as compared to slow-growing cell lines (Figure 1), indicating that MPA mainly affects the fast-cycling compartment.

## MPA inhibited cell proliferation, arrested cell cycling and induced cell apoptosis in fast-growing cancer cell line

To further understand how MPA acts on fast-growing cancer cells, HeLa cells (the most sensitive cell line to MPA emerged from our panel of cancer cell lines) were treated with clinically relevant MPA concentrations [14] and analyzed in more detail for the effects of MPA on cellular expansion, cell cycle, and programmed cell death. MPA counteracted HeLa cell proliferation and colony-forming potential in a time- and dose-dependent manner (Figure 2A). Indeed, even a relatively low concentration (1 µg/mL) of MPA already substantially impeded colony formation; whereas higher concentrations (2-5 µg/mL) completely inhibited colony formation. The result reports 322 ± 27 colonies/500 cells were formed in untreated, but only 148 ± 27 colonies were formed in 1 µg/mL MPA treated groups (mean ± SEM, n = 6, $P < 0.01$) (Figure 2B). Accordingly, the size of CFU was significantly smaller in MPA treated compared to untreated groups (96 ± 5 pixels vs 278 ± 8 pixels, mean ± SEM, n = 30, $P < 0.01$) (Figure 2C). Furthermore, MPA dose-dependently provoked the G0/G1-phase arrest (Figure 2D). In addition, MPA dose-dependently triggered both early and late cell apoptosis (Figure 2E). These data suggest that MPA profoundly interferes with the physiology of fast-growing cancer cells and raises questions as to how cancers can escape the effects of MPA.

## IMPDH2 is a relevant target for MPA in inhibiting cancer cell growth

The clinical effects of MPA are presumed to be mediated through inhibition of IMPDH enzymatic activity and subsequent inhibition of *de novo* nucleotide biosynthesis. Although two isoforms of IMPDH exist, the type 2 isoform (IMPDH2) exhibits a 5-fold higher sensitivity to inhibition by MPA as compared to the type 1 isoform (IMPDH1) [3].

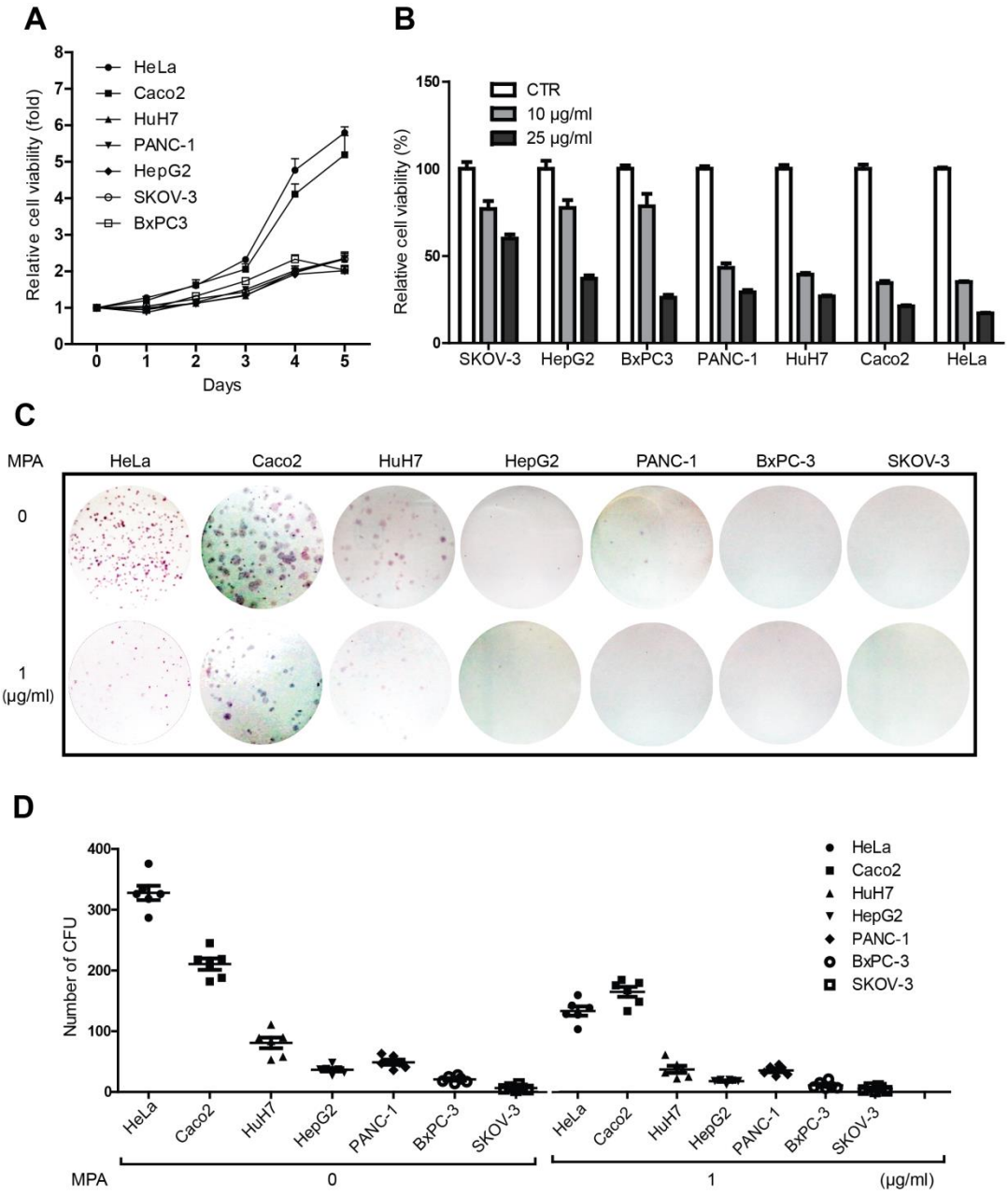


**Figure 1. MPA inhibited cell proliferation and colony formation of different cancer cell lines.** (A) Growth curve of seven different cancer cell lines show that HeLa cells grow faster than the other cell lines tested (mean ± SD, n = 6). (B) MPA inhibited cell proliferation of all seven cancer cell lines as determined by MTT, data shown cells were treated by MPA for 72 h (mean ± SD, n = 5). (C) and (D) MPA inhibited single cell colony formation of seven cancer cell lines (mean ± SD, n = 6, ***P < 0.001).

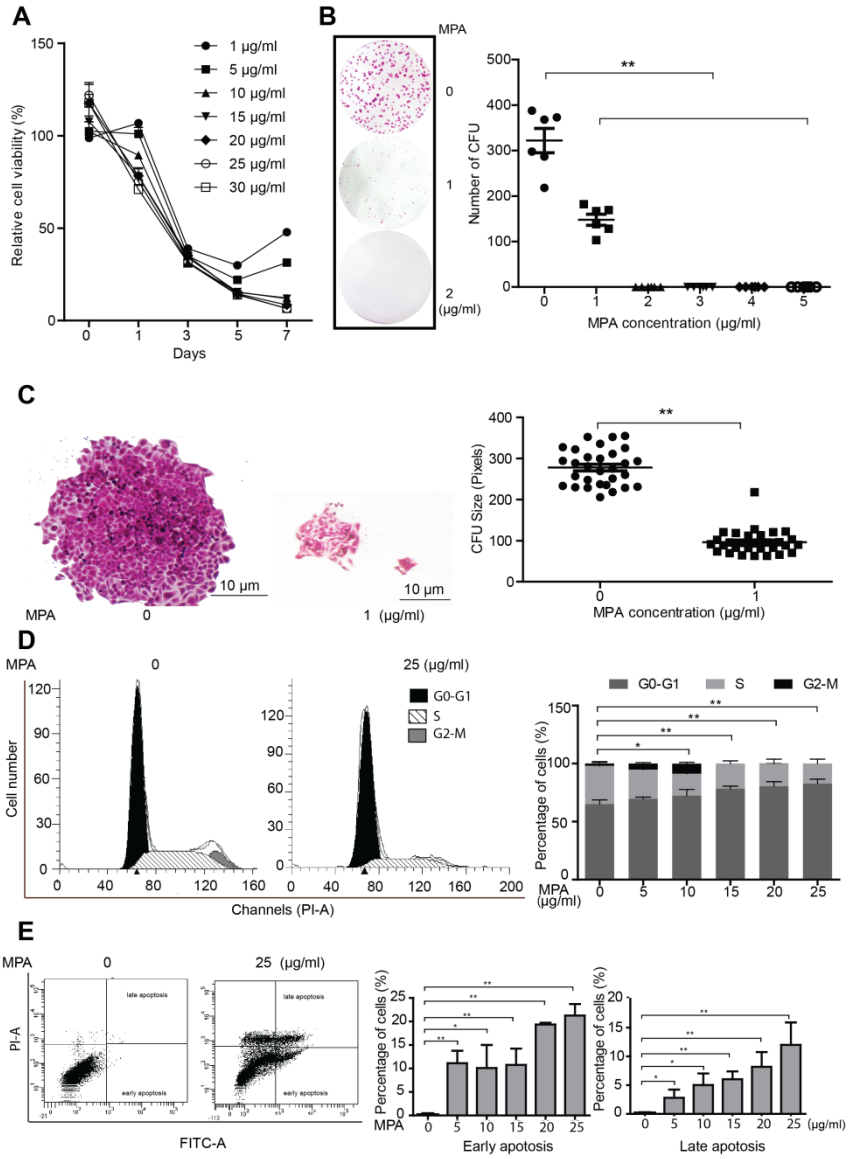


**Figure 2. MPA counteracts proliferation of a fast-growing cancer cell line.** (A) Clinically-relevant MPA concentrations, potently inhibit proliferation of the HeLa cell line as assessed by MTT activity (mean ± SD, n = 5). (B) Clinically-relevant MPA concentrations impair colony formation of HeLa cells (mean ± SD, n = 6). (C) Clinically-relevant MPA concentrations impair colony growth of HeLa cell as determined by image analysis (mean ± SEM, n = 30, **P < 0.01). (D) MPA treatment causes G0/G1 phase cell cycle arrest. The left panel shows cell cycle phase distribution of a vehicle-treated culture, whereas the middle panel shows cell cycle phase distribution in a MPA-treated culture. The right panel shows a quantification of the MPA effects on the cell cycle of HeLa (mean ± SD, n = 3. *P < 0.05; **P < 0.01). (E) FACS analysis of cellular apoptosis through Annexin-V positivity and PI incorporation. The left panel provides an example of a vehicle-treated HeLa culture, whereas the middle panel provides an example of the effects seen following MPA treatment. The quantification in the right panel shows statically significant stimulation of both early and late apoptosis in the 5-25 µg/mL MPA concentration (mean ± SD, n = 3, *P < 0.05; **P < 0.01).

IMPDH2 is assumed to be the major target of MPA. Moreover, IMPDH2 is often up-regulated in cancer [15], suggesting that IMPDH2 is the relevant target for MPA in the experiments described above. To substantiate this notion, we employed a lentiviral vector expressing an experimentally mutated *IMPDH2* (mut*IMPDH2*) fused to *GFP* [16, 17]. The product of this construct has normal IMP dehydrogenase activity but lacks the binding site for MPA and thus confers MPA-resistance. Transduction of this vector resulted in successful expression of this mutated allele in HeLa cells (Figure 3A). In the CFU assay, forced expression of this mutated *IMPDH2* provoked resistance to MPA treatment (Figure 3B and 3C). Furthermore, the mut*IMPDH2* cells prevented MPA-induced apoptosis (Figure 3D). These results are consistent with a key role of IMPDH2 in mediating the effects of MPA in our experimentation.

## MPA delayed tumor initiation, inhibited cancer cell proliferation and induced cell apoptosis *in vivo*

Insight into the effects of MPA on tumor cell *in vivo* was obtained in experiments, in which nude mice were used for subcutaneous engraftment of the HeLa cell line. 20 hours after inoculation, mice were intraperitoneally injected with MPA for 20 consecutive days. In this xenograft model, treatment of MPA (60 mg/kg body weight) significantly ($P < 0.05$) delayed tumor initiation (Figure 4A). In the 240 mg/kg body weight of MPA treated group, one mouse failed to form tumor; while tumor formation also tended to be delayed in the other mice (Figure 4B). Thus MPA counteracts growth of experimental tumors in this model. Immunohistochemical staining of tumors harvested from these mice demonstrated significant down-regulation ($P < 0.05$) of IMPDH2 at the protein level following treatment with MPA (Figure 4C). Concomitantly, MPA inhibited tumor cell proliferation, as shown by a significant reduction ($P < 0.05$) of proliferating cells assessed by the percentage of p-histone H3 positive cells (Figure 4D). Furthermore, MPA treatment provokes substantial apoptosis in the tumor cell compartment, as evidence from the significant increase in the percentage of cleaved

caspase 3 positive cells (Figure 4E). These results show that MPA counteracts tumor growth elicited by a fast-growing cancer cell *In vivo.*

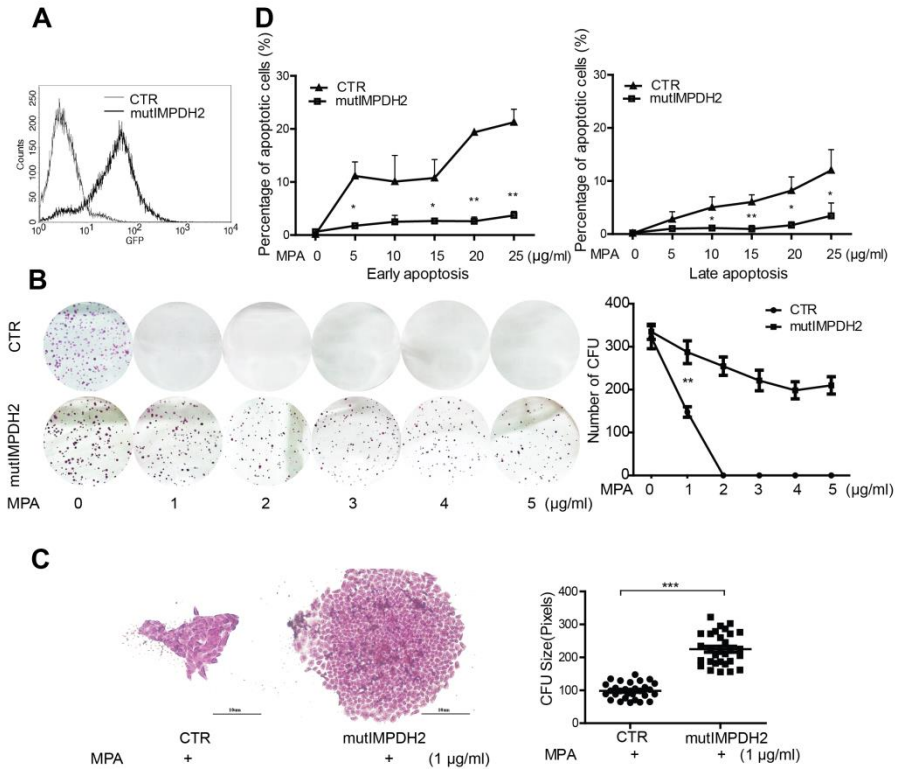


**Figure 3. Forced-expression of a mutated IMPDH2, lacking the MPA binding site, results in resistance to MPA.** (A) An IMPDH2 variant having normal IMP hydrogenase activity but lacking the MPA binding site was fused to a GFP reporter (mutIMPDH2) and expressed in HeLa cells by a lentiviral vector. FACS analysis showed robust GFP expression in the transduced HeLa cells but not in mock-transduced cells. Transduced cells appear to be resistant to MPA in both colony formation (B) (mean ± SD, n = 6, **P < 0.01) and cell proliferation assays (C) (mean ± SEM, n = 30, ***P<0.001). (D) MPA-mediated induction of both early apoptotic cells as well as late apoptotic cells is significantly reduced in mutIMPDH2 HeLa cells (mean ± SD, n = 3. *P < 0.05; **P < 0.01).

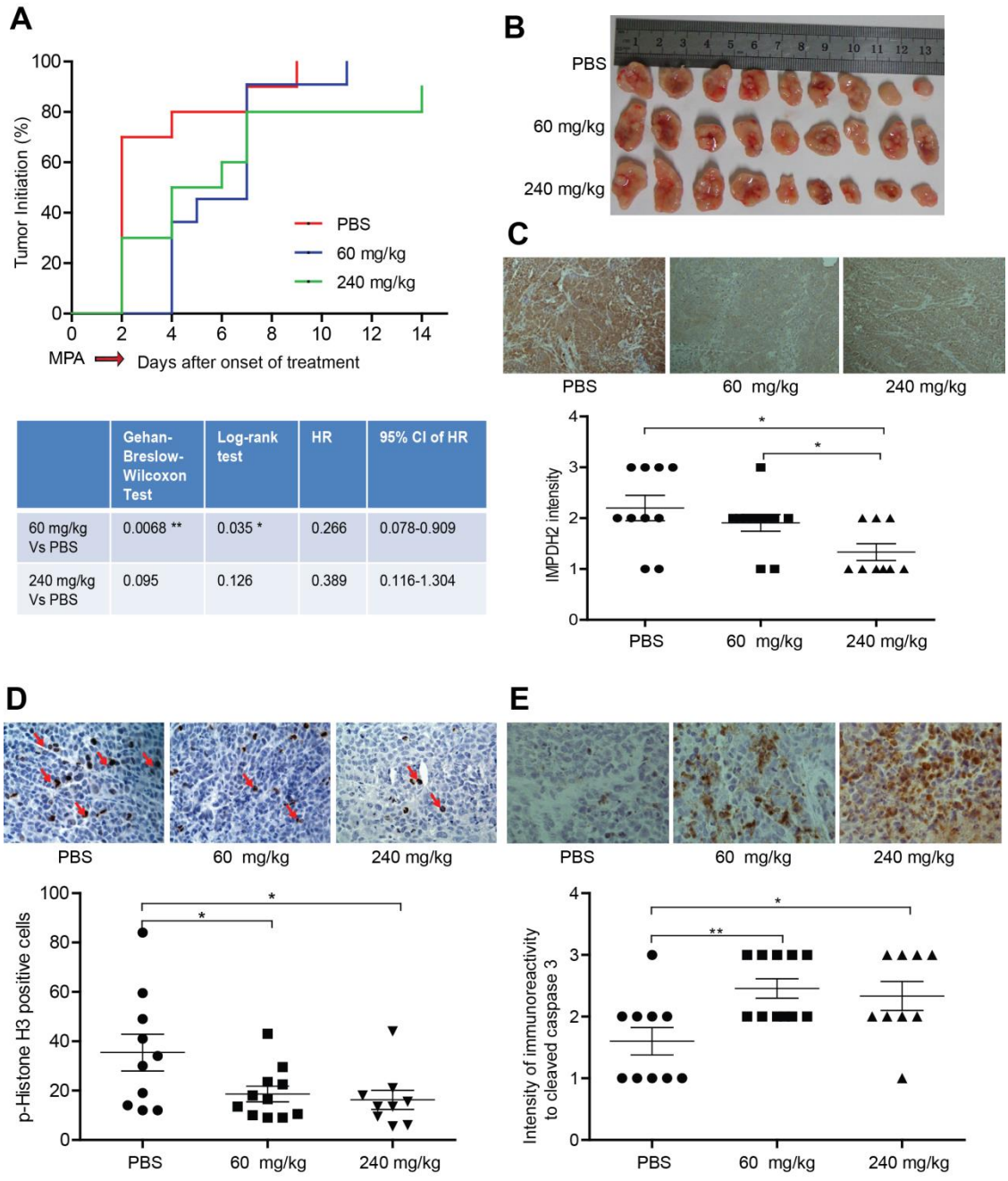


| | Gehan-Breslow-Wilcoxon Test | Log-rank test | HR | 95% CI of HR |
|---|---|---|---|---|
| 60 mg/kg Vs PBS | 0.0068 ** | 0.035 * | 0.266 | 0.078-0.909 |
| 240 mg/kg Vs PBS | 0.095 | 0.126 | 0.389 | 0.116-1.304 |

**Figure 4. MPA delayed tumor initiation, inhibited cell proliferation and provokes tumor apoptosis in mice.** (A) MPA treatment significantly delays tumor initiation by HeLa cells in nude mice. (B) Following the experiment, animals were sacrificed and tumors were harvested. The photograph illustrates the macroscopic appearance of the tumors in the respective groups. (C) Immunohistochemical staining of harvested tumor tissue sections revealed a significant down-regulation of IMPDH2 protein levels following treatment with MPA. (D) Treatment of MPA significantly reduced the percentage of p-histone H3 positive (proliferating) cells in the tumors. (E) MPA treatment of HeLa-grafted nude mice significantly increased the numbers of anti-cleaved caspase 3 immunoreactive (apoptotic) cells (mean ± SEM, PBS, n = 10; 60 mg/kg, n = 11; 240 mg/kg, n = 9, *P < 0.05; **P < 0.01).

## Existence of slow-cycling cancer cells compartment in fast-growing tumors

Substantial evidence indicated that slow-cycling cancer cells can evade therapeutic agents and repropagate the tumor [18]. In order to identify whether there are slow-cycling cancer cells in our experimental system, we established a lentiviral based Tet-on label-retaining system that enables us to isolate slow-cycling cells for further functional characterization. To this end, cells were transduced with two vectors. One vector expresses a reverse Tet trans activator (rtTA), dsRed fluorescent protein and a neomycin-resistance cassette. The other vector expresses a Histone-GFP fusion protein driven by a tetracycline response element (TRE) and puromycin-resistance gene (Supplementary Figure S1A). Stable cell lines can be established by co-transducing with these two vectors and the clones can be selected either via drug resistance or by cell sorting based on fluorescence. This constitutes a genotoxic free and cell proliferation independent approach to identify slow-cycling cells. Upon induction by doxycycline, all the cells are labeled with GFP. After doxycycline withdrawal, dividing cells lose their GFP signal; whereas quiescent or slow-cycling cells retain their GFP expression, which thus serves as a label for LRCs (Figure 5A and Supplementary Figure S1).

HeLa cells engineered with Histone-GFP$^{tet\text{-}on}$ were subcutaneously engrafted in immunodeficient mice (Figure 5B). Once a small tumor was formed, Histone-GFP expression was induced by doxycycline in the drinking water of the animal. Following doxycycline withdrawal, mice were sacrificed at different time points. As shown by both FACS and Immunohistochemical staining, a small population of LRCs was detected in tumors (Figure 5C and 5D). Thus we concluded that even fast-growing tumors harbor LRC compartment.

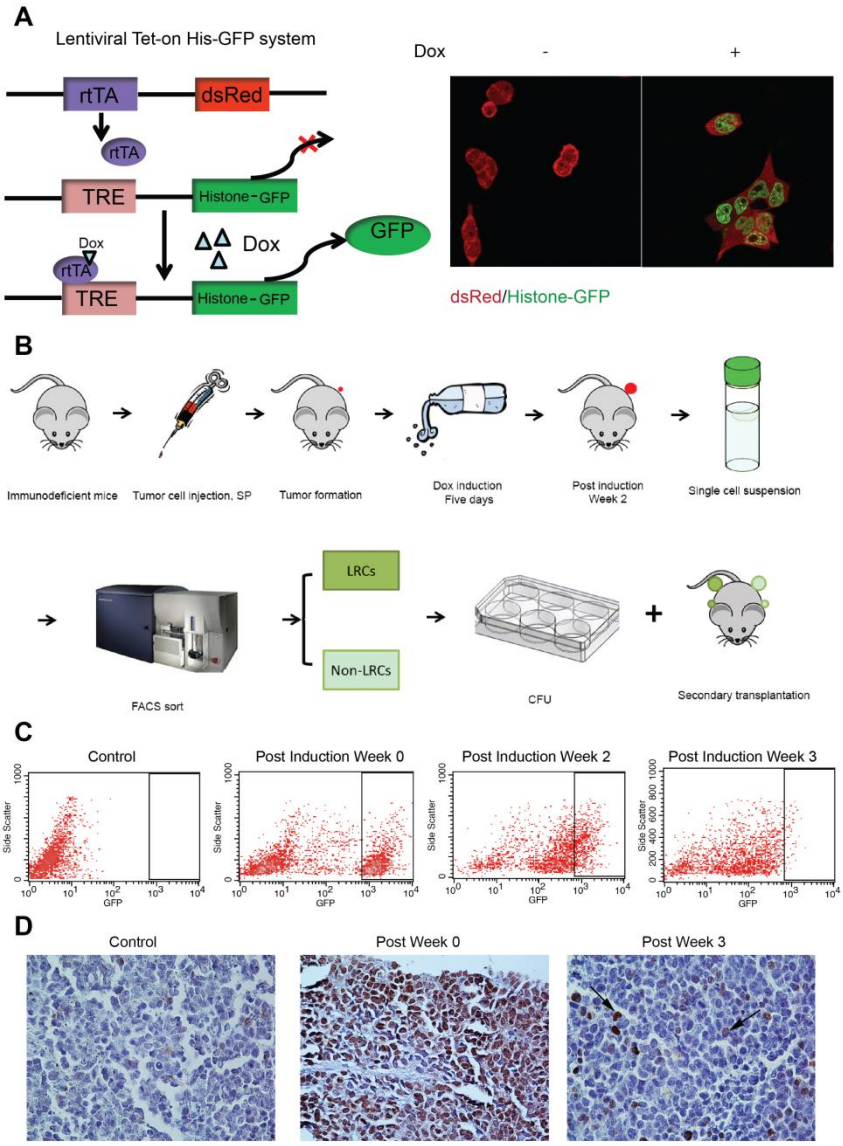


**Figure 5. Identification of slow-cycling cancer cells using a lentiviral label-retaining system.** (A) Illustration of principle the lentiviral Tet-on Histone-GFP strategy employed. Confocal imaging confirms the specific induction of nuclear Histone-GFP expression in HeLa cells upon doxycycline treatment. (B) Schematic representation of the experimental approach to identify, isolate and characterize the slow-cycling cells, or termed as label-retaining cells (LRCs) *in vivo*. (C) FACS characterization of Histone-GFP expression in transduced HeLa cell during 3 weeks following release from doxycycline induction. (D) Immunohistochemical staining of harvested xenograft tumor tissues confirms the presence of nuclear anti-GFP immunoreactivity in these tissues.

## Slow-cycling cells are superior in tumor formation and display more resistance to MPA

To functionally characterize LRCs, LRCs and non-LRCs were isolated from HeLa cell-derived tumors using FACS sorter (Figure 5B and Supplementary Figure S3). Surprisingly, *ex vivo* CFU assay showed that LRCs were significantly more efficient in colony formation (non-LRCs: 2.8 ± 1.3 colonies/100 cells; LRCs: 8.1 ± 2.2, mean ± SEM, n = 19, $P < 0.001$) when compared to fast-cycling cells (Figure 6A). Consistently, LRCs are more efficient in forming tumors, both with regard to size and number in immunodeficient mice upon subcutaneous engraftment (Figure 6B).

Subsequently, we evaluated the relative sensitivity of LRCs and non-LRCs to MPA. Both populations were sorted and colony forming potential was assessed in the presence or absence of MPA. Compared with the control groups, treatment with MPA (10 μg/mL) significantly inhibited the colony formation efficiency of non-LRCs but not of LRCs (where only minor effects were seen; Figure 6C). Thus, slow-cycling cancer cells when compared to fast-cycling cancer cells appear more resistant to MPA and may thus constitute the MPA-resilient reservoir in cancers.

## Discussion

IMPDH is a key enzyme in *de novo* guanine nucleotide biosynthesis and is thus a target for oncologic disease. MPA works as a potent IMPDH inhibitor that is used as an immunosuppressive drug [3]. A phase I trial in patients with advanced multiple myeloma showed a positive correlation between clinical responses and depletion of the intracellular deoxyguanosine triphosphate levels by mycophenolate mofetil (MMF), the prodrug of MPA. MMF was administered up to a maximum dose of 5 g/day, which is 2-3 times higher than general use in organ transplantation patients, but was well tolerated in this study [19]. In renal transplant patients, a tendency towards a lower risk of malignancy in MMF-treated patients versus non–MMF-treated has been reported in a large, prospectively conducted, observational cohort study [20]. However, another

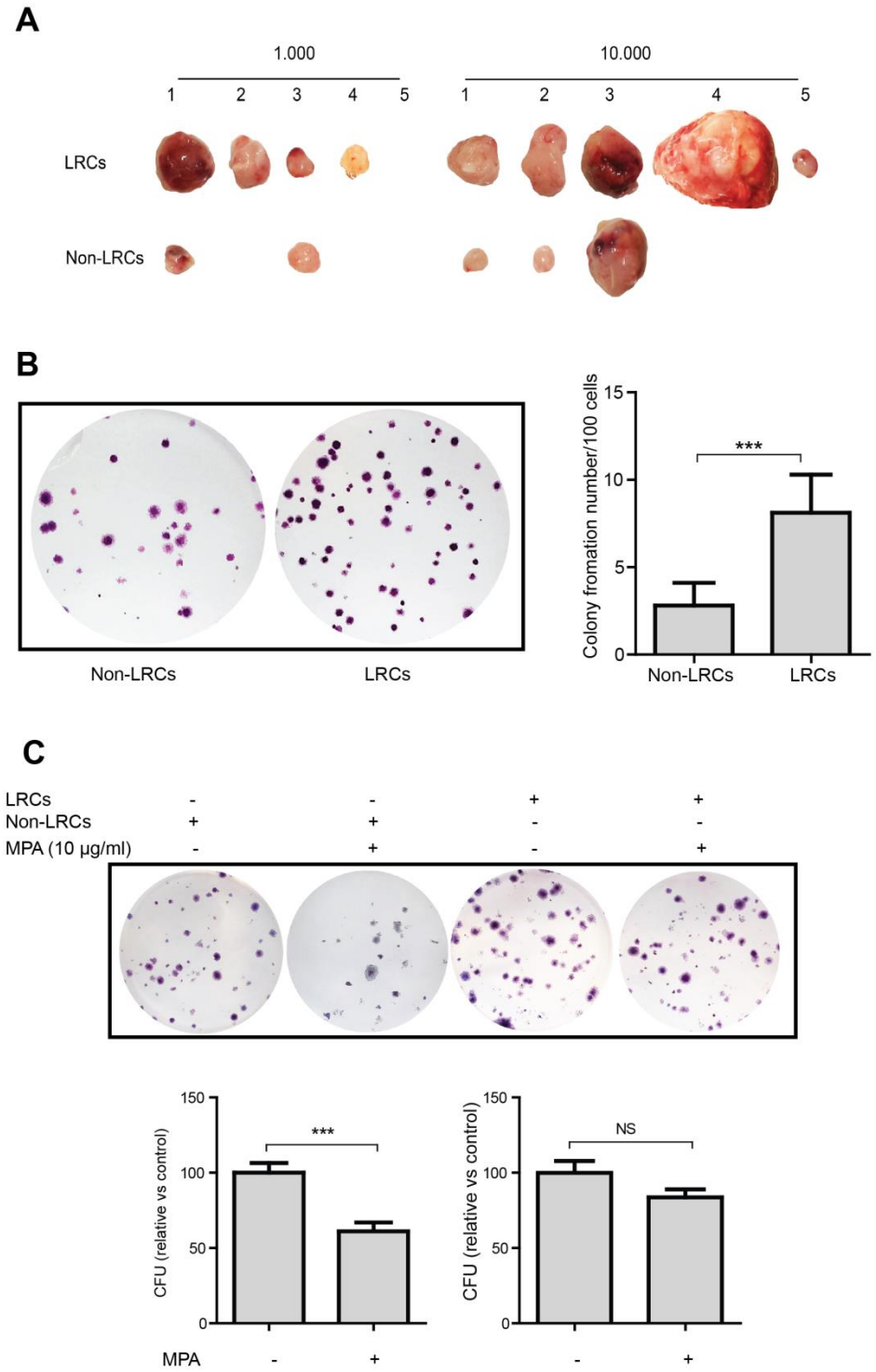


**Figure 6. Grafted label-retaining cells are superior in tumor initiation and more resistance to MPA.** (A) The macroscopic appearance of the tumors formed following secondary grafting of LRCs and non-LRCs respectively. (B) Colony formation following grafting LRCs and Non-LRCs harvested from xenograft tumor tissues (mean ± SEM, n = 19, ***P<0.001). (C) Colony formation by LRCs and Non-LRCs harvested from xenograft tumor tissues, when treated with MPA at a concentration of 10 µg/mL (mean ± SEM, n = 17, ***P<0.001).

clinical study in pancreatic cancer failed to show any beneficial effects [21]. We found that only fast-cycling, but not slow-cycling, cancer cells are sensitive to the inhibitory effects of MPA. Thus, dissecting the heterogeneity of cancer may help to understand the distinct responsiveness to MPA treatment.

A unique aspect of this study is the use of a label retaining technique that enables to identify and isolate LRCs. Classically, nucleotide analogs, such as 5-iodo-2'-deoxyuridine and Bromodeoxyuridine, are commonly used to identify LRCs. These agents can be used to identify LRCs, but the cells are not able to be isolated for functional study [22]. Thus, fluorescent-coupled nucleotide analogs were developed for identification and isolation of LRCs. However, these agents are not competent for *in vivo* application [23]. Although nucleotide analogs were also able to label cells *in vivo*, subsequent isolation of LRCs from the tissue is often a challenge that hampers further functional investigation [22]. Another major drawback is that most of these labeling methodologies rely on cell division to label cells. Therefore, the real quiescent cells in fact cannot be labeled. Consequently, the introduction of modified nucleotides into cells profoundly alters the status of the cells [24]. Integrating lentiviral-based Tet-on cell labeling system has circumstanced these limitations. Up on induction of the GFP fluorescent protein, all the cells can be labeled without genotoxic effect. It can be used for identification and isolation of slow-cycling cells both *in vitro* and *in vivo*. In this study, we used a Histone-GFP fusion protein that localized in the cell nucleus with prolonged half-life [25]. Thus, this technique bears broad implications for studying cell cycling. Indeed, we found the existence of slow-cycling cancer cell compartment within the fast growing tumors formed by HeLa cells. These cells are superior in tumor initiation and more resistant to MPA. We speculate that the existence of slow-cycling cancer cells in different patient population may affect the ultimate responsiveness of MMF/MPA treatment [19-21].

IMPDH2 is up-regulated in proliferating cells [26], including in various types of cancer cells [27, 28], and exhibits a 5-fold higher (compared to IMPDH1) sensitivity to

MPA. Mechanistically, the effect of MPA appears through inhibition of its canonical target, IMPDH2. Ectopic expression of a mutated *IMPDH2* (mut*IMPDH2*) largely nullifies the anti-proliferative effects of MPA. Since IMPDH is the key enzyme in purine nucleotide synthesis pathway, we studied the effects of modulating purine nucleotide pool on cell growth. Increasing the nucleotide concentration by supplementation of exogenous guanosine did not have major effect on cell growth (Supplementary Figure S4). In addition, we surprisingly found that supplementation of exogenous guanosine counteracts only to a minor extent to the inhibitory effect of MPA (Supplementary Figure S5). Although the anti-proliferative of MPA is mainly dependent on targeting IMPDH2, depletion of nucleotide could only explain part of its mechanism-of-action.

Interestingly, a recent study has demonstrated a double functionality for IMPDH in drosophila. It can also act as a transcription factor in stress conditions that inhibits cell proliferation [29]. Thus we speculate that IMPDH2 might be a ligand-regulated transcription factor and MPA might act as a ligand. Indeed, IMPDH2 is predominantly located in cytoplasm in normal condition of cultured HeLa cells, but efficiently translocated into nucleus upon MPA treatment (Supplementary Figure S6A). Consistently, a mutated *IMPDH2* lacking the binding site of MPA was not able to translate into nucleus even with treatment of MPA (Supplementary Figure S6B). These results appear to support the previous observation in Drosophila cells and our hypothesis. Furthermore it is already known that MPA works as a ligand to activate the activity of peroxisome proliferator activated receptors, such as PPARγ [30], a critical nuclear receptor on adipocyte differentiation. However, gene silencing of PPARα and PPARγ did not affect the sensitivity of HeLa cells to MPA treatment, excluding their potential involvement (Supplementary Figure S7). The scenario that MPA acts as a ligand for ligand-regulated transcription factors to regulate cancer cell growth is certainly interesting and therefore deserves further investigation.

In summary, this study demonstrated that through inhibiting IMPDH2, MPA was capable of constraining the growth of fast-cycling cancer cells. Using a lentiviral Tet-on cell labeling technique, we identified slow-cycling cancer cells within the fast-growing tumors that are superior in tumor initiation but more resistant to MPA. Thus, it is very necessary to develop regimens that can effective target slow-cycling cancer cells. Combining these regimens with agents targeting fast-cycling cancer cells, such as MPA, may be a viable option in cancer therapy.

## Conclusion

Slow-cycling cancer cells within fast-growing tumors were identified. These cells, compared to fast-cycling cells, were superior in tumor initiation and resistant to IMPDH2 inhibition by MPA. Thus, simultaneous targeting slow and fast-cycling cells are necessary to eradicate cancer.

## Acknowledgements

The authors would like to thank Dr. Lifeng Ni from the Animal Care at Hangzhou Normal University, Hangzhou, China for helping with the animal experiments. We also thank Professor Riccardo Fodde (Department of pathology, Erasmus Medical Center Rotterdam, Netherland) for providing Plasmids pLV.EX3D/EF1A-rtTA (M2)-dsRed-Express2 and pLV.EX2D/TRE-eGFP.

# Supplementary Information

Supplementary Figure 1

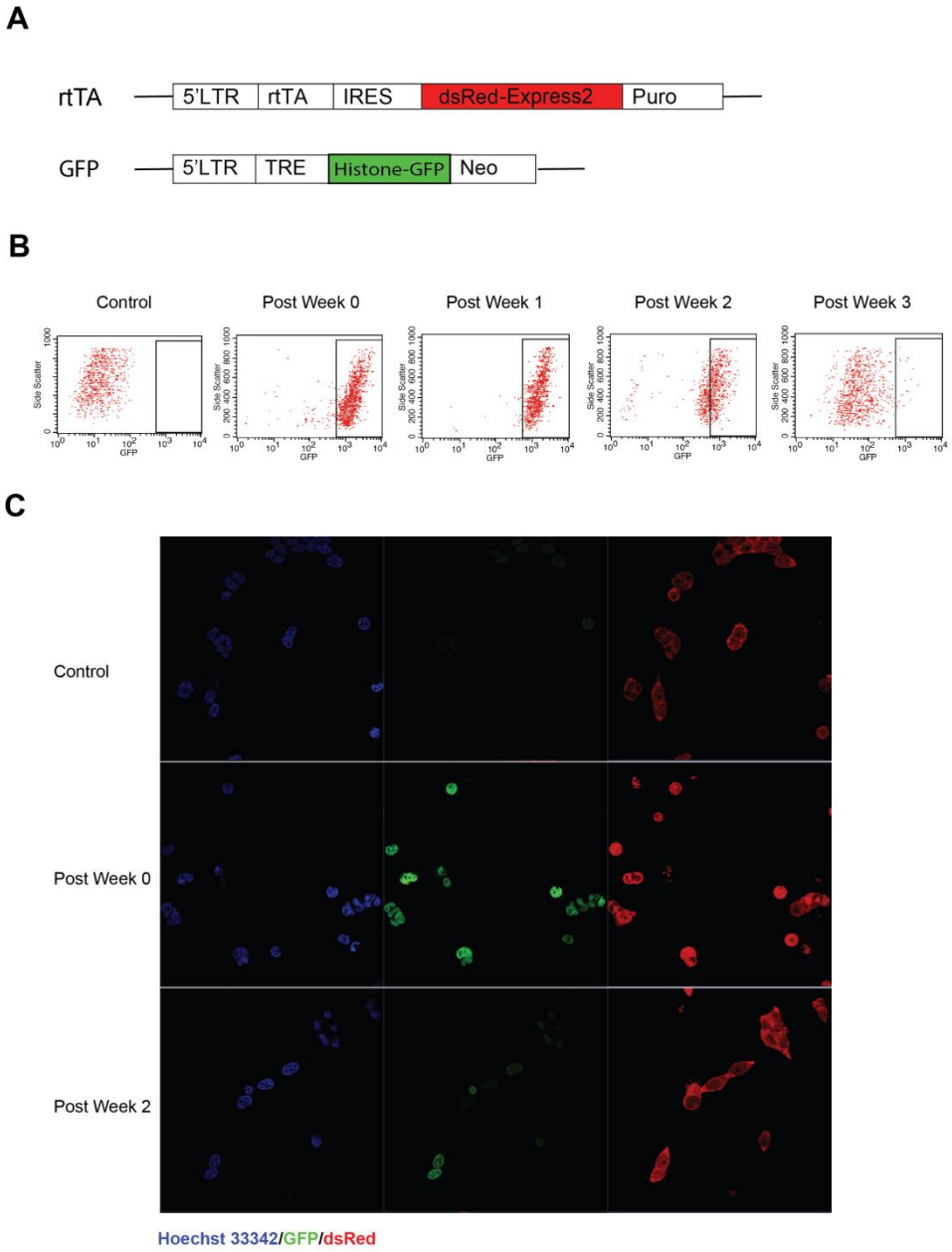


**Figure S1.** Label retaining Hela$^{tet\text{-}on}$ cell line expressing histone2B-GFP in a Tet-inducible fashion. (A) Plasmids pLV.EX3D/EF1A-rtTA (M2)-dsRed-Express2 and pLV.EX2D/TRE-eGFP were used. (B) and (C) GFP retaining condition *in vitro* could be detected even 3 weeks after doxycycline withdraw.

Supplementary Figure 2

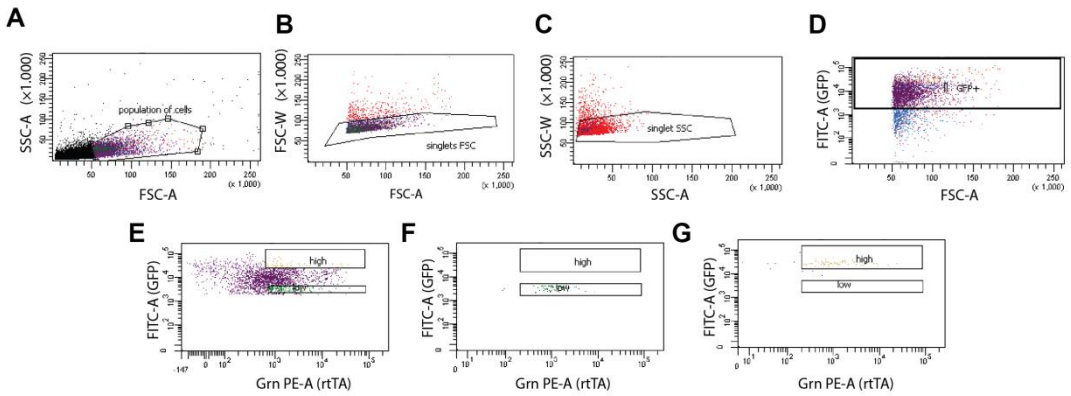


**Figure S2.** Tumor tissue were dissociated into single cell suspension and sorted for Non-LRCs ($GFP^{low}$dsRed) and LRCs ($GFP^{high}$dsRed) by FACS.

Supplementary Figure 3

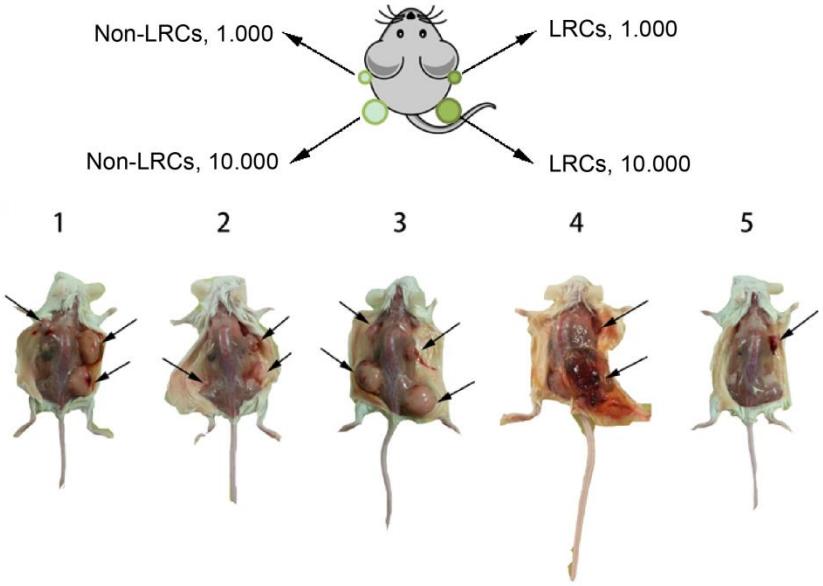


**Figure S3.** Non-LRCs and LRCs were injected subcutaneously into mice with cell number of 1.000 and 10.000 on four sites. Arrows indicate tumor formation.

Supplementary Figure 4

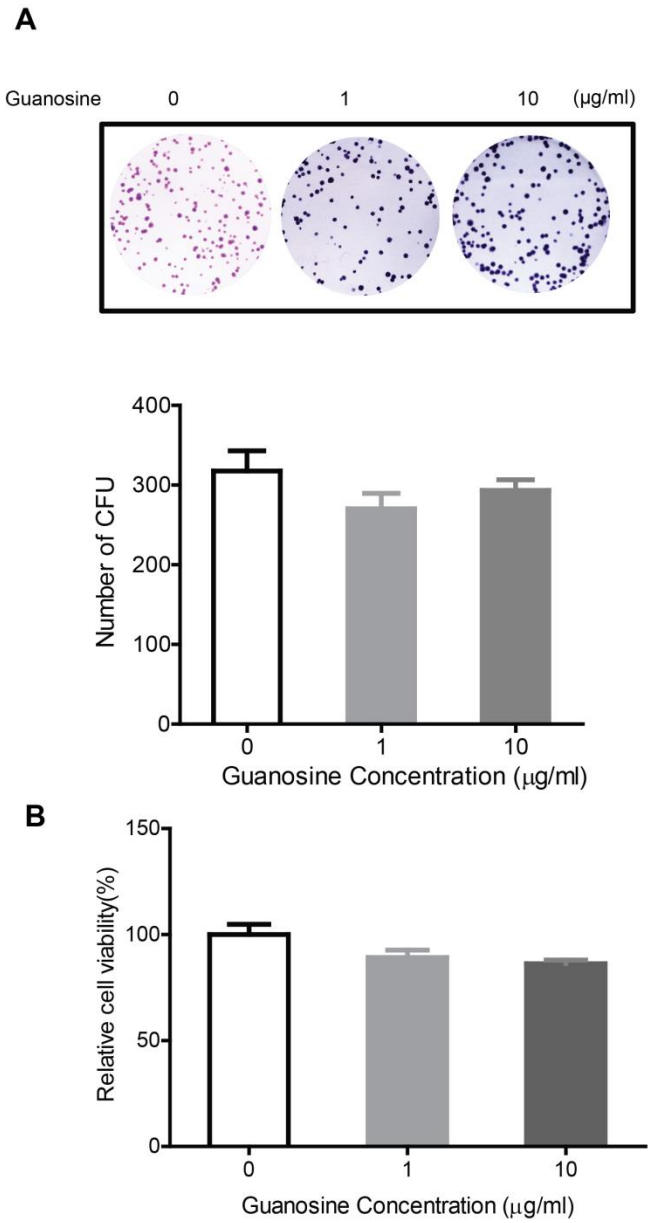


**Figure S4.** Guanosine alone did not significantly affect cell proliferation. (A) CFU appearance and numbers. (B) MTT assay.

Supplementary Figure 5

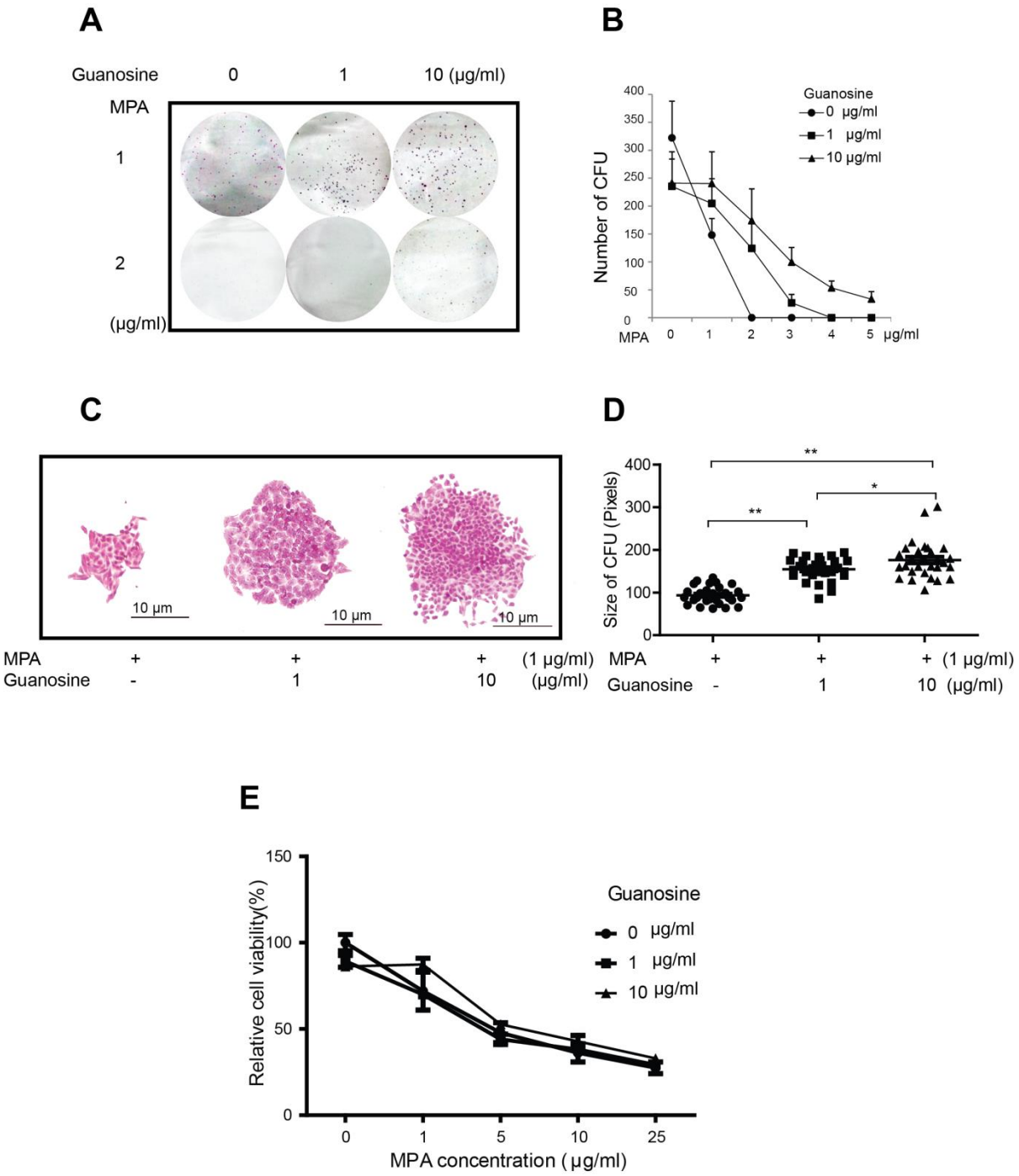


**Figure S5.** Anti-proliferative effects of MPA were partially restored by supplementation of exogenous guanosine. (A) and (B) The number of CFU, (C) and (D) The size of CFU were partially restored by supplementation of exogenous guanosine during treatment of the HeLa cell line with MPA (mean ± SD or SEM, n = 6 or 30, respectively, *P < 0.05; **P < 0.01).

Supplementary Figure 6

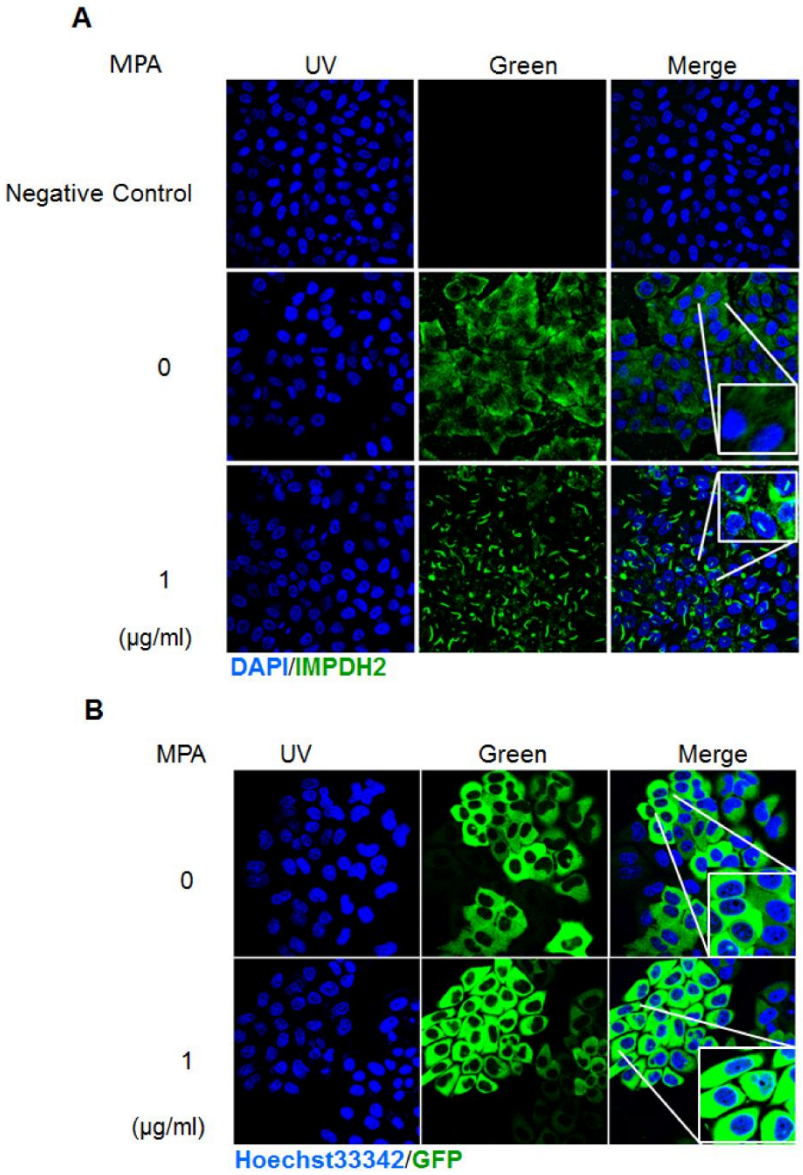


**Figure S6.** Cellular localization of IMPDH2 protein. (A) IMPDH2 protein predominately located in cytoplasm, but translocate into nucleus upon MPA treatment in HeLa cells. Blue: DAPI nuclear staining. Green: antibody against human IMPDH2. (B) A mutated IMPDH2 (fused with GFP) lacking the binding site of MPA was not able to translate into nucleus even with treatment of MPA in HeLa cells. Blue: DAPI nuclear staining. Green: GFP

Supplementary Figure 7

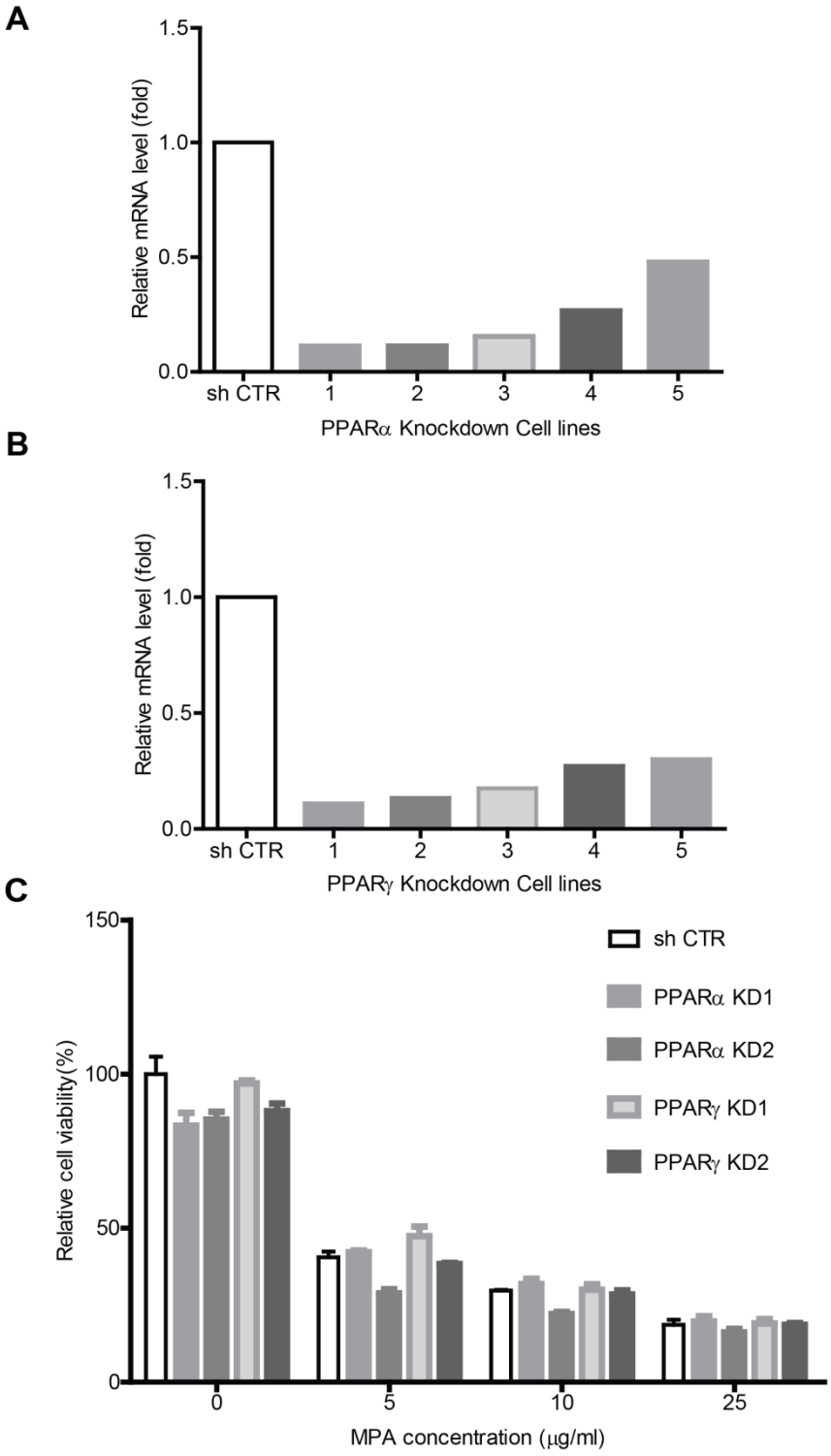


**Figure S7.** Knockdown of PPARα or PPARγ did not affect the sensitivity of HeLa cells to MPA treatment. (A) and (B) Relative mRNA levels of PPARα or PPARγ in HeLa cells transduced with 5 different lentiviral shRNA clones, GAPDH was used as an internal reference. (C) Clone 1 (KD1) and 2 (KD2) for each gene were selected to perform MTT assay.

Supplementary Table S1

STR genotyping of seven cancer cell lines

| STR | Panc-1 | BxPC-3 | Caco2 | HeLa | HepG2 | Huh7 | SKOV-3 |
|---|---|---|---|---|---|---|---|
| D3S1358 | 17 | 14/16 | 14/17 | 18/18 | 15/16 | 15/15 | 14/14 |
| TH01 | 7/8 | 9 | 6 | 7/7 | 9/9 | 7/7 | 9/9,3 |
| D21S11 | 28 | 29 | 30 | 27/28 | 29/31 | 30/30 | 30/31,2 |
| D18S51 | 12 | 12 | 12 | uitval | 13 | uitval | 16/17/18 |
| Penta_E | 7/14 | 12/14 | 7 | uitval | 15/20 | 11/11 | 5/13 |
| D5S818 | 11/13 | 11 | 12/13 | 12/14 | 11/13 | 12/12 | 11/11 |
| D13S317 | 11 | 11 | 11/13/14 | 12/14 | 9/13 | 10/11 | 8/11 |
| D7S820 | 8/10 | 10/13 | 11/12 | 8/12 | 10/10 | 10/11 | 13/14 |
| D16S539 | 11 | 9/11 | 12/13 | 10/10 | 12/13 | 10/10 | 12/12 |
| CSF1PO | 10/12 | 13 | 11 | 9/10 | 10/11 | 11/11 | 11/11 |
| Penta_D | 14 | 14 | 9 | 8/8 | 9/13 | 12/12 | 12/13 |
| AMEL | X | X | X | XX | XY | XX | XX |
| vWA | 15 | 14/18 | 16/18 | 16/18 | 17/17 | 16/18 | 17/18 |
| D8S1179 | 14/15 | 13 | 12/14 | uitval | 15/16 | 14/14 | 14/15 |
| TPOX | 8/11 | 8 | 9/11 | 8/12 | 8/9 | 8/11 | 8/11 |
| FGA | 21 | 20/21 | 19 | 21 | 22/25 | 22/22 | 24/25 |
| Match | 87% | 81% | 77% | 84% | 74% | 94% | 71% |

The STR match threshold is range from 71% to 94%.

STR genotyping information comes from the website: http://strdb.cogcell.org/

## References


1. Hanahan D, Weinberg RA. Hallmarks of Cancer: The Next Generation. Cell 2011;144:646-674.

2. Natsumeda Y, Ohno S, Kawasaki H, et al. Two distinct cDNAs for human IMP dehydrogenase. J Biol Chem 1990;265:5292-5.

3. Carr SF, Papp E, Wu JC, et al. Characterization of human type I and type II IMP dehydrogenases. J Biol Chem 1993;268:27286-90.

4. Moosavi MA, Yazdanparast R, Sanati MH, et al. 3-Hydrogenkwadaphnin targets inosine 5'-monophosphate dehydrogenase and triggers post-G1 arrest apoptosis in human leukemia cell lines. Int J Biochem Cell Biol 2005;37:2366-79.

5. Guidicelli G, Chaigne-Delalande B, Dilhuydy MS, et al. The necrotic signal induced by mycophenolic acid overcomes apoptosis-resistance in tumor cells. PLoS One 2009;4:e5493.

6. Fellenberg J, Kunz P, Sahr H, et al. Overexpression of inosine 5'-monophosphate dehydrogenase type II mediates chemoresistance to human osteosarcoma cells. PLoS One 2010;5:e12179.

7. Fellenberg J, Bernd L, Delling G, et al. Prognostic significance of drug-regulated genes in high-grade osteosarcoma. Mod Pathol 2007;20:1085-94.

8. Inai K, Tsutani H, Yamauchi T, et al. Differentiation induction in non-lymphocytic leukemia cells upon treatment with mycophenolate mofetil. Leuk Res 2000;24:761-8.

9. Takebe N, Cheng X, Fandy TE, et al. IMP dehydrogenase inhibitor mycophenolate mofetil induces caspase-dependent apoptosis and cell cycle inhibition in multiple myeloma cells. Mol Cancer Ther 2006;5:457-66.

10. Tressler RJ, Garvin LJ, Slate DL. Anti-tumor activity of mycophenolate mofetil against human and mouse tumors in vivo. Int J Cancer 1994;57:568-73.

11. Govindasamy N, Murthy S, Ghanekar Y. Slow-cycling stem cells in hydra contribute to head regeneration. Biol Open 2014;3:1236-44.

12. Schillert A, Trumpp A, Sprick MR. Label retaining cells in cancer--the dormant root of evil? Cancer Lett 2013;341:73-9.

13. Morris RJ, Potten CS. Slowly cycling (label-retaining) epidermal cells behave like clonogenic stem cells in vitro. Cell Prolif 1994;27:279-89.

14. Patel CG, Akhlaghi F. High-performance liquid chromatography method for the determination of mycophenolic acid and its acyl and phenol glucuronide metabolites in human plasma. Ther Drug Monit 2006;28:116-22.

15. Chen K, Man K, Metselaar HJ, et al. Rationale of personalized immunosuppressive medication for hepatocellular carcinoma patients after liver transplantation. Liver Transpl 2014;20:261-9.

16. Liang W, Wang D, Ling X, et al. Sirolimus-based immunosuppression in liver transplantation for hepatocellular carcinoma: a meta-analysis. Liver Transpl 2012;18:62-9.

17. Yam P, Jensen M, Akkina R, et al. Ex vivo selection and expansion of cells based on expression of a mutated inosine monophosphate dehydrogenase 2 after HIV vector

transduction: effects on lymphocytes, monocytes, and CD34+ stem cells. Mol Ther 2006;14:236-44.

18. Moore N, Houghton J, Lyle S. Slow-cycling therapy-resistant cancer cells. Stem Cells Dev 2012;21:1822-30.

19. Takebe N, Cheng X, Wu S, et al. Phase I clinical trial of the inosine monophosphate dehydrogenase inhibitor mycophenolate mofetil (cellcept) in advanced multiple myeloma patients. Clin Cancer Res 2004;10:8301-8.

20. Robson R, Cecka JM, Opelz G, et al. Prospective registry-based observational cohort study of the long-term risk of malignancies in renal transplant patients treated with mycophenolate mofetil. Am J Transplant 2005;5:2954-60.

21. Rodriguez-Pascual J, Sha P, Garcia-Garcia E, et al. A preclinical and clinical study of mycophenolate mofetil in pancreatic cancer. Invest New Drugs 2013;31:14-9.

22. Pan Q, Nicholson AM, Barr H, et al. Identification of lineage-uncommitted, long-lived, label-retaining cells in healthy human esophagus and stomach, and in metaplastic esophagus. Gastroenterology 2013;144:761-70.

23. Xin HW, Ambe CM, Hari DM, et al. Label-retaining liver cancer cells are relatively resistant to sorafenib. Gut 2013;62:1777-86.

24. Xin HW, Hari DM, Mullinax JE, et al. Tumor-initiating label-retaining cancer cells in human gastrointestinal cancers undergo asymmetric cell division. Stem Cells 2012;30:591-8.

25. Wang Y, Sacchetti A, van Dijk MR, et al. Identification of quiescent, stem-like cells in the distal female reproductive tract. PLoS One 2012;7:e40691.

26. Thomas EC, Gunter JH, Webster JA, et al. Different characteristics and nucleotide binding properties of inosine monophosphate dehydrogenase (IMPDH) isoforms. PLoS One 2012;7:e51096.

27. Hager PW, Collart FR, Huberman E, et al. Recombinant human inosine monophosphate dehydrogenase type I and type II proteins. Purification and characterization of inhibitor binding. Biochem Pharmacol 1995;49:1323-9.

28. Zimmermann A, Gu JJ, Spychala J, et al. Inosine monophosphate dehydrogenase expression: transcriptional regulation of the type I and type II genes. Adv Enzyme Regul 1996;36:75-84.

29. Kozhevnikova EN, van der Knaap JA, Pindyurin AV, et al. Metabolic enzyme IMPDH is also a transcription factor regulated by cellular state. Mol Cell 2012;47:133-9.

30. Makoto Ubukata HT, Misaki Ohashi, et al. Mycophenolic acid as a latent agonist of PPARr. Bioorganic & Medicinal Chemistry Letters 2007;17:4767-4770.

# CHAPTER 6

## Summary and Discussion

The research of stem cells has always attracted tremendous attention, not only because they can be utilized as potential therapeutic agents for treating various diseases, but also due to their possible participation in the tumor formation and progression. However, both of the good and evil aspects for liver stem cells require extensive investigation. The present thesis has attempted to demonstrate that how liver stem cells behave in livers in physiological homeostasis, upon injury, as well as carcinogenesis (**Figure 1**).

**Stem Cells in Intestine and Liver**

Although the intestine and liver are both endodermal organs, they are highly different in biological behavior and function. The intestinal epithelium proliferates every 3-5 days to compensate for the loss of functional cells. However, the hepatocytes in human liver normally live over 200 days before they are replaced by new cells. Apart from these apparent differences, the stem cells from those two organs also behave differently during the organ homeostasis and upon injury.

The intestine harbors a dedicated cycling stem cell population, which is responsible to fuel the rapid turnover of intestine. At the bottom of intestinal crypts, $LGR5^+$ cells are consistently self-renewing and generating rapidly dividing daughter cells [1]. In contrast, liver LGR5 cells are an intermediate stem cell population which not present in homeostatic period but only emerged upon liver injury (**Chapter 2**).

In the intestine, the quiescent/slow cycling label retaining cells (LRCs) occupy the +4 position from the crypt base. Those label retaining cells are marked by polycomb complex protein 1 oncogene (BMI1) [2], leucine-rich repeats and immunoglobulin-like domains protein 1 (LRIG1) [3], mouse telomerase reverse transcriptase (mTERT) [4], RNA-binding protein MEX3A (MEX3A) [5] or Hop homeobox (HOPX) [6]. Upon the depletion or dysfunction of LGR5 stem cells, those quiescent stem cells will be activated to repopulate the stem cell niche. The function of quiescent stem cells in intestine is more like a distinct reserve stem cell population.

Similar to intestine, the liver label retaining cells also express Lrig1, mTert and Mex3a (**Chapter 2**). Unlike intestine, the label retaining cell is not a subpopulation or backup of LGR5 stem cell. The liver label retaining cells present in the homeostatic liver, retaining the GFP label over 1 year, which can expand and further differentiate into functional cells *in vitro*. Interestingly, LRCs give birth to Lgr5 stem cell, as well as other progenitor/stem

cell populations, including SOX9 and CD44 cells. This is also consistent with our finding that LGR5 can be absent in the initiation and expansion of liver organoids (**Chapter 2**). These results imply that liver contains a hierarchical structure that quiescent stem cells could maintain the homeostasis and respond to injury by give rise to a multiply stem/progenitor cells. However, innovative techniques should be developed for identifying the quiescent stem cells in human liver, thus further providing effective therapeutic agents for future regeneration medicine.

**LGR5 Marks Cancer Stem Cell and Represents a New Therapeutic Target in Liver Cancer**

In colon/intestine, LGR5 has been reported as the most important marker for normal stem cell, as well as the tumor initiating cells [1, 7-11]. In **Chapter 2**, we have illustrated that LGR5 marks proliferative stem cells in the liver that are triggered by tissue injury. Thus, we further investigate the existence and function of LGR5 cells in liver tumor.

Our study demonstrated that LGR5 cells appear in the DEN induced liver tumors. The percentage of LGR5 cells was significantly higher in tumor proper compared to the tumor surrounding, as well as the frequency observed in healthy or acute/chronically injured livers (**Chapter 4**). To further demonstrate the function of LGR5 cells, we established a organoid culture system from primary liver tumors (**Chapter 3**). Employing this model, we observed that tumor LGR5 cells have stronger *in vitro* organoid initiation ability and *in vivo* tumor initiation capability. We also revealed that LGR5 positive cells were more resistant to treatment, compared to LGR5 negative cells. More interestingly, the ablation of the LGR5 expressing cells in liver tumor would impede the *in vivo* tumor growth.

Because cancer stem cells are highly tumorigenic and treatment-resistant, several pharmaceutical companies have started programs aiming at eliminating the cancer stem cell population. The main strategy involves 1) inhibiting cancer stem cell related key pathway, including WNT and NOTCH pathway[12]; 2) targeting quiescent cancer stem cells by an anti-CD36 antibody[13]; 3) using antibody-drug conjugates to ablate cancer stem cells [11]. In the colon and the intestine, LGR5 has been identified as a potential cancer therapy target [9-11]. The anti-LGR5-antibody-drug conjugates have been reported to target the LGR5 expressing cells in intestinal cancer effectively and further impede the growth of tumor, without unacceptable disturbance of the function of normal LGR5 stem cells [11].

Thus, It will be of particular interest to further study targeting liver LGR5 cancer stem cell based treatment.

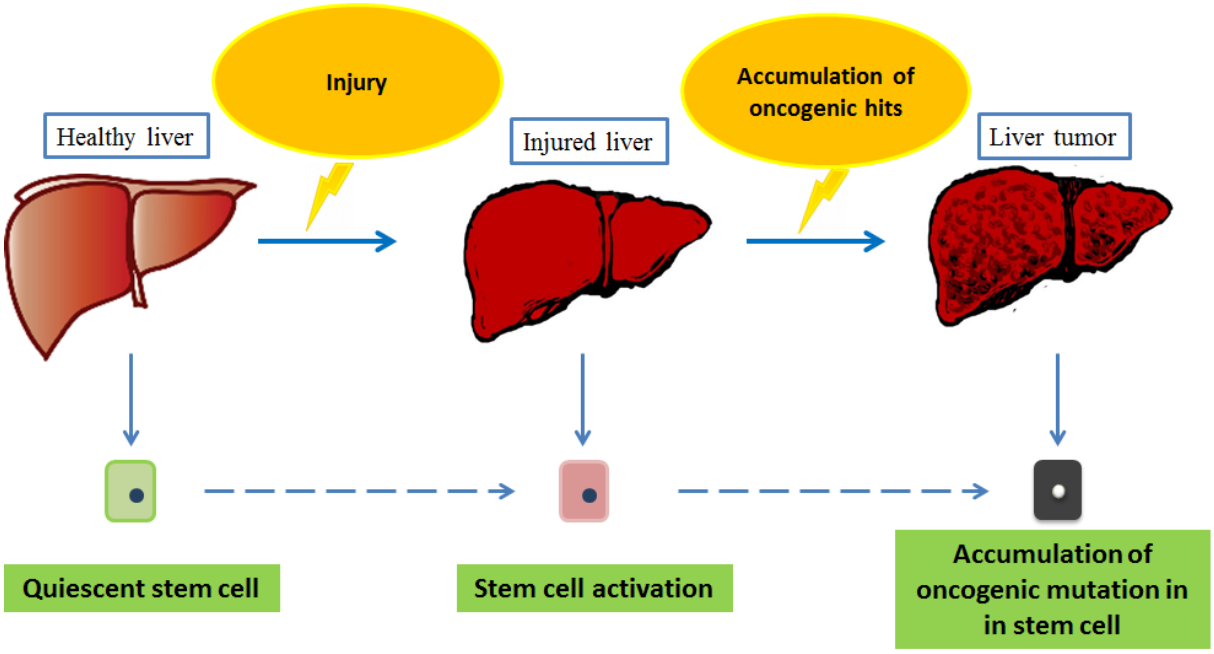


**Figure 1. Dynamics of Stem Cells in Liver Homeostasis, Injury and Carcinogenesis**

**Perspectives**

- Long-term label retaining cells represent a quiescent stem cell pool in the liver. It is maintained during liver homeostasis and respond to liver injury by giving rise to different stem/progenitor cells, including LGR5, SOX9 and CD44 positive cells. Likely, a combination of multiply stem/progenitor cells, rather than a single proliferative stem cell population, contributes to tissue repair in response to injury.

- LGR5 cells are present in liver tumor and represent a cancer stem cell population. Targeting LGR5 cancer stem cells provides a novel avenue for combating liver cancer. Extensive investigation is warranted to further develop effective therapies that can kill the cancer stem cells and prevent the tumor re-growth/recurrence. Considering the heterogeneous background of liver cancer, multi-target-based therapies should also be further investigated.

## References:


1. Barker N, van Es JH, Kuipers J, et al. Identification of stem cells in small intestine and colon by marker gene Lgr5. Nature 2007;449:1003-7.

2. Sangiorgi E, Capecchi MR. Bmi1 is expressed in vivo in intestinal stem cells. Nat Genet 2008;40:915-20.

3. Powell AE, Wang Y, Li Y, et al. The pan-ErbB negative regulator Lrig1 is an intestinal stem cell marker that functions as a tumor suppressor. Cell 2012;149:146-58.

4. Montgomery RK, Carlone DL, Richmond CA, et al. Mouse telomerase reverse transcriptase (mTert) expression marks slowly cycling intestinal stem cells. Proc Natl Acad Sci U S A 2011;108:179-84.

5. Barriga FM, Montagni E, Mana M, et al. Mex3a Marks a Slowly Dividing Subpopulation of Lgr5+ Intestinal Stem Cells. Cell Stem Cell 2017;20:801-816 e7.

6. Takeda N, Jain R, LeBoeuf MR, et al. Interconversion between intestinal stem cell populations in distinct niches. Science 2011;334:1420-4.

7. Boddupally K, Wang G, Chen Y, et al. Lgr5 Marks Neural Crest Derived Multipotent Oral Stromal Stem Cells. Stem Cells 2016;34:720-31.

8. Haegebarth A, Clevers H. Wnt signaling, lgr5, and stem cells in the intestine and skin. Am J Pathol 2009;174:715-21.

9. de Sousa e Melo F, Kurtova AV, Harnoss JM, et al. A distinct role for Lgr5+ stem cells in primary and metastatic colon cancer. Nature 2017;543:676-680.

10. Shimokawa M, Ohta Y, Nishikori S, et al. Visualization and targeting of LGR5+ human colon cancer stem cells. Nature 2017;545:187-192.

11. Junttila MR, Mao W, Wang X, et al. Targeting LGR5+ cells with an antibody-drug conjugate for the treatment of colon cancer. Sci Transl Med 2015;7:314ra186.

12. Batlle E, Clevers H. Cancer stem cells revisited. Nat Med 2017;23:1124-1134.

13. Pascual G, Avgustinova A, Mejetta S, et al. Targeting metastasis-initiating cells through the fatty acid receptor CD36. Nature 2017;541:41-45.

# CHAPTER 7

## Nederlandse Samenvatting

## Dutch Summary

Multipotente stamcellen zijn cellen die ongespecialiseerd kunnen blijven en door deling hun aantal kunnen vermeerderen, maar die ook zich (tot een beperkt aantal) gespecialiseerde celtypes kunnen differentiëren. Ze zijn essentieel bij het in stand houden van de grootte van organen door afgedankte cellen te vervangen en spelen een belangrijke rol bij regeneratie na beschadiging. De hoop dat leverstamcellen bij kunnen dragen aan gecontroleerd herstel van beschadigde levers in een klinische setting bestaat al lang. Daarnaast bestaat het vermoeden dat leverkanker ontstaat uit zogenaamde kankerstamcellen en dat het uitschakelen van leverkankerstamcellen een nieuwe aanpak zou kunnen vormen bij het bestrijden van deze (in het geval van gemetastaseerde ziekte) ongemeen dodelijke en therapieresistente ziekte. In dit proefschrift probeer ik deze leverstamcellen beter te begrijpen en op deze wijze leverstamcel-gerichte therapie in het verschiet te brengen. De betrokken vragen die ik mij in dit proefschrift stel werk ik uit in **hoofdstuk 1**.

In haar algemeenheid kan men zeggen dat stamcelcompartimenten in de lever anders lijken dan in de (dunne) darm. Beide organen delen een gemeenschappelijke embryonale oorsprong in dat zij alle twee ontstaan uit de endodermale kiemlaag, maar de fysiologie van beide organen is erg verschillend. De darm is een abortieve structuur, die blootstaat aan extreme mechanische en microbiologische belasting. De darm reageert op deze belasting door haar absorbtieve epitheel elke twee tot vijf dagen volledig te vernieuwen. De geassocieerde proliferatieve last wordt gedragen door het zogenaamde LGR5+ celcompartiment, dat dan ook snel deelt en haar onmiddellijke nakomelingen, in de crypten van de darmen. In **hoofdstuk 2** bekijk de aard en functie van het LGR5+ celcompartiment in de lever. De lever is een schijnbaar solide orgaan, dat bestaat uit duizenden kleine celformaties, van 1 mm doorsnede, die het bloed verwerken en een cruciale rol speelt in de biochemische homeostase van het lichaam alsmede het ontgiften van het bloed. Levercellen moeten naar schatting in gewone omstandigheden na ongeveer tweehonderd dagen vernieuwd worden. In mijn proefschrift toon ik aan dat de gewone gezonde lever niet een substantieel LGR5+ stamcelcompartiment bevat. Wordt de lever beschadigd, bijvoorbeeld door een insult met xenobioticum zoals koolstoftetrachloride, dan verschijnt een LGR5+ compartiment in de zich regenererende lever, die het herstel van het orgaan lijken te ondersteunen. Men kan zich voorstellen dat bij leverziekten ondersteuning van de LGR5+ positieve cel een positief effect zal hebben

op het herstelproces. Uit vervolg experimenten bleek echter dat het belang van deze LGR5+ cellen in dit opzicht waarschijnlijk beperkt is.

In de darm wordt het snel delende LGR5+ compartiment onderhouden door een dieper stamcel compartiment, dat juist niet deelt. Als LGR5+ cellen verloren gaan (denk bijvoorbeeld aan chemotherapie of stralingsschade, maar ook huis, tuin en keuken verlies van deze cellen tijdens het normale leven) dan worden deze diepe stamcellen wakker en genereren ze nieuwe snel delende LGR5+ cellen. Deze diepe stamcellen zijn dus een reservoir waar het LGR5+ compartiment uit kan putten als dat nodig is. Ik kon echter vaststellen dat in de lever LGR5+ stamcellen noodzakelijk nog voldoende zijn bij het herstel van de lever na schade. Wel bevat de een diep slapend stamcelcompartiment dat aan de top staat van een complexe stamcel hiërarchie van dochter stam- en progenitorcellen dat weliswaar in staat is om nieuwe LGR5+ cellen te genereren, maar ook vele andere nakomelingen heeft. Deze populatie van diepe, slapende stamcellen lijkt dan ook het meest interessant bij het denken over regeneratieve geneeskunde met betrekking tot de lever.

Zulke cellen bleken ook interessant te zijn in de context van leverkanker. Ik onderzocht in welke mate LGR5+ cellen aanwezig waren in levertumoren en ik kon vaststellen dat leverkanker veel meer van dergelijke cellen bevatte in vergelijking tot het gezonde weefsel naast de kanker (**hoofdstuk 4**). Ook waren deze LGR5+ cellen veel talrijker in de tumor dan gezien werd in gezonde levers of zelfs levers met acute of chronische ontsteking. Dus terwijl LGR5+ cellen niet noodzakelijk zijn voor het oncologisch proces in de lever, zijn ze er wel mee geassocieerd. Deze bevinding riep dan ook vragen op of de LGR5+ in de lever wellicht dan ook een rol zouden spelen in de verklaring voor waarom leverkanker zo ongewoon chemotherapieresistent is of in ieder geval een factor in de progressie van leverkanker zouden kunnen zijn. Data uit **hoofdstuk 3** lijken een dergelijke these te ondersteunen. Hier onderzocht ik organoiden (dit zijn kleine in de kweekschaal groeiende structuren die de meeste eigenschappen van het oorspronkelijke weefsel behouden en daarom uitstekend geschikt zijn voor wetenschappelijke experimentatie). Ik vond dat organoiden afgeleid van LGR5+ cellen vaker succesvol tot stand kwamen, dat zij vaker echte tumoren konden maken en dat zij meer resistent zijn tegen behandeling dan organoiden afgeleid van andere cellen. De verleiding is dus groot om deze LGR5+ cellen te zien als potentieel doelwit voor verbeterde behandeling van leverkanker.

In een laatste experimenteel hoofdstuk (**hoofdstuk 5**) probeer ik op grove wijze te testen in welke verschillende subpopulaties van leverkanker inderdaad echt belangrijk zijn in het verklaren van therapie resistentie. Om dit te bereiken, sorteerde ik kankercellen in twee groepen: een groep langzaam deelde en een groep die snel deelde. Ik zag dat de langzaam delende groep veel minder goed op therapie reageerde en ook dat deze groep veel gevaarlijker was wat betreft uiteindelijke grootte van de tumor. Het is dus inderdaad zo dat er verschillende groepen kankercellen zijn met verschillende relevantie voor het oncologisch proces.

Ik bediscussieer al deze data in **hoofdstuk 6.** Samengevat, kan ik stellen dat mijn data in belangrijke mate een hiërarchie in stamcel compartimenten in haar algemeenheid, maar ook in oncologische ziekte, ondersteunen waarvan de precieze onderlinge interactie de reactie op een insult (hetzij chemische schade voor het stamcelcomplex in gezonde organismen, hetzij de reactie op chemotherapie bij kanker) bepaald. Met deze kennis zou het mogelijk moeten zijn om meer doelgerichte therapie te ontwikkelen voor het behandelen van zowel leverschade alsook leverkanker, althans ik hoop met dit proefschrift daartoe een eerste aanzet te hebben gegeven.

# Appendix

## Publications

## PhD portfolio

## Curriculum Vitae

## Acknowledgement

# List of Publications

1. **Wanlu Cao**, Kan Chen, Michiel Bolkestein, Yuebang Yin, Nesrin Tuysuz, Luc J. W. van der Laan, Derk ten Berge, Dave Sprengers, Herold J. Metselaar, Jaap Kwekkeboom, Ron Smits, Maikel P. Peppelenbosch and Qiuwei Pan. The Dynamics of Proliferative and Quiescent Stem Cells in Liver Homeostasis and Injury. ***Gastroenterology***. 2017 Oct; 153(4).

2. **Wanlu Cao**, Meng Li, Yuebang Yin, Buyun Ma, Monique M.A. Verstegen, Jiaye Liu, Kan Chen, Michiel Bolkestein, Dave Sprengers, Luc J. W. van der Laan, Jaap Kwekkeboom, Ron Smits, Maikel P. Peppelenbosch and Qiuwei Pan. Modeling liver cancer and therapy responsiveness using organoid cultures derived from primary mouse liver tumors. (***Carcinogenesis***, conditionally accepted)

3. Wang W, Yin Y, Xu L, Su J, Huang F, Wang Y, Boor PPC, Chen K, Wang W, **Cao W**, Zhou X, Liu P, van der Laan LJW, Kwekkeboom J, Peppelenbosch MP, Pan Q. Unphosphorylated ISGF3 drives constitutive expression of interferon-stimulated genes to protect against viral infections. ***Sci Signal***. 2017 Apr 25;10(476).

4. PI3K-Akt-mTOR axis sustains rotavirus infection via the 4E-BP1 mediated autophagy pathway and represents an antiviral target. Yin Y, Dang W, Zhou X, Xu L, Wang W, **Cao W**, Chen S, Su J, Cai X, Xiao S, Peppelenbosch MP, Pan Q. **Virulence**. 2017 May 5:1-16.

5. The RNA genome of hepatitis E virus robustly triggers antiviral interferon response. Wenshi Wang, Changbo Qu, Jianhua Zhou, **Wanlu Cao**, Lei Xu, Buyun Ma, Mohamad S. Hakim, Yuebang Yin, Tiancheng Li, Maikel P. Peppelenbosch, Qiuwei Pan. ***Hepatology***, accepted.

6. **W Cao**, M Li, P Liu, J Liu, M Bolkestein, K Chen, L.J.W.Van Der Laan, D Sprengers, H J Metselaar, J Kwekkeboom, R Smits, M.P.Peppelenbosch and Q Pan. Hepatic LGR5 stem cells contribute to liver carcinogenesis. ***Journal of Hepatology***. Volume 66, Issue 1, Supplement, 2017, Pages S77-S78.

7. Zhou X, Huang F, Xu L, Lin Z, de Vrij FM, Ayo-Martin AC, van der Kroeg M, Zhao M, Yin Y, Wang W, **Cao W**, Wang Y, Kushner SA, Peron JM, Alric L, de Man RA, Jacobs BC, van Eijk JJ, Aronica EM, Sprengers D, Metselaar HJ, de Zeeuw CI, Dalton HR, Kamar N, Peppelenbosch MP, Pan Q. Hepatitis E virus infects neurons and brains. ***J Infect Dis***. 2017 Feb 11.

8. Hoekstra E, Das AM, Swets M, **Cao W**, van der Woude CJ, Bruno MJ, Peppelenbosch MP,

Kuppen PJ, Ten Hagen TL, Fuhler GM. Increased PTP1B expression and phosphatase activity in colorectal cancer results in a more invasive phenotype and worse patient outcome. ***Oncotarget***. 2016 Apr 19;7(16):21922-38.

9. Chen K, **Cao W**, Li J, Sprengers D, Hernanda PY, Kong X, Van Der Laan LJ, Man K, Kwekkeboom J, Metselaar HJ, Peppelenbosch MP, Pan Q. Differential Sensitivities of Fast- and Slow-cycling Cancer Cells to Inosine Monophosphate Dehydrogenase 2 Inhibition by Mycophenolic Acid. ***Mol Med***. 2015 Oct 13.

10. **Cao W**, Peppelenbosch MP, Pan Q. Virus-host interactions in HBV-related hepatocellular carcinoma: more to be revealed? ***Gut***. 2015 May;64(5):852-3.

11. Hernanda PY, Chen K, Das AM, Sideras K, Wang W, Li J, **Cao W**, Bots SJ, Kodach LL, de Man RA, Ijzermans JN, Janssen HL, Stubbs AP, Sprengers D, Bruno MJ, Metselaar HJ, ten Hagen TL, Kwekkeboom J, Peppelenbosch MP, Pan Q. ***Oncogene***. 2015 Sep 24;34(39):5055-68.

# PhD Portfolio

| | |
|---|---|
| Name PhD student | Wanlu Cao |
| Erasmus MC | Department of Gastroenterology and Hepatology |
| PhD Period: | September 2013 – January 2018 |
| Promotor: | Prof. Maikel P. Peppelenbosch |
| Copromotor | Dr. Qiuwei Pan |

## General Courses

- Laboratory Animal Science course (Art.9)
- Biomedical Research Techniques XIII & XIV
- Microscope Image Analysis: From Theory to Practice
- Basic and translational oncology course
- Scientific Integrity for PhD students

## Oral Presentations at national/international Conferences

- April, 22. Hepatic LGR5 Stem Cells Contribute to Liver Carcinogenesis. International Liver Congress™ 2017, Amsterdam, the Netherlands.
- March, 24. Hepatic LGR5 Stem Cells Contribute to Liver Carcinogenesis. Dutch Experimental Gastroenterology and Hepatology Meeting 2017. Eindhoven, the Netherlands.
- March, 24. Establishment of Malignant Organoid Model from Primary Mouse Liver Tumors Dutch Experimental Gastroenterology and Hepatology Meeting 2017. Eindhoven, the Netherlands
- March, 21. Hepatic LGR5 Stem Cells Contribute to Liver Carcinogenesis. MolMed Day 2017. Rotterdam, the Netherlands.
- April, 16. The dynamic and coherence of slow and fast cycling stem cells in homeostatic and injured liver. International Liver Congress™ 2016, Barcelona, Spain.
- March, 17. The dynamic and coherence of slow and fast cycling stem cells in homeostatic and injured liver. Dutch Experimental Gastroenterology and Hepatology Meeting 2016. Eindhoven, Netherlands
- March, 3. The dynamic and coherence of slow and fast cycling stem cells in homeostatic and injured liver. MolMed Day 2016. Rotterdam, the Netherlands.

## Awards and Honors

**Young Investigator Travel Awards**

- ILC Full Bursary (€650), International Liver Congress™ 2017, Barcelona, Amsterdam.

- ILC Full Bursary (€650), International Liver Congress™ 2016, Barcelona, Spain.

**Best Abstract Awards**

- Hepatic LGR5 Stem Cells Contribute to Liver Carcinogenesis. International Liver Congress™ 2017, Amsterdam, the Netherlands.

# Curriculum Vitae

Wanlu Cao was born in May 12, 1989, in Qidong, Jiangsu province, China. She grew up and attended her primary, middle and high school in her hometown.

In 2006, she started her study of Biological Engineering at the University of China Pharmaceutical University, Nanjing, Jiangsu province (4 years). In 2010, she started a master research in the same university. She studied at the School of Life Science & Technology, under the supervision of Prof. Min Wang. Her main interest was to investigate the antiangiogenic activity of the vascular endothelial growth factor receptor. She obtained her Master degree in 2013.

In 2013, with the support of China Scholarship Council, she got an opportunity to start her PhD research at the department of Gastroenterology and Hepatology, Erasmus Medical Center, the Netherlands. Under the supervision of Prof. Maikel P. Peppelenbosch and Dr. Qiuwei Pan, she mainly focused her investigations on the dynamics of stem cells in liver homeostasis, injury and carcinogenesis.

# Acknowledgement

It is a long, demanding and interesting journey towards obtaining a PhD. I would like to express my sincere gratitude to those who have offered me invaluable help during the five years of my PhD study. I truly appreciate your help in the completion of this thesis.

To my promotor, Prof. Dr. Maikel P Peppelenbosch, thank you so much for your great support. You always give me inspiring and innovative suggestions.(as sir know-everything). I have learned so many things from our weekly group meeting, especially when my projects were stuck in somewhere (well, this happens all the time). Without your help, I can never survival from my PhD and finally present this thesis.

To my co-promotor Dr. Qiuwei Abdullah Pan. You have taught me so many things, starting with how to do presentations, to design a project, to write a manuscript and so on. You saved me out of scientific dilemma for so many times. It is you that really enlighten me to understand how to be a better scientific researcher.

To Luc, it is my great honor to have you as the inner committee member. You are such a talented and knowledgeable person who always bring up with sparking and inspiring ideas. it is really enjoyable time to discuss scientific questions with you. Your ideas enrich my research, give me more confidence to work as a scientist in the future.

To Ron, really appreciate for your help and all the valuable suggestions for my projects. I still remember in my first year of PhD, you told me that: you should ask the question, then, you will have half the chance to get the answer; if you do not ask, the chance will be 0 (which is translated from a Dutch proverb). Every time when I hesitate to do something which I should do, this sentence comes to my mind. Without your help, it is an impossible mission for me to finally graduate as a PhD. Thank you so much!!!

To Prof. Riccardo Fodde, it is my honor to have the chance to learn from you. The first time that we met was that Abdullah brought me to introduce our project to you. Besides all the rigorous and interesting scientific suggestions, you also told us like: which word is more accurate in describing that situation; what is the difference between two similar scientific words. At that moment, I started to realize that you are just the kind of scientist who I want to take as an idol forever.

To Dave, you always give me a lot of precious suggestion from the clinical view. As time goes on, when I start to conceive a new projects now, I also start with: what is the clinical meaning? what is my final target? You also encourage me a lot during our weekly meeting. Thank you so much!

To Jaap, you give me so many valuable and important suggestions about my projects as well as the manuscript. Wish the best to you and your entire family.

To 王旻教授和张娟老师，谢谢您二位在硕士期间给予我的所有的帮助，您二位同样也是我一开始在科研之路上的领路人。祝您工作顺利，阖家幸福。

To Monique (Verstegen), many thanks to you. Since we work in the similar area, we can always have interesting and inspiring discussion about organoid. Especially there are limited people working in the organoid initially, it is so nice to discuss with you about all the scientific details, which makes me not work alone.

To Matt, I still cannot forget that day, when I left EMC around 10:30 p.m. and met you in the front door of Sophia. Then, you told me that you still have 5-6 hours of experiments to finish (this is a regular situation for you), which means almost the whole night. Then, I really started to understand the following sentence: Genius is one per cent inspiration, ninety-nine per cent perspiration. Wish you have a brighter future and there is no doubt about this.

To Derk, Nesrin and Wouter, thank you so much for your help in the label retaining project, especially in the establishment of organoid model. Wish you have a wonderful future!!!

To Zeliha and Mirjam, thank you for your help in the RNA sequencing, wish the best to you and your future.

To Michiel and Asha, you give me so so many help in cryosection, mice and different types of staining. It's so happy to cooperate with you. Hope I will have the chance to visit you both in Germany someday in the future.

To Marcel, thank you so much for your help on the FIS assay for liver organoid. You are such a gentle and nice person. Wish all the best to you.

To Gwenny, you are so smart and so energetic. You are professional in science area and so nice in daily life. You know so many scientific knowledge as well as so many songs. "Work hard, play harder" I really learn this proverb from you. Wish all the best to you.

To Pratika, thank you so so much. You gave me so many help in the first year of my PhD. And to your lovely daughter Amreta and your husband. I really enjoy the time staying with your family. They are all really nice people. We talk a lot about marriage, friendship and love. Those are all precious memory to me. Wish the best to you and your entire family. Hope to see you someday in the future.

To Auke, you give me so many help in so many things. Even when you are also busy with something, you still would like to help us out of some issues. You are really a helpful and gentle person. Wish the best to you and your entire family.

To Yingying, thank so much for letting me meet you in the lab and becoming friends for the past five years. We have so many fantastic memories that I even do not know where to start. When I was shy in the beginning, it was you that encourage me to participate in more social activities, which let me meet so many wonderful friends in the following years. My 28 birthday cakes, the first time Andrew called me Lulu, so many times you told me that: you should believe in yourself. Thank you for having you. Love you.

To Meng. 千言万语，谢谢你出现并且成为我的好朋友，损友且段友。有朋友在身边，做科研好像也就没有那么辛苦了。希望你也早日顺利毕业，早日找到你的如意良人。愿友谊长存。

To Estella, you are so smart and such a nice person. You are so brave in expressing your points of view. Being friend with you for five years, I am also on the way to be a stronger person. You always encourage me to try a lot of different things. And we always can share our lives in the lab almost every day (not the last year of PhD, we are too busy). Thank you so much for those memorable moments.

To Jiaye, my Paranimfen. You give me so many help in experiments, especially in the last year of my PhD. You are smart and hard-working. In the meantime, you also have you unique way to explore this world. I am really impressive that you always know how to find out the cheapest tickets and hotels. I believe that you definitely will become a good researcher and doctor. All the best to you and your future.

To Yuebang, thank you for giving me so many help in the organoid culture. You are so smart and you work so hard. Wish you a bright future.

To Xu lei. You always work so hard and always so modest. Wish all the best to you and your brighter future.

To Shan. Seeing your strict attitude towards scientific work, I can definitely figure out that you are also a good doctor. Hope you can also defense your PhD as soon as possible. Wish the best to you, your wife and your lovely little princess.

To Kan, thank you for your help to my experiments. You give me a great deal of encouragement as well as precious suggestion. For a really long time, we walked home together and talked everything happened that day. You just like a sister to me. All the best wishes to you, your husband and your son. See you in China.

To Effie, we started to know each other almost in the last year of your PhD. At that period, we walked home together with Kan. You are really a simple and sweat person. Now you have already became a strong and independent group leader in your new workplace. Hope to meet you in China soon. Wishes all the best to you.

To Cindy, you are really a smart girl and I really enjoy our trip to EASL in Barcelona. You also gave me a lot of help before and after I came to EMC. Thank you so much and all the best to your future.

To Wenhui, my first roommate in Rotterdam. In the beginning of our PhD, we really spent a lot of time together. Your presence really makes me not feel lonely. All of those memories are so precious to me. Wish the best to you and your entire family.

To Wenshi，深感你是一个有大智慧和大能力的人，同时你也是一个非常好的朋友，愿鹏程万里，阖家幸福。

To Pengyu, you are a knowledgeable and smart person. I have to admit that I use the same word as Lei in his acknowledge to you. But when I saw that sentence, I just feel exactly the same feeling. I always believe that you definitely will become a 科研大牛 in the future.

To Amy, you know how to insist and be yourself even when others do not understand you. I really learned a lot from you. Wish all the happiness to you.

To Shihao, you are knowledgeable and hard-working. 然道阻且长，且等你大放光芒.

To Shaoshi, you have your unique point of view towards life, science and future. By discussing with you, I also learned a lot. You show us a different way to think about life. Wish all the best to you.

To Wen, you really have a nice attitude towards life. We are both the Paranimfen of Kan, thus I have the chance to know a little bit more about you. I am really impressive by your way of thinking about life, family and friendship. With all the best for your brighter future.

To Buyun, you are smart and hard-working. I believe that you will definitely become a good and outstanding researcher in the future.

To Bobby, it's so nice to have the chance to see your changes. Maybe you also have the feeling that PhD period will indeed makes someone think more deeply about life, not only about science or research. I believe that you will become a really good researcher in the future. All the best wishes to you.

To Sunrui. I have to say: among all the researchers, you are the best singer; Among all the singers, you are the best scientific researcher. It is really nice to have two areas which you are both good at. Wish all the best to you.

To Zhouhong, I am really impressive by your professional and responsible attitude towards your work. You definitely will have a bright future.

To Ling. Although we just met each other for several months, you have already helped me a lot in my experiments. You are definitely a talented scientific researcher. Wish all the best to your brighter future.

To Zhijiang, Xumin, Yang Qin, Li Yang, Li Yunlong and Yu Peifa. 虽然我们才刚认识，还没有机会好好的熟悉, 但是我相信你们一定是未来的科研之星，祝你们前程似锦，一帆风顺。

To Marieke, you gave so so so many help in the experiments. Without you, I can never accomplish my projects. You are so professional, so patient and so nice to me. And I really enjoy all of our talking about your wedding, dog, holiday and so on. Wish the best to you and your family.

To Evelyn, you are such a smart and beautiful girl. I still cannot forget your story about the frog and sock. Wish you all the best for your bright future.

To Emma, you are very wisdom and positive all the time. During your stay in MDL, we have so many lab parties and you always encourage us to join the party. You definitely will have a wonderful future.

To Wesley and Cindy, both of you are such nice and smart person. Thank you for letting me sharing the important moment with you. It feels so good to see Wesley's PhD defense, getting married and especially the baby angle joining your family. Wish all the best for your entire family.

To Rik, you are a handsome, smart and nice person. You always can bring laughs and happiness into the lab. Wish the best to you and your future.

To Martijn, you are a smart and happy person. It is really fun to play the game of The Werewolves of Miller's Hollow with you and other colleagues during the camping. Those are really happy memories to me. And also congratulation to your defense. Wish the best to your future.

To Suk Yee, you are such a smart and happy girl. It is such a unique feeling to talk with you, because we can switch the language between English and Chinese. You just like a person who can bring sunshine to friends. I will just become happy during the talking with you. You definitely will have a brighter future and wish you can find your Mr. Right as soon as possible.

To Anthonie. You are always so happy no matter in the lab or in the parties, And it is so cute to see you and your son have the same hairstyle. Wish the best for your family.

To Kim, you are such a nice person. For me, it will just be happy when see you in the lab. I really enjoy the time when you plan and describe your future with you family. Hope I can have the chance to visit you when you finally move to your dreamland.

To Petra, you are such an elegant and nice lady. Maybe you do not know this, but actually you are an idol for me. You really have a lifestyle which I admire so much. I really like the Rotterdam Tour you give, playing piano with your daughter and etc. Hope all the best for your future.

To Monique (de Beijer), my neighbor in the lab. You like to sit in the left side of the flow cabinet and I love the right side. And we always work until late in the night. That's why we are always neighbors in the lab. You are so smart and work so hard. I could feel the passion and unlimited energy from you for the scientific research. Wish the best to your bright future.

To Floris, my friend, also my neighbor in the lab as well as in the office. You are so smart and always so happy. You really make good plan for your life, both for career and family. I really wish the best for your future.

To Ruby, I am really happy to hear that there will be a new PhD student in your group working on liver organoid. The feeling is just: yeah, finally, I will have an ally. You are a smart and active person. And I am lucky to work together with you. Wish you have a sweat, lovely weeding soon and as well as a bright future.

To Lisanne, I really feel that life only gives you with all the good, but not any bad. You are smart, beautiful, energetic and elegant. Wish all the best to you.

To Vincent, you always work so hard. I definitely believe that you will become an outstanding doctor in the coming days. Wish all the best to you.

To Shanta, thank you for sharing so much precious experience in IHC/IF. Besides your help from your expert area, you also help me a lot in the first 1-2 years. Because I was very shy initially, you are always open to talk with me. That's really helped me to adjust to the new environment, especially in the first year of my PhD.

To Raymond and Leonie, thank you for giving me so so so much help. Whenever we have different types of problems/emergencies/super emergencies, you always can help me out. Give my best wishes to you and your entire family.

To Patrick, you are really a nice, gentle, helpful and optimistic person. Wish all the best to you.

To Kelly, we are familiar with each other because we are both working on organoid and mice. Our style is like: Yes, I am on the way to the EDC. Oh yes, I am in the middle of passaging organoids. And you are always just a hero to save my organoid out of danger, because there are always some components running out, which I can borrow from you. You are really a sweat and nice girl. Wish all the best to your future.

To Natasha, every time when I see you in lab, I just feel happy. To me, You are a girl full of sunshine and energy. You also belong to the "team organoid", which enables us to see each other a lot on weekends, different holidays, early in the morning and late in the night. Wish all the best to you.

To Marla, thank you so much for helping me with the b-catenin staining. Wish the best to you.

To Pauline, you inspired me a lot. For me, it is already so difficult to handle all the scientific issues. But you need to take care both of the career and family. Wish all the best to you and your entire family.

To Jan, you are always so happy, gentle and helpful. The feeling is just like: you give the world with love and the world return back to you also with love. Really looking forward to meet you lovely wife and children. Wish all the best to you and your entire family.

To Buddy, thank you so much for helping us with the ordering all the time. You are always so patient and helpful. Wish all of the best to you.

To Thijmen, you are really a gentleman. Although we did not have so many chances to talk, I heard a lot about you from Kan. She mentioned that you kindly taught her pronunciation, which impressed me a lot with your warm heart. Wish you the best to your future career.

To Gulce, you are not only smart but also hard-working. Almost every time when I work until late, you are still in the lab. Wish all of the best to you and your future.

To Sonja, thank you for giving me so much precious suggestions during our weekly GIO meeting. I learned so many things from you. Although we work in different areas, you are indeed an idol for me. You are energetic, smart and beautiful. Wish all the best to you and your future.

To Gertine, thank you so much for your help on my experiments. Wish all the best to you.

To Paula, thank you for teaching us how to pitch a tent. I really enjoy those fantastic camping moments. Wish all the best to you and your entire family.

To Lauke, you will definitely become a good doctor & scientific researcher in the future. Because you are smart and also work so hard. no matter it is Weekend, 10 p.m. or Christmas day, you can always find Lauke in the lab or in the office. I definitely believe that you will have a brighter future.

To Noe, you are smart and also work so hard. Plus, I am really interested that, how can you adapt to the weather in Rotterdam as a Spainish? This question really bothers me for a long time. Give my best wishes to your PhD and future.

To Shaojun, I am really impressive by your dream about “吃软饭”. Wish your dream will come true as soon as possible (just kidding). You are a polite, smart and funny person. I believe that you definitely will have a brighter future.

To Ilknur, you are really a sweat and nice girl. You give me so much encouragement. Hope we can cooperate some day in the future. Give my best wishes to you.

To Michiel (Mommersteeg), I really enjoy the trip to the Beer festival. Now I have the feeling that: it is more easy to make friends with Dutch people with beer around (For our Chinese people, it is in a restaurant).

To Jorke, you also belong to that kind of people who bring sunshine around you. You are always so happy and full of energy. Wish all the best to your future.

To Yik, another member of “team organoid”. You are a sweat and beautiful girl. Wish all the best to your future.

To Manzhi, you really know what you want and also know how to achieve you target. I learned a lot from you. You will definitely have a bright future.

To Liu Menggang 师兄, you just like an older brother to us. You are a good doctor and also a good husband. Wish all the best to you and your entire family.

To all the colleagues from EDC, Ingeborg, Eva, Vincent, Miranda, Jennifer, Charlotte, Sabine, Henk (Dronk), Michelle, Ineke and Dr. Mathieu Sommers. Thank you so so much. You gave me so many help for the past five years. All the best wishes to you.

All the co-authors, thank you for the contribution to my thesis and to the journal publications.

I would like to give my great thanks to the financial support from the China Scholarship Council.

All MDL members to those who have left and who are present, Professor Hugo de Jonge, Hanneke, Andrea, Andre, Thomas, Martine (Meulemans), Frances, Jasper, Ksenia, Dowty, Wouter, Janine, Diahann, Wendy, Gijs, Alexander, Kateryna, Kairong, Hakim, Cynthia, Emmeloes, Kostas, Eelke, Renee, Henk, Rachid, Ben, Terry, Aniek, and so on. I want to thank you for helping me during the five years. I have indeed enjoyed my time with you in the lab. Best wishes to all of you!

To 酷爱美食且酷爱推荐美食同时热爱科研的展民、我感觉是万能的无敌美少女丹莉莉，直爽美丽智慧的目前已晋级为额娘的黄玲，超级会在狼人杀中伪装自己的同伟、稍微有点神秘但是超级温暖且睿智的侯珺，南半球一哥的优秀毕业生长斌、喜欢并擅长摄影的吴斌、无敌潇洒且成功转行的潇磊，帅气幸福的未来之星文浩以及文浩幸福之来源之聪慧小美女瑶瑶，集智慧于美貌于一身的且已订婚的无敌美少女高雅、另外一个集智慧于美貌于一身的且居然坚持六点起床的高文、智慧超群且号召力无敌的刘凡老师、无敌且貌美的请务必收下我的膝盖的辣妈温蓓、智慧青春美少女小俊、温柔睿智大美女陈思，宅且智慧着的月光族魁魁（开销巨头为吃且居然不胖）、绝对是加班 no.1 大半夜可以在 EMC 找到的平臻、优秀毒舌且理解不了为啥还是单身的鲁涛、热爱且会生活的白冠男、温柔小甜心王璐，总是很开心的徐笑非，绝对学霸的活泼美少女张旭熙，目前口头禅是我们开公司吧的美女若愚、睿智但是好久不见的凯音、可爱又美丽的睿智小少女陈金鸾，同门师弟晓路，由于“it’s ugly”的故事一战成名的周峘（di），永远会被国影说服或者怎么都没有办法说服国影的唐颖、如果不是在跑步就是在去健身路上的健康美少女波波以及其他可爱的朋友们，很荣幸可以遇到如此优秀的你们，过去的岁月充盈着我们的笑語晏晏，愿大家的未来幸福美好，我们友谊长存。

To 刘敏和云宝，虽然我们不在一个国家，但是你们永远是我遇到任何苦难和收获喜悦的时候，第一时间想倾诉和分享的人。你们使我更坚强。

To 我的未婚夫李海鑫。谢谢你一直陪着我，给于我坚持下去的动力。过去的五年对于我们来说是艰难的。但是同时又是很有收获的。你的陪伴和鼓励，使得我的科研之路变的没有那么的漫漫无绝期。

最后也是最重要的是，感谢我最亲爱的爸爸妈妈。是你们给了我内心最深处的坚持下去的力量。科研之路非常坎坷，但是因为你们，我从来就没有想过要放弃。没有你们，就没有我。我爱你们，我爱你们。